

**A STUDY ON FIBROSIS AND ADIPOGENESIS DURING
MUSCLE REGENERATION IN MOUSE MODEL**

(マウス筋再生過程における線維化および脂肪化に関する研究)

The United Graduate School of Veterinary Science

Yamaguchi University

MOHAMED ABDELHADY ALI MAHDY

March 2017

CONTENTS

Page

General introduction.....	1
Chapter 1: Comparison of muscle regeneration following cardiotoxin and glycerol injury	
Abstract.....	5
Introduction.....	7
Material and methods.....	9
Results	16
Discussion.....	23
Figures.....	30
Chapter 2: Early ultrastructural events of muscle damage following cardiotoxin and glycerol injury	
Abstract.....	41
Introduction.....	42
Material and methods.....	44
Results	46
Discussion.....	51
Figures.....	57
Summary.....	65
Acknowledgments.....	67
References.....	68
Published papers.....	82

GENERAL INTRODUCTION

Experimental animal models enable studying muscle regeneration in a controlled and reproducible manner (Horie *et al.*, 2014) and consequently developing new therapies for treating congenital and acquired myopathies (Karalaki *et al.*, 2009). However, the cellular events and time course of regeneration differs depending on the type of injury (Musarò, 2014). Cardiotoxin (CTX) is extensively used in muscle research to induce injury and regeneration (Czerwinska *et al.*, 2012; Gayraud-Morel *et al.*, 2009; Liu *et al.*, 2012; Uezumi *et al.*, 2010), it induces similar degenerative changes to those in muscular dystrophies and inflammatory myopathies (Ramadasan-Nair *et al.*, 2014). While glycerol-induced injury is a novel model to induce ectopic adipocytes during muscle regeneration (Pisani *et al.*, 2010; Uezumi *et al.*, 2010), it induces similar degenerative changes to those in patients with Duchenne muscular dystrophy (DMD) (Kawai *et al.*, 1990). Although Lukjanenko *et al.* (2013) compared the regeneration process in glycerol and CTX injury models by immunohistochemistry and genomic profiling, the detailed response of non dystrophic muscle to injuries induced by CTX and glycerol is largely unknown.

Despite of the remarkable capacity of skeletal muscle to regenerate in response to injuries and diseases (Yan *et al.*, 2003), fibrosis and fat infiltration are observed in skeletal muscle in some pathological and experimental conditions resulting in impaired regeneration. Muscle fibrosis, the excessive accumulation of connective tissue, is a characteristic feature of muscular dystrophies (Pessina *et al.*, 2014) and severe injuries as lacerations, contusions and strains (Uezumi *et al.*, 2014). Fibrosis impairs normal muscle regeneration (Serrano *et al.*, 2011) through forming barrier between muscle and capillaries (Desguerre *et al.*, 2009). In addition, it decreases the amount of target muscle available for treatment (Kharraz *et al.*, 2014). While fat infiltration is associated with different pathological conditions as myopathies, sarcopenia, cachexia (Brioché *et*

al., 2016), and advanced cases of DMD (Uezumi *et al.*, 2014). An increased level of fat infiltrations decreases muscle quality and strength and impaired mobility (Addison *et al.*, 2014).

Muscular dystrophies are characterized by progressive weakness due to myofibers degeneration with progressive replacement of muscle tissue with fibrous and fat tissue (Živković and Clemens, 2015). DMD is characterized by repetitive cycles of muscle necrosis and regeneration (Wallace and McNally, 2009) with constant muscle fibrosis in young age (Kharraz *et al.*, 2014). *mdx* mouse, the most commonly used genetic model, shows limited fibrosis in limb muscles of aged mice (after 18-24 months), while fibrosis is developed in diaphragm muscle only (Gutpell *et al.*, 2015) which hinders evaluation of anti-fibrosis treatment. Alternatively, breeding two years old animals requires much time and money (Desguerre *et al.*, 2012). Therefore, it is important to develop either new protocol to advance muscle fibrosis in young *mdx* mice or develop new models for muscle fibrosis at early stages of life (Pessina *et al.*, 2014).

Transforming growth factor (TGF)- β 1, a potent profibrotic cytokine, is associated with fibrosis development in many tissues and muscular dystrophies (Prisk and Huard, 2003) it is up regulated in most pathologies either in its active or latent form (Pohlars *et al.*, 2009). In addition, *in vitro* studies revealed that TGF- β 1 is an inhibitor of osteogenic (van Zoelen *et al.*, 2016), and adipogenic differentiation (Choy and Derynck, 2003). Recently, Pessina *et al.* (2014) demonstrated the fibrotic effect of combining exogenous TGF- β 1 with CTX-induced injury in wild-type muscles, they showed significant fibrosis in combined treatment while TGF- β 1 treatment alone did not induce fibrosis.

Previous studies explored alternative methods to enhance fibrosis in the limb muscle of *mdx* mice to mimic human muscular dystrophy such as repeated mechanical micro-injuries (Desguerre *et al.*, 2012), laceration, denervation, chronic exercise, and injection of myotoxic

agents (Pessina *et al.*, 2014). In addition to genetic models, there is a need to develop new experimental methods to efficiently enhance fibrosis in hind limbs (Kharraz *et al.*, 2014). Moreover, studying muscle fibrosis in normal, non-dystrophic, mice will help understanding the mechanism, cells and factors that play role in fibrosis development (Pessina *et al.*, 2014).

Aims of research

The overall aim of this thesis is to investigate the detailed response of non-dystrophic muscle following injuries induced by CTX and glycerol to determine the appropriate injury model for studying muscle fibrosis and adipogenesis.

In Chapter 1, the outcome of muscle regeneration following injury induced by glycerol was compared with the widely used CTX-induced injury and the structural changes in IMCT during muscle regeneration were demonstrated using SEM-cell maceration technique. In addition, the effects of TGF- β 1 on muscle regeneration and adipogenesis in glycerol-injured muscle were investigated.

In Chapter 2, the early ultrastructural events following CTX and glycerol muscle injuries were demonstrated to investigate the possible mechanisms by which CTX and glycerol damage skeletal muscle and to clarify the relationship between these events and difference in regeneration between the two injury models.

Chapter 1

Comparison of muscle regeneration following cardiotoxin and glycerol injury

ABSTRACT

In the current study, skeletal muscle regeneration in normal mice was investigated following two types of injuries, cardiotoxin (CTX) and glycerol, to compare their effects on the morphological characteristics of muscle during the regeneration process, moreover, the alteration of the intramuscular connective tissue (IMCT) structure during regeneration was studied by scanning electron microscopy (SEM) following digestion of the cellular elements of the muscle with sodium hydroxide.

Tibialis anterior (TA) muscles of adult male C3H/HeN mice were injured either with CTX or glycerol. Muscle degeneration was greater in CTX-injured muscle than glycerol-injured muscle at day 4 after injury. Although muscle regeneration started at the same time in both CTX- and glycerol-injured muscles, CTX-injured muscle showed better organization and larger myotube diameter than glycerol-injured muscle at day 14 after injury. On the other hand, adipocytes infiltration was detected in glycerol-injured muscle but not detected in CTX-injured muscle. Furthermore, different patterns of endomysial collagen deposition were notable during regeneration between CTX-injured muscle and glycerol-injured muscle.

Next, the effects of exogenous transforming growth factor (TGF)- β 1 treatment on muscle regeneration and adipogenesis were investigated in glycerol-injured muscle. TGF- β 1 was either co-injected with glycerol, as an early treatment, or injected at day 4 after glycerol-induced injury, as a late treatment. Muscle samples were collected at day 7 after initial injury. Myotube density was significantly lower in the early treatment group than in the glycerol-injured group. Moreover, the Oil Red O-positive area was significantly smaller in the early treatment group than in the glycerol-injured group and late treatment group. Furthermore, TGF- β 1 treatment increased endomysial fibrosis and induced immunostaining of α -smooth muscle actin, a marker

for myofibroblasts. In conclusion, the current results suggest that changes in IMCT play an important role in controlling the efficiency of muscle regeneration following injury. Moreover, the greater inhibitory effects of early TGF- β 1 treatment than those of late TGF- β 1 treatment during regeneration in glycerol-injured muscle suggest that TGF- β 1 has a more potent effect on the early stage of muscle regeneration and adipogenesis.

INTRODUCTION

Skeletal muscle has a powerful capability for regeneration following different types of injuries such as strains and contusions and diseases such as muscular dystrophies (Best and Hunter, 2000), and the regenerated muscle in normal conditions resembles the undamaged muscle morphologically and functionally (Charge and Rudnicki, 2004). However, disturbance of the regeneration process results in fibrosis and adipocyte infiltration.

Several experimental models of muscle injury have been used to study skeletal muscle regeneration in a controlled and consistent manner. These models include chemical models such as cardiotoxin (CTX) (Czerwinska *et al.*, 2012), bupivacaine (Nishizawa *et al.*, 2003; Politi *et al.*, 2006), and glycerol (Pisani *et al.*, 2010) injection and mechanical models such as freezing injury (Warren *et al.*, 2007) and crush injury (Zimowska *et al.*, 2009). However, time course as well as characteristics of muscle regeneration differs according to the type of injury.

Intramuscular connective tissue (IMCT) is an essential component of skeletal muscle. It has several functions; it provides a scaffold for arrangement of myofibers, nerves and vessels, it transmits contractile force within the muscle, and it provides an appropriate environment for differentiating myoblast (Osse and Brandan, 2002). Moreover, it regulates muscle development, regeneration and function through controlling the activities of different mononuclear cells as immune cells, stem cells and fibroblasts (Garg and Boppart, 2016). Appropriate deposition of IMCT is essential for efficient regeneration, preserving muscle structure and supporting the muscle contractile function (Serrano *et al.*, 2011), however, deviations in the intensity and timing of this process result in fibrosis. Endomysial fibrosis is an important feature in Duchenne muscular dystrophy, it forms barrier between capillaries and myofibers and associated with decline of satellite cells (SCs) and infiltration of alternatively activated macrophages (Desguerre

et al., 2009), moreover, changes in muscle environment surrounding stem cells increase the severity of its pathological features (Kharraz *et al.*, 2014). Therefore, better understanding of the changes in the morphology of IMCT during regeneration helps to understand the pathogenesis of muscle diseases and develop therapies for improving muscle regeneration.

In the current study, comparison of muscle regeneration following CTX, the commonly used myotoxin to induce muscle injury, and glycerol, the newly used method to induce muscle injury was done. In addition the effects of exogenous treatment of TGF- β 1 on muscle regeneration and adipogenesis in glycerol-injured muscle were investigated. Recently, Lukjanenko *et al.* (2013) compared muscle regeneration in glycerol-induced injury and CTX-induced injury by immunohistochemistry and genomic profiling. However, to the best of my knowledge, no study had previously evaluated the changes of IMCT structure during the degeneration and regeneration process following injuries induced by CTX and glycerol. The different changes during muscle degeneration and regeneration in chemically-injured models help to understand the different events occur in muscular dystrophies and to develop new therapies for these dystrophies.

MATERIALS AND METHODS

Animal care and ethical approval

Adult male C3H/HeN mice at 6-8 weeks of age, weighting about 20-24 g body weights, were purchased from CLEA Japan (Tokyo, Japan). The present study was conducted on male mice to avoid sex-specific differences in muscle regeneration in female mice (Fearing *et al.*, 2016; McHale *et al.*, 2012).

Animals were housed during the experiment in the Experimental Animal Facility of Tottori University, Japan. First, animals were kept for two days to be acclimated to the facility before experiments. They were housed in plastic cages supplied with sawdust floor and were fed a pelleted diet (CLEA Rodent Diet; CE-2, CLEA Japan) with free access to drinking water. The facility was provided with controlled temperature (22-24°C), humidity (40-60%) and light (12-h light-dark cycle). Animal care was performed in accordance with Tottori University's guidelines for the care and use of laboratory animals in research. All experimental procedures were approved by the Animal Research Committee, Tottori University, Japan (Approval number: 15-T-24).

Experimental muscle injury

Anesthesia was prepared as a mixture of 0.2 mL pentobarbital sodium (Somnopentyl; Kyoritsu Seiyaku, Tokyo, Japan), 0.8 mL midazolam (Dormicum 10 mg; Astellas Pharma, Tokyo, Japan), 1 mL butorphanol (Vetrophale; Meiji Seika Kaisha, Tokyo, Japan), and up to 10 mL normal saline (0.9% NaCl; Otsuka Pharmaceutical, Tokushima, Japan). Mice were weighed using a digital scale ELT-402 (Sartorius, Gottingen, Germany). Anesthesia was injected intraperitoneally [0.02 mL/g body weight] using a 27g X 3/4" needle (Terumo, Tokyo, Japan).

The anterolateral aspect of the left hind limb was disinfected with 70% ethanol (Wako, Osaka, Japan) and the skin was shaved.

Mice were divided into two groups ($n = 18$ in each group). The first group was injected with 50 μL of 10 μM CTX from *Naja mossambica mossabica* (C9759, Sigma-Aldrich, St. Louis, MO, USA), the second group with 50 μL of 50% glycerol (v/v) (Wako, Osaka, Japan) in sterile phosphate-buffered saline (PBS; pH 7.4). Intramuscular injections were done at the middle part of tibialis anterior (TA) muscle using U-100 insulin syringes (BD, Fukushima, Japan). Mice were kept on a heating pad at approximately 38°C to maintain body temperature until full recovery.

Sampling and histological analysis

Mice were sacrificed by cervical dislocation after inhalation anaesthesia with isoflurane (Intervet, Tokyo, Japan). Skin over TA muscle was shaved and incised using fine scissors and fine tip forceps and then the TA muscle was separated by fine scissor. Injured TA muscles were collected at 4, 7 and 14 days after injury (three mice for each time point). The opposite non-injured TA muscles were used as controls.

For histological analysis, muscles were fixed in 4% paraformaldehyde solution, dehydrated in graded ethanol series (Wako), cleared in xylene (Wako) and embedded in paraffin. Serial cross-sections (5 μm in thickness) were obtained using sliding microtome (RUB-2100H; Yamamoto, Saitama, Japan) and stained with hematoxylin and eosin (HE) for histological analysis.

For detection of fibrosis, muscle sections were stained with 0.1% Sirius red stain (Polysciences, Warrington, Pennsylvania, USA) dissolved in a saturated aqueous solution of picric acid (katayama chemicals, Osaka, Japan) for 1 h at room temperature. Sections were

washed with acidified water (contain 0.5% acetic acid), dehydrated and mounted with Eukitt mounting medium (O. Kindler GmbH, Freiburg, Germany).

Scanning electron microscopy

Muscle samples were fixed with 2.5% glutaraldehyde (Wako) in 0.1 M phosphate buffer, pH 7.3, overnight at 4°C, post fixed in 1% OsO₄ (Merck, Darmstadt, Germany) for 2 h, dehydrated in an ascending graded series of ethanol (Wako), critical point drying, coated with platinum after mounting on metal stubs and observed by SEM (S-800; Hitachi, Tokyo, Japan).

Transmission electron microscopy

Muscles were cut into small pieces using a razor, fixed in 3% glutaraldehyde overnight (Li *et al.*, 2009) then post-fixed in 1% OsO₄ for 3 h, dehydrated in ethanol, embedded in rubber molds with epoxy resin (Okenshoji, Tokyo, Japan) and polymerized in an oven at 60°C for about 36 h. Semi-thin section (1µm in thickness) were cut with glass knives using a PT-X Power Tome Ultramicrotome (RMC, Arizona, USA) and stained with toluidine blue (Merck). Ultrathin sections (70 nm in thickness) were cut, mounted onto coated copper grids (Nisshin EM, Tokyo, Japan), and stained with uranyl acetate and lead citrate. Grids were examined using a JEM-1400 transmission electron microscope (JOEL, Tokyo, Japan) operated at 80 KV.

Cell Maceration/Scanning electron microscopy

This technique helps to analyze the structural changes in the extracellular matrix of skeletal muscle (Gillies *et al.*, 2011) through visualization of the three-dimensional arrangement of the collagen fibers of IMCT. Samples were prepared using cell maceration technique as described in

previous studies (Nishimura *et al.*, 1999; Ohtani *et al.*, 1988), in which the cellular elements of the muscle had been digested leaving the collagen fiber network. Briefly, small pieces of TA muscles were fixed with 2.5% glutaraldehyde in a 0.1 M phosphate buffer solution for 3 days, pH 7.3, and then immersed in 10% aqueous solution of NaOH for 4 days followed by rinsing in distilled water for 5 days (with changing NaOH solution and distilled water every 12 h). The samples were fixed in 1% tannic acid for 3 h. After rinsing in distilled water for several hours, the samples were post-fixed in 1% OsO₄ for 1 h, dehydrated in ethanol, freeze-fractured in liquid nitrogen, and freeze dried with t-butyl alcohol (Inoue and Osatake, 1988). Samples were coated with gold after mounted on metal stubs and examined using a scanning electron microscope (S-800; Hitachi) operated at 10 kV.

Intramuscular injection of TGF- β 1

To study the effects of TGF- β 1 on muscle regeneration and adipogenesis in glycerol-injured muscle, 50 ng of TGF- β 1 [Recombinant Human TGF- β 1 (HEK293 derived); Peprotech, New Jersey, USA] was injected intramuscularly (Pessina *et al.*, 2014). Mice were divided into three groups ($n = 14$ in each group): an early treatment group that received 50 ng of RhTGF- β 1 co-injected with glycerol, a late treatment group that received 50 ng of RhTGF- β 1 at day 4 post glycerol injury, and a group that received glycerol only. TA muscles were collected at day 7 after initial glycerol injury. Paraffin sections were obtained from the middle part of the muscle.

Oil Red O staining (ORO)

Muscles were fixed in 4% paraformaldehyde solution (pH 7.4), cryoprotected in 15% sucrose and then 30% sucrose (Wako) in PBS until they sank (Waddell *et al.*, 2010), embedded in

Tissue-Teck OCT (Optimum Cutting Temperature; Sakura, Tokyo, Japan) compound, and frozen at -80°C. Cryosections (10 µm in thickness) were obtained from the middle part of the muscle at -20 °C using a Leica CM-3050S cryostat (Leica Biosystems, Nussloch, Germany). Lipid accumulation was assessed by ORO in 60% triethylphosphate (Wako, Tokyo, Japan), and the nuclei were counterstained using Mayer's Hematoxylin.

Immunofluorescence and immunohistochemistry

Paraffin sections were deparaffinized and permealized with 0.5% Triton X-100 (Nacalai, Kyoto, Japan). All washings were done with PBS containing 0.1% BSA (Sigma-Aldrich). For immunofluorescence, sections were incubated with donkey serum (GTX30972; Gene-Tex, CA, USA) for 30 min at room temperature. The sections were incubated overnight at 4°C with primary antibodies, including mouse anti-neonatal myosin antibody (1:50, sc-53097; Santa Cruz Biotechnology, Santa Cruz, USA) and rabbit anti-collagen type I antibody (1:200, NB600-408; Novus Biologicals, Littleton, USA), followed by incubation with a secondary antibody conjugated to Alexa Fluor (R&D Systems, Minneapolis, USA) at a dilution of 1:200 for 30 min. Nuclei were stained with 1 µg/mL Hoechst 33342 (Molecular Probe, Leiden, Netherlands) for 10 min were then mounted with fluorescence mounting medium (Dako Japan, Kyoto, Japan) and examined by a fluorescent microscope (Olympus IX71, Olympus, Tokyo, Japan).

For immunohistochemistry, endogenous peroxidase activity was eliminated with 3% hydrogen peroxide (Wako) in distilled water for 10 min. Non-specific binding was blocked with 5% BSA for 2 h in a humidified chamber. Sections were incubated with rabbit anti- α smooth muscle actin (SMA) antibody (1:200, NB600-531; Novus Biologicals) and rabbit anti-F4/80 antibody (1:500, sc-26643-R; Santa Cruz) for detection of myofibroblasts and macrophages

(Kawanishi *et al.*, 2016), respectively. Immunoreactivity was detected with 3, 3'-diaminobenzidine (DAB) (Dako). Nuclei were stained with haematoxylin. Negative control sections without a primary antibody were included in every staining.

Morphometric analysis

For morphometric analysis, three mice for each time point were used and three representative sections/mouse were chosen. Four non-overlapping fields/section were photographed at X10 objective lens. Digital images were taken with a digital camera (DP71, Olympus). The captured images were analyzed using Image-J software (v1.46r, National Institutes of Health, Maryland, USA). The myotube density was calculated as the number of myotubes, containing central nuclei/field (Horsley *et al.*, 2001). The minor axis diameters (smallest diameters) of at least 500 myotubes per animal were measured. Sirius red-positive areas were quantified after adjustment of the threshold and expressed relative to the total muscle area (Wang *et al.*, 2013). For quantification of collagen type I and adipocyte in the muscle tissue, the areas stained with anti-collagen type I antibody and ORO, respectively, were quantified and expressed relative to the total muscle area.

Reverse transcriptase-polymerase chain reaction (RT-PCR)

Total RNA was extracted using Trizol reagent (Ambion Life Technologies, Carlsbad, California, USA) according to the manufacturer's protocol. The quantity and quality of total RNA were determined by using a spectrophotometer (Ultraspec 1100 Pro; Amersham, Freiburg, Germany). For cDNA synthesis, 0.5 µg of total RNA was reverse-transcribed using ReverTra Ace RT Master Mix with gDNA remover (Toyobo, Osaka, Japan). Gene expression was analyzed using

semi-quantitative RT-PCR. PCR reactions were performed using Quick Taq HS DyeMix (Toyobo) and a thermal cycler (T100; Bio-Rad, California, USA). The primer sequences and product sizes are shown in Table 1. PCR products were analyzed by electrophoresis in 2% agarose gel at 100 V and visualized using ethidium bromide (Sigma-Aldrich).

Evans blue dye (EBD) uptake

EBD is used as an *in vivo* marker for detecting damaged myofibers (Wooddell *et al.*, 2011). Mice were injected intraperitoneally with 1% EBD (Wako) in sterile saline (0.1 mL/10 g body weight). Muscles were collected 20 h after EBD injection. Then muscle cryosections were examined by a fluorescent microscope. Nuclei were stained with Hoechst.

Statistical analysis

Data were expressed as means \pm standard deviation (SD). Statistical analysis was performed using SPSS software (IBM SPSS Statistics; Chicago, Illinois, version 21). Results were analyzed by one-way analysis of variance (ANOVA) followed by Dunnett's *post-hoc* test to compare the injured groups with the non-injured control and to compare TGF- β 1-treated groups with the glycerol-injured group. The t-test followed by Bonferroni's *post-hoc* test was used for comparing between treatments. Statistical significance was defined as $P < 0.05$.

RESULTS

Time courses of muscle regeneration following CTX and glycerol-induced injuries

Myofibers in the intact non-injured muscles had polygonal shapes with peripheral nuclei (Fig. 1A).

Four days after injury

Both injuries induced muscle degeneration with inflammatory cellular infiltration at day 4 after injury (Fig. 1B and 1C). However, muscle degeneration was greater in CTX-injured muscle than in glycerol-injured muscle, moreover, large number of cellular infiltration with vacuolated myofibers could be seen in CTX-injured muscle.

Seven days after injury

Small regenerating myotubes characterized by relatively large central nuclei and basophilic staining appeared by day 7 in both injury models with enlarged interstitial spaces (Fig. 1D and 1E). The myotube density was higher in CTX-injured muscle than in glycerol-injured muscle; about 1.4-fold higher than that in glycerol-injured muscle. Moreover, adipocytes infiltration was detected between the regenerated myotubes in glycerol-injured muscle only. In contrast, no adipocytes could be detected in CTX-injured muscle (Fig. 1E).

Fourteen days after injury

At day 14, CTX-injured muscle had many regenerated myotubes of varying diameters (Fig. 1F). In contrast, glycerol-injured muscle had fewer regenerated myotubes with adipocytes infiltration (Fig. 1G). The myotube density in CTX-injured muscle was about

1.1-fold higher than that in glycerol-injured muscle. The average myotube diameter was significantly increased at day 14 compared with that at day 7 in both injury models ($P<0.05$). The average myotube diameter was significantly larger in CTX-injured muscle than in glycerol-injured muscle ($P<0.05$) (Fig. 3A). Moreover, the regenerating myotubes in CTX-injured muscle showed better organization compared to those in glycerol-injured muscle.

Collagen deposition during muscle regeneration following CTX and glycerol-induced injuries

Sirius red stain was used to visualize collagen deposition during regeneration. Both models showed an increased collagen deposition during regeneration (Fig. 2). Although collagen deposition was significantly higher in CTX-injured muscle than that in glycerol-injured muscle at both day 4 and day 7 ($P<0.05$) (Fig 3B), it decreased significantly in CTX-injured muscle compared to glycerol-injured muscle at day 14. On the other hand, collagen deposition increased with regeneration in glycerol-injured muscle.

Scanning electron microscopy

To confirm the effect of glycerol on muscle regeneration, glycerol-injured muscles were examined with SEM. Myofibers in the intact non-injured muscle were closely arranged and had polygonal shapes (Fig. 3C). Glycerol-injured muscle showed damage of the myofibers as well as the perimysial connective tissue at day 4 after injury, while the surviving myofibers were disorganized, rounded in shape and have smaller diameters than that in non-injured muscle, in addition, the extracellular spaces were increased (Fig. 3D). At day 7, small rounded myotubes with small spherical-shaped lipid droplets could be observed between them (Fig. 3E). At day 14,

the extracellular spaces between the myofibers decreased and being infiltrated with lipid droplets which were surrounded by a membrane and contain fat in amorphous state. Lipid droplets were connected with thin delicate reticular fibers (Fig. 3F).

Transmission electron microscopy (TEM)

Myofibers in the non-injured muscle had peripherally located nuclei under the basal lamina. The quiescent SC was located between the myofiber and the basal lamina. It was characterized by a large nucleus with condensed heterochromatin and little cytoplasm (Fig. 4A).

Four days after injury

The degenerated myofibers in CTX-injured muscle showed disintegrated cytoplasm with pyknotic nuclei while the basal lamina was intact (Fig. 4B). While the degenerated myofibers in glycerol-injured muscle showed amorphous cytoplasm with loss of myofibrils and disruption of the basal lamina (Fig. 4C). Mononuclear cells were either invade the degenerated myofibers or present in the extracellular space. Most of these cells were identified as macrophages; having ovoid nucleus and cell projections.

Seven days after injury

At day 7, large number of oval, spindle-shaped and elongated myoblasts could be observed in both injured muscles. They were identified by their large nuclei and distinct nucleoli. In addition, numerous myotubes could be observed, they had one or more central nuclei and few myofibrils. However, myoblasts detected in CTX-injured muscle were close together. Some myoblasts appeared as apparently fused (Fig. 4D). While

myoblasts in glycerol-injured muscle were separated from each other (Fig. 4E) with some adipocytes could be detected between myoblasts and myotubes.

Fourteen days after injury

At day 14, myotubes with central nuclei and densely backed myofibrils were detected in both injured muscles. In CTX-injured muscle, some myotubes showed both central and peripheral nuclei, indicating that they still in the process of maturation, while others showed peripheral elongated nuclei, indicating that they became matured (Fig. 4F). While in glycerol-injured muscle, all myotubes had central nuclei, indicating that they were still immature (Fig 4G).

Three dimensional structure of IMCT

To study alteration of the IMCT structure in response to either CTX- or glycerol-induced injuries, muscles were prepared by cell-maceration technique to study collagen fiber network after removing the cellular structures. Non-injured muscle showed endomysial connective tissue surrounded empty tubular structures that were occupied by myofibers before maceration, they were arranged in a honeycomb structure (Fig. 5A).

Four days after injury

At day 4, the CTX-injured muscle exhibited alteration of the honeycomb structure, endomysial tubes of varying sizes and shapes and an increased endomysial connective tissue, it appeared as wavy sheets (Fig. 5B) while the glycerol-injured muscle showed loss of the honeycomb structure, disruption of the endomysial connective tissue, irregular collagen fibers with mushy-shape and few number of endomysial tubes (Fig. 5C).

Seven days after injury

At day 7, the CTX-injured muscle restored the honeycomb appearance of the connective tissue, however, there were an increased perimysial and endomysial connective tissue with marked fibrosis around blood vessels (Fig. 5D), while the glycerol-injured muscle showed appearance of small number of endomysial tubes separated with spaces in between, these spaces comprise collagen fibril baskets remained after removal of adipocytes during preparation of samples (Fig. 5E).

Fourteen days after injury

The thickness of the endomysial sheath was decreased in CTX-injured muscle at day 14 (Fig. 5F), but still thicker than the normal level. On the other hand, the glycerol-injured muscle showed large number of endomysial tubes of varying diameters separated with collagen fibril baskets with thickened perimysial connective tissue (Fig. 5G).

TGF- β 1 treatment impaired muscle regeneration in glycerol-injured muscle

TGF- β 1 treatment impaired muscle regeneration at day 7 after injury as evidenced by decreased myotube density that is, a decrease in the number of myotubes containing central nuclei and expressing neonatal myosin. The percentage of myotubes was significantly lower (38.1%, $P < 0.05$) in the early treatment group than in the glycerol-injured group, while there was no significant difference in the percentage of myotubes (28.8%, $P > 0.05$) between the late treatment group and glycerol-injured group (Fig. 6).

Next, mRNA expression levels of the myogenic factors *MyoD* and *myogenin* were analyzed. TGF- β 1 treatment down-regulated the expression of both myogenic factors compared to the

levels in the glycerol-injured group. Moreover, the early treatment group showed lower expression levels than those in the late treatment group (Fig. 6C).

TGF- β 1 treatment induced extensive fibrosis in glycerol-injured muscle

Next, collagen deposition was assessed by collagen type I immunostaining. TGF- β 1 treatment induced greater collagen deposition than that in the glycerol-injured group: about 2.5-fold ($P < 0.05$) and 1.3-fold greater ($P > 0.05$) in the early and late treatment groups, respectively (Fig. 6). Collagen deposition was distributed in the endomysial spaces between myotubes.

TGF- β 1 treatment inhibited adipocyte accumulation in glycerol-injured muscle

TGF- β 1 treatment significantly decreased the ORO-positive area by about 88.3% and 59.3% in the early and late treatment groups, respectively (Fig. 6). The mRNA expression levels of the adipogenic factors *CEBP β* and *PPAR γ* were analyzed. TGF- β 1 treatment down-regulated the mRNA expression of both adipogenic transcriptional factors compared to the levels in the glycerol-injured group. Moreover, the early treatment group showed lower expression levels than those in the late treatment group (Fig. 6C).

TGF- β 1 treatment induced α -SMA immunostaining

TGF- β 1 treatment induced differentiation of myofibroblasts, α -SMA-positive cells, at day 4 after injury, whereas α -SMA-positive cells were not detected in the glycerol-injured group at the same time point (Fig. 7). TEM analysis was performed for confirmation. Many fibroblasts, characterized by large nuclei, spindle shape and well-developed rough endoplasmic reticulum in their cytoplasm, were detected in the glycerol-injured muscle. In contrast, many myofibroblasts,

characterized by larger size, multiple cytoplasmic processes and abundant mitochondria, were detected in the TGF- β 1-treated muscle (Fig. 7).

TGF- β 1 treatment impaired phagocytosis of necrotic myofibers

The area of residual necrosis, as shown by HE stain, at day 7 after injury was larger in the TGF- β 1-treated muscles than in the glycerol-injured muscles. Moreover, the area of residual necrosis was larger in the early TGF- β 1-treated muscles than in the late TGF- β -treated muscles. These results were confirmed by EBD uptake. Numerous EBD-positive myofibers were present in the TGF- β 1-treated muscles. In contrast, few EBD-positive myofibers were present in the glycerol-injured muscles (Fig. 8A). Macrophage infiltration was assessed at day 4 after injury by F4/80 immunostaining. As expected, the average number of F4/80-immunopositive cells was significantly smaller in the TGF- β 1-treated muscles than in the glycerol-injured muscles (Fig. 8B).

DISCUSSION

The aim of the present study is to compare muscle regeneration in mice following two different types of injuries; CTX and glycerol. In addition to investigate the changes of IMCT structure and their impact on muscle regeneration process in these injury models.

Injection of myotoxic agents into skeletal muscle is the most frequently used method to study muscle regeneration (Gayraud-Morel *et al.*, 2009). CTX-induced injury produces pathological changes which are similar to the pathological changes recorded previously in muscle dystrophies and inflammatory myopathies (Ramadasan-Nair *et al.*, 2014). Moreover, glycerol-induced injury produces degenerative changes comparable to those seen in Duchenne muscular dystrophy (Kawai *et al.*, 1990) and dysferlinopathy (Ho *et al.*, 2004). Therefore, studying muscle fibrosis in normal, non-dystrophic, mice will help to understand the different mechanisms, cells and factors responsible for fibrosis development (Pessina *et al.*, 2014), and consequently help to develop new therapeutics to prevent muscle fibrosis.

Different regeneration outcomes in response to CTX- and glycerol-induced injuries

Muscle regeneration started at day 7 after injury in both injury models, however, the morphometrical analysis showed better regeneration in CTX-injured muscle than in glycerol-injured one which indicated by higher number of regenerated myotubes, larger diameters and better organization than in glycerol-injured muscle at day 14 after injury. Similar results were reported in a previous study (Lukjanenko *et al.*, 2013). The difference in regeneration between the two injury models could be attributed to their different effects on muscle. Sanes (2003) showed that the outcome of muscle regeneration following injury depends on the degree of disruption to the basal lamina. Ultrastructural analysis of injured muscles revealed differences

between degenerated myofibers in the two injured muscles; CTX-injured muscle showed disintegrated cytoplasm, pyknotic nuclei and intact basal lamina while glycerol-injured muscle showed amorphous cytoplasm and disruption of the basal lamina. The present results are consistent with those of the previous studies which reported that CTX induces myofiber necrosis and degeneration leaving intact basal lamina (Harris, 2003), while glycerol disrupts myofiber cell membrane (Kawai *et al.*, 1990). The present SEM findings confirm the before mentioned results, the endomysial tubes were preserved after CTX-induced injury while they were destructed after glycerol-induced injury. The basal lamina surrounding SCs plays an essential role in muscle regeneration; contact of SCs with undamaged basal lamina provides guidance signals for SCs migration (Kharraz *et al.*, 2013). In addition, collagen VI accumulation was increased at early stages after CTX-induced injury, it regulates SC activity both *in vitro* and *in vivo* (Urciuolo *et al.*, 2013). These results further support the current results.

The present study revealed adipocyte infiltration following glycerol-induced injury, which indicates impaired regeneration, but no adipocyte infiltration could be detected following CTX-induced injury. This is in parallel with the results of Uezumi *et al.* (2010) who concluded that muscle environment after day 4 of injury inhibits adipogenesis in CTX-injured muscles, on the contrary, it facilitates adipogenesis in glycerol-injured muscles. It was reported that glycerol affects macrophage function negatively resulting in impaired regeneration with fat deposition (Pisani *et al.*, 2010). Adipocyte infiltration was reported following CTX-induced injury in old mice but not in young mice (Liu *et al.*, 2012). Moreover, mouse strain plays a role in adipocyte deposition following CTX injection; no adipocyte was detected in C57BL/6 mice either after single or repeated CTX injections, while adipocyte accumulation was detected after repeated CTX injections, in C3H/HeN, BALB/c and DBA/2 mice strains, but could not be detected in any

examined mice strain following single CTX injection (Fukada *et al.*, 2010), these results support the results of the current study.

Changes in IMCT affected muscle regeneration

Proper muscle regeneration depends largely on cell-cell communications and extracellular matrix (ECM) composition (Fiore *et al.*, 2016). Changes in the morphology of the perimysial collagen fibers alters both the mechanical properties of ECM as well as the muscle function (Zhao *et al.*, 2008). CTX-injured muscle showed an increased IMCT at the levels of perimysial and endomysial connective tissue at day 7 after injury by SEM-maceration, moreover, the present morphometrical analysis revealed an increased collagen deposition in CTX-injured muscle during the early stages of regeneration, reached peak at day 7 then decreased at the later stages. The present results are in line with the results of Pessina *et al.* (2014) who reported mild and transient fibrosis following CTX injury and the results of Fiore *et al.* (2016) who reported highest collagen deposition at day 7 after notexin injury due to fibroadipogenic progenitors proliferation. It is worth mentioning that transitional ECM maintains SC proliferation through enhancing of DNA synthesis (Calve *et al.*, 2010). Efficient regeneration in CTX-injured muscle was correlated with the transient collagen deposition at early stage of regeneration. This could be explained in light of the previous observations by Murphy *et al.* (2011) who reported that interactions between fibroblasts and SCs are essential for muscle regeneration; positive fibroblast-SCs interactions in early stages promote muscle regeneration followed by suppression of fibroblasts activity at later stages to decrease muscle fibrosis.

TGF- β 1 treatment impaired muscle regeneration in glycerol-injured muscle

TGF- β 1, a potent profibrotic cytokine, is associated with the pathogenesis of fibrosis in many tissues and muscular dystrophies (Prisk and Huard, 2003). A recent *in vivo* study demonstrated fibrotic effect of exogenous TGF- β 1 treatment on wild-type muscles; injection of TGF- β 1 alone did not induce fibrosis, but when it was combined with CTX injury, significant fibrosis was induced (Pessina *et al.*, 2014). The present results have shown that CTX induced transient endomysial fibrosis while endomysial fibrosis increased at day 14 after glycerol-induced injury. As a result, it is hypothesized that combination of glycerol and TGF- β 1 might increase fibrosis at early regeneration stage. Therefore, the effects of exogenous TGF- β 1 treatment at different time points on muscle regeneration and adipogenesis in glycerol-injured muscles were investigated. Early TGF- β 1 treatment significantly reduced myotube density compared to that in the glycerol-injured muscles. Moreover, TGF- β 1 treatment down-regulated mRNA expression of the myogenic factors *MyoD* and *myogenin*. Similar results were obtained previously in an *in vitro* study (Lamarche *et al.*, 2015; Li *et al.*, 2008). Inhibition of *MyoD* and *myogenin* mRNA expression indicates impairment of SC proliferation and differentiation (Zhang *et al.*, 2010). TGF- β 1 delays differentiation of C2C12 myoblasts (Schabort *et al.*, 2009; Wicik *et al.*, 2010) through down-regulation of the expression of gene transcription factors as well as the expression of genes encoding proteins involved in cell differentiation (Wicik *et al.*, 2010). Furthermore, immunoneutralization of TGF- β 1 improves muscle regeneration (Zimowska *et al.*, 2009). The decreased levels of *MyoD* and *myogenin* mRNA expression together with the reduction in myotube density in the TGF- β 1-treated group could be explained by the notion that TGF- β 1 impairs muscle regeneration through inhibition of SC proliferation and differentiation (Cohn *et al.*, 2007).

TGF- β 1 treatment induced extensive fibrosis and myofibroblasts differentiation

Collagen deposition was significantly greater in the early treatment group than in the glycerol-injured group as well as in the late treatment group. These results are in consistent with the results of a recent study showing that exogenous TGF- β 1 treatment promotes fibrous tissue accumulation in injured muscle (Pessina *et al.*, 2015). Moreover, the increased deposition of collagen type-1 in the interstitial space of the injured muscle negatively affects muscle regeneration (Desguerre *et al.*, 2012) which provide further explanation of the impaired regeneration following TGF- β 1 treatment. On the other hand, TGF- β 1 has the potential to up-regulate α -SMA protein synthesis and accumulation of myofibroblasts. These findings are supported by the results obtained by Malmstrom *et al.* (2004) showing that TGF- β 1 induces myofibroblast differentiation through α -SMA expression.

TGF- β 1 treatment suppressed adipogenesis in glycerol-injured muscle

Early TGF- β 1 treatment suppressed adipogenesis and down-regulated expression of the adipogenic transcription factors *C/EBP β* and *PPAR γ* in the glycerol-injured muscle. These results are in agreement with results of previous *in vitro* studies showing that TGF- β 1 inhibits adipocyte differentiation (Choy and Derynck, 2003; Lu *et al.*, 2013) through targeting the adipocyte transcription factors *C/EBP β* and *C/EBP δ* (Choy and Derynck, 2003). Moreover, TGF- β 1 significantly suppressed the expression of *C/EBP α* and *PPAR γ* (Tsurutani *et al.*, 2011).

TGF- β 1 treatment impaired clearance of necrotic myofibers

Efficient regeneration requires migration of macrophages to the injured site to phagocytose the necrotic myofibers (Tidball and Villalta, 2010). Therefore, residual necrosis can be used as an

indirect evaluation of macrophage function (Wang *et al.*, 2014). TGF- β 1-treated muscles have larger areas of residual necrosis than those in glycerol-injured muscles. Moreover, numerous EBD-positive myofibers were found in TGF- β 1-treated muscles. These results are consistent with results obtained by Accornero *et al.* (2014) showing that TGF- β 1 increases myofiber membrane fragility through a reactive oxygen species-dependant mechanism, resulting in greater myofiber necrosis. A larger number of necrotic myofibers in injured muscles at day 7 after injury suggests impaired phagocytic function of macrophages in removal of necrotic debris (Zhao *et al.*, 2016). To further confirm this hypothesis, macrophage infiltration was evaluated by using F4/80 immunostaining, a marker for macrophages. TGF- β 1 treatment significantly reduced the population of macrophages at day 4 compared to that in the glycerol-injured muscles. The results obtained by Werner *et al.* (2000) that showed TGF- β 1 inhibits macrophage activation support the present results showing a larger necrotic area in TGF- β 1-treated muscles associated with a significantly smaller population of macrophages. Moreover, the results of the previous study showed that impaired macrophage function negatively affects muscle regeneration with development of fibrosis (Cheng *et al.*, 2008), further supporting the results of the current study showing significantly lower myotube density with significantly greater collagen deposition following early TGF- β 1 treatment.

In conclusion, the present results suggest that changes in IMCT play an important role in controlling the efficiency of muscle regeneration following injury. Moreover, the stronger inhibitory effects of TGF- β 1 at early treatment than those of late treatment during regeneration in glycerol-injured muscle suggest that TGF- β 1 has a more potent effect on the early stage of muscle regeneration and adipogenesis. Moreover, combination of TGF- β 1 with glycerol-induced

injury provides a simple model to enhance muscle fibrosis for future studies. Further studies are needed to verify its application to hasten fibrosis in hind limbs of young *mdx* mouse.

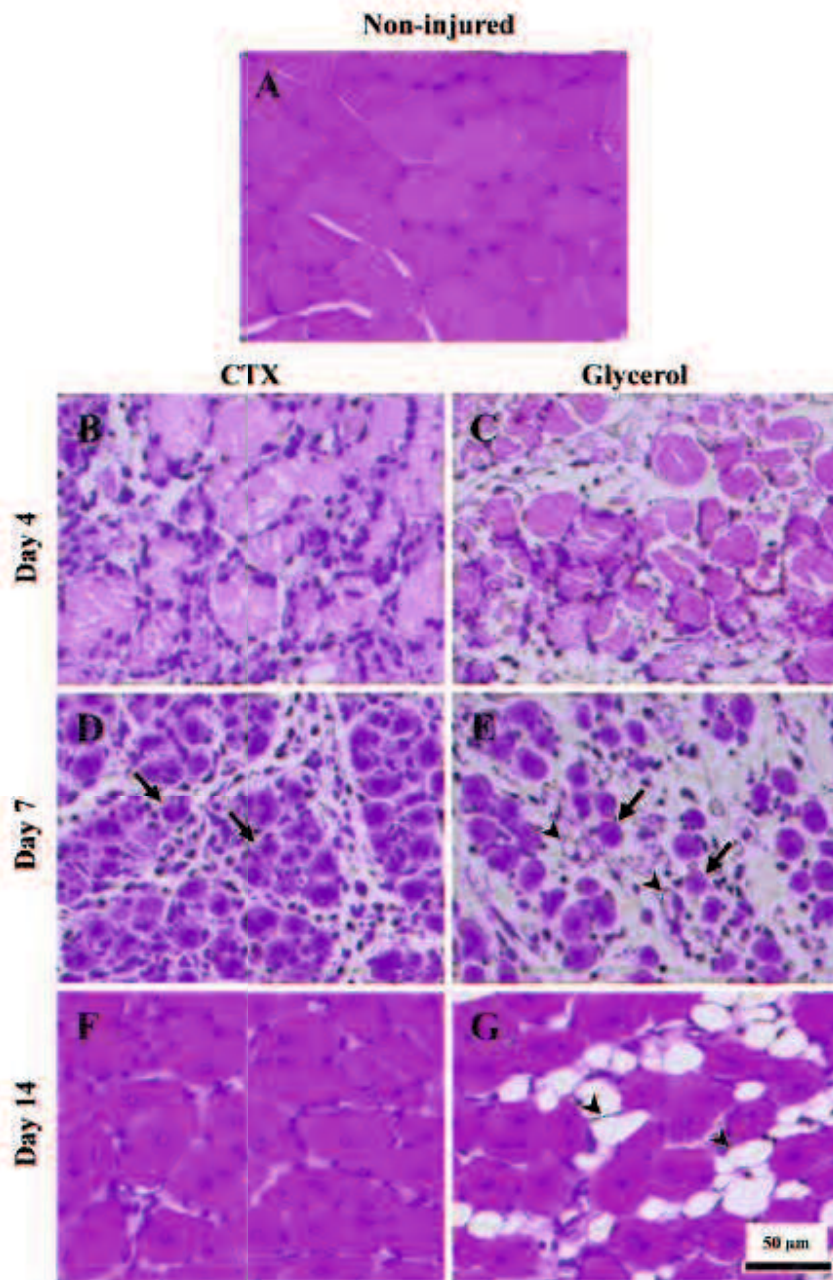


Figure 1. Morphological changes of TA muscle following either CTX- or glycerol-induced injuries. (A) Non-injured muscles, (B, D, F) CTX-injured muscles and (C, E, G) glycerol-injured muscles at 4, 7 and 14 days after injury were stained with HE stain. Regenerating myotubes with central nuclei (arrows) appeared in both models at day 7, while adipocytes (arrowheads) could be detected only in glycerol model.

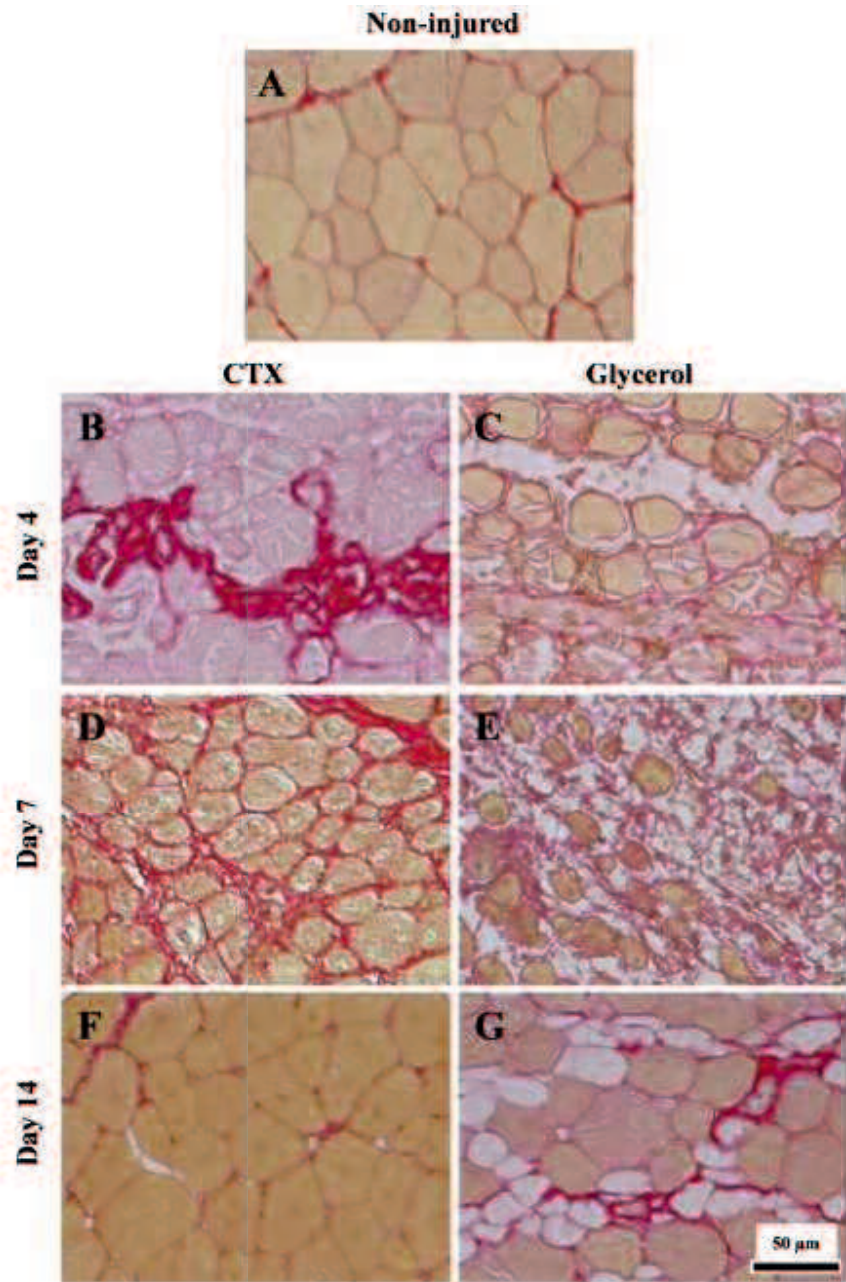


Figure 2. Histochemical analysis of collagen fiber in TA muscle following either CTX- or glycerol-induced injuries. (A) Non-injured muscles, (B, D, F) CTX-injured muscles and (C, E, G) glycerol-injured muscles at 4, 7 and 14 days after injury were stained with Sirius red stain.

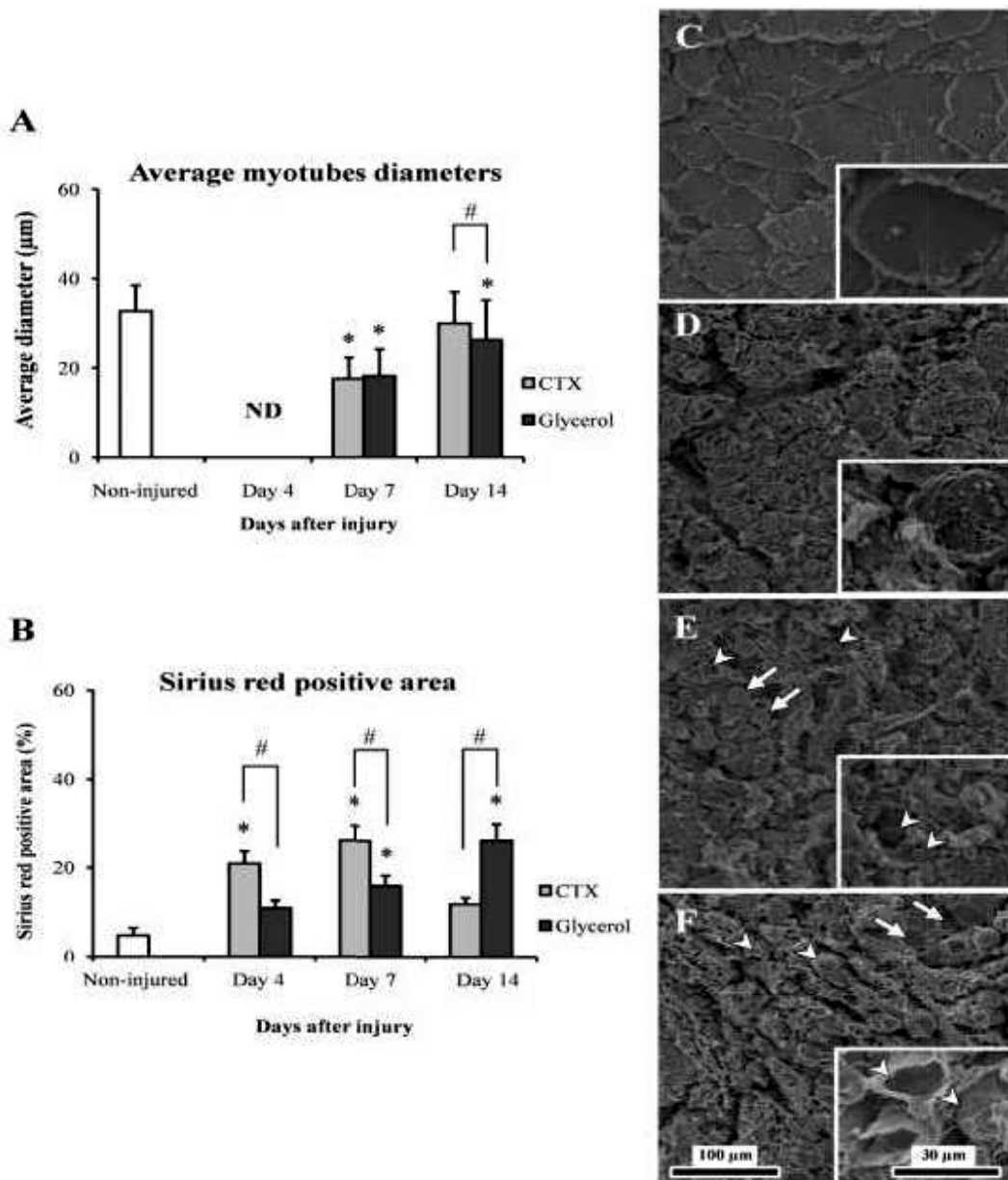


Figure 3. (A) Changes in myotubes diameters after CTX- or glycerol-induced injuries. (B) Quantification of Sirius red positive area. (C) SEM micrograph of non-injured and (D, E, F) glycerol-injured TA muscle at 4, 7 and 14 days post injury. Inset showing higher magnification. Regenerating myotubes (arrows) were infiltrated with adipocytes (arrowheads). Data are expressed as means \pm SD, (ND, not detected, * indicates significant difference from non-injured muscle, # indicates significant difference between two models, $P < 0.05$).

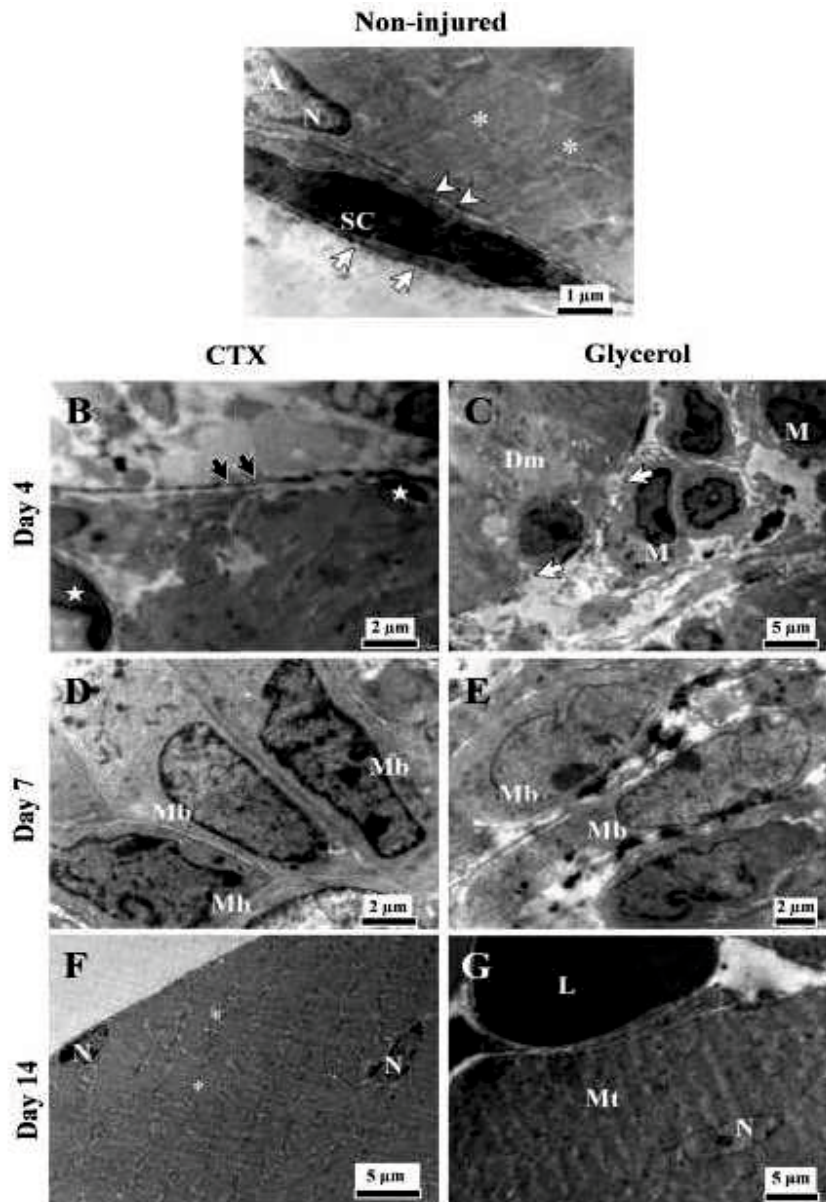


Figure 4. TEM micrographs of muscle regeneration. (A) Non-injured myofiber with peripheral nucleus (N), normal myofibrils (asterisks) and satellite cell (Sc) was located under basal lamina (arrows) and separated from myofiber by plasma membrane (arrowheads), (B, C) degenerated myofiber (Dm) at day 4 with disintegrated cytoplasm and pyknotic nucleus (star), intact basal lamina (black arrows) in CTX-injured muscle, and macrophages (M), disrupted basal lamina (white arrows) in glycerol-injured muscle, (D, E) regenerative changes at day 7 showed myoblasts (Mb) (F) myotube with central and peripheral nuclei (N), normal myofibrils (asterisk), (G) immature myotube (Mt) with central nucleus (N) and lipid droplet (L).

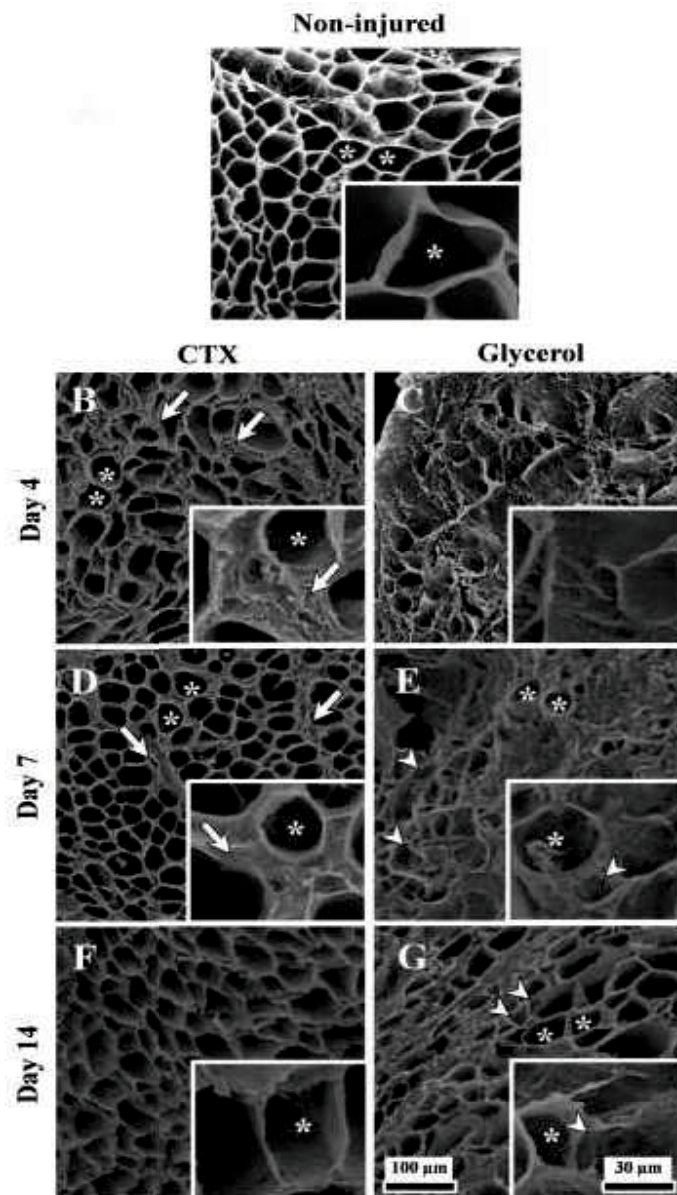


Figure 5. Structural changes of the IMCT of macerated TA muscle following either CTX- or glycerol-induced injuries. (A) Non-injured, (B, D, F) CTX-injured muscles and (C, E, G) glycerol-injured muscles at 4, 7, 10 and 14 days post injection. Endomysial collagen (arrows) surrounding endomysial tubes (asterisks). Collagen baskets of adipocytes (arrow heads) could be observed in glycerol-injured model but not in CTX- injured model. Inset showing higher magnification.

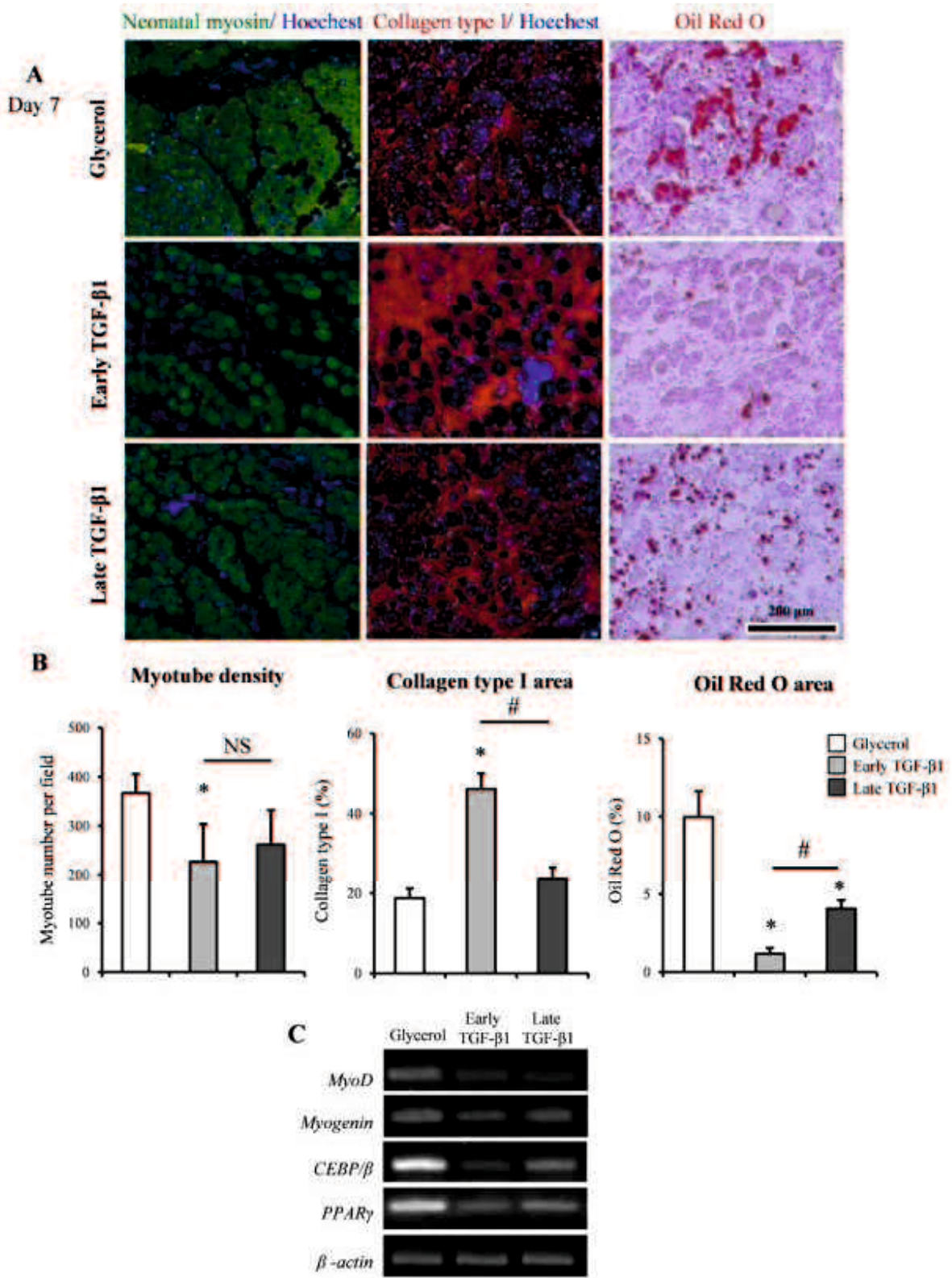


Figure 6. TGF- β 1 treatment impaired muscle regeneration, increased endomysial fibrosis, and inhibited adipogenesis in glycerol-injured muscles. (A) Muscle sections from the glycerol-injured, early TGF- β 1 treatment and late TGF- β 1 treatment groups at day 7 after injury were immunostained with anti-neonatal myosin (green) and anti-collagen type I (red) with nuclei stained with Hoechst (blue) and stained with Oil Red O stain for detection of adipocytes. (B) TGF- β 1 treatment decreased the myotube density, increased collagen type I area, and decreased the Oil Red O-positive area. (C) Semi-quantitative RT-PCR analysis of mRNA expression of the myogenic factors *MyoD* and *Myogenin* and the adipogenic factors *C/EBP β* and *PPAR γ* in glycerol-injured, early TGF- β 1 treatment and late TGF- β 1 treatment groups at day 7 after injury.* indicates a significant difference from glycerol-injured muscle, # indicates a significant difference between early and late treatment groups, and NS indicates non-significance ($P < 0.05$).

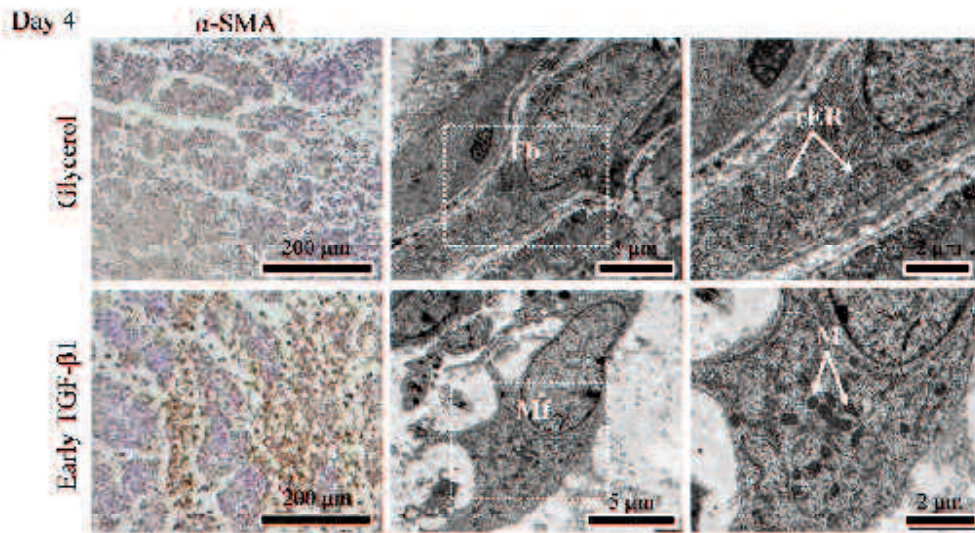


Figure 7. TGF- β 1 treatment induced α -SMA protein expression and myofibroblasts accumulation. Fibroblasts (Fb) were detected in glycerol-injured muscle and myofibroblasts (Mf) were detected in early TGF- β 1-treated muscle. Higher magnification of the dotted rectangle showing abundant rough endoplasmic reticulum (rER) and abundant mitochondria (M).

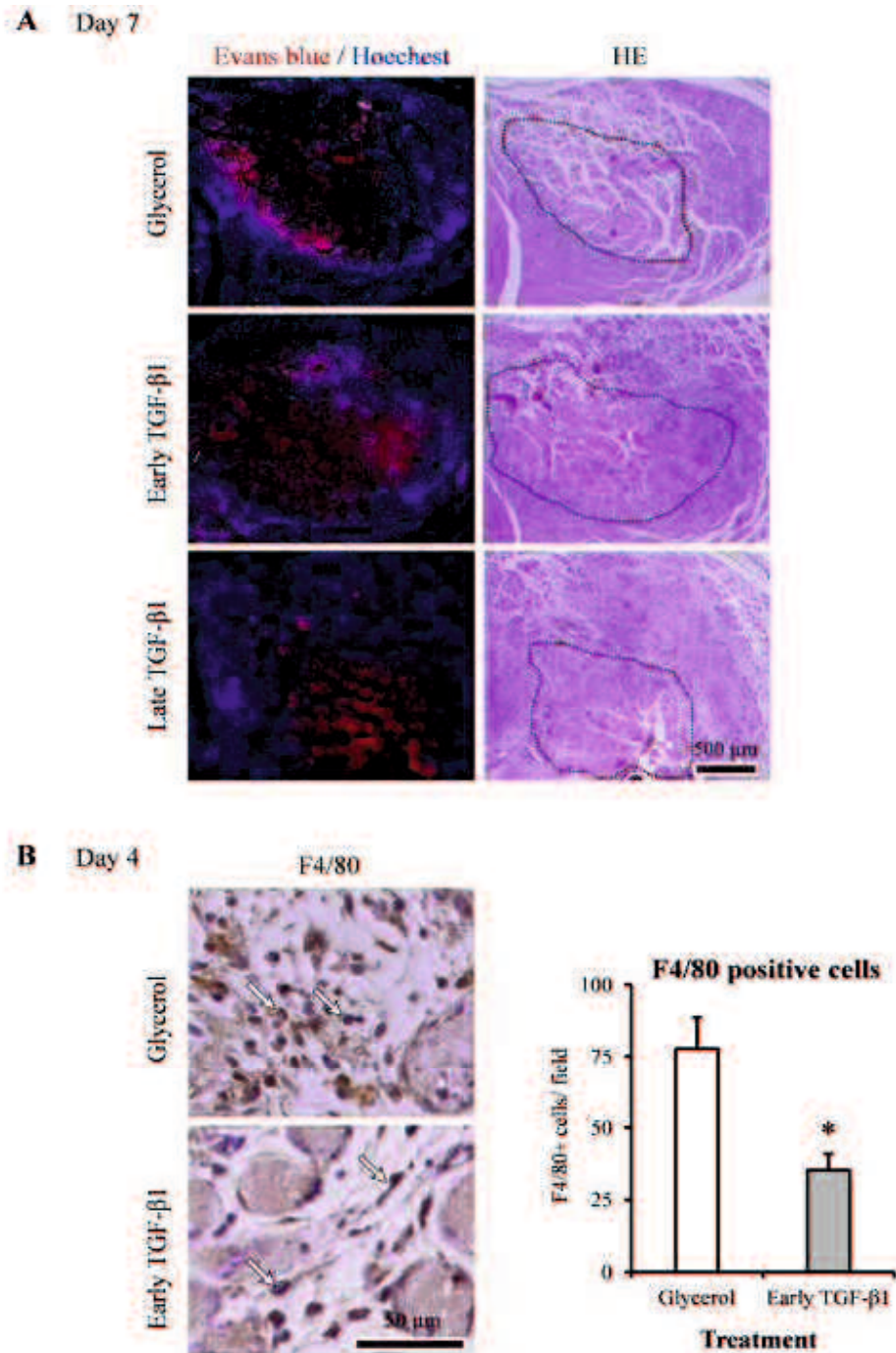


Figure 8. TGF-β1 treatment impaired clearance of necrotic myofibers. (A) Light micrographs showing Evans blue dye-positive myofibers, nuclei stained with Hoechst and the same areas stained with HE stain. Dotted line indicates residual necrosis area. (B) TGF-β1 treatment impaired macrophage infiltration at day 4 after glycerol injury. F4/80-positive macrophages were quantified. * indicates a significant difference from glycerol-injured muscle ($P < 0.05$).

Table 1 Primer sequences for semi-quantitative polymerase chain reaction

Gene	Forward primer	Reverse primer	Product size (bp)
<i>MyoD</i>	5'-GCAGAATGGCTACGACACC-3'	5'-TGGGTTCCCTGTTCTGTG-3'	222
<i>Myogenin</i>	5'-TGAATGCAACTCCCACAG-3'	5'-CGTAAGGGAGTCCAGATTGT-3'	92
<i>C/EBPβ</i>	5'-GCAAGAGCCGCGACAAG-3'	5'-GGCTCGGGCAGCTGCTT-3'	153
<i>PPARγ</i>	5'-TGCACTGCCTATGAGCACTTCA-3'	5'-CATCACGGAGAGGTCCACAGA-3'	102
<i>β-actin</i>	5'-TCATCACTATTGGCAACGAGC-3'	5'-AACAGTCCGCCTAGAAGCAC-3'	400

Chapter 2

Early ultrastructural events of muscle damage following cardiotoxin and glycerol injury

ABSTRACT

The present study describes the early changes of skeletal muscle damage in response to two types of injuries, cardiotoxin (CTX) and glycerol, by light microscopy and transmission electron microscopy. Tibialis anterior (TA) muscles were injured either with CTX or glycerol and the injured muscles were taken at intervals starting from 1 h up to 4 days after injury and subjected to both histological and ultrastructural analyses. Injury by CTX induced mitochondrial accumulation, swelling and lysis, while injury by glycerol induced vesicles accumulation with focal disruption of the basal lamina, which indicates that the two injuries damage myofibers by different mechanisms. Moreover, earlier inflammatory reaction and in larger numbers was noticed after CTX-induced injury than after glycerol-induced injury. Morphometric analysis revealed that satellite cells (SCs) activation started at 6 h after both injuries, as indicated by an increase in the length and cytoplasmic-to-nuclear ratio. However, CTX-injured muscles showed significantly longer SCs with a higher cytoplasmic-to-nuclear ratio than those in glycerol-injured muscles at day 4. In conclusion, the present findings demonstrated that CTX and glycerol induced myofiber damage through different mechanisms; CTX affected myofiber mitochondria, while glycerol affected the myofiber cell membrane and altered osmosis. In addition, CTX-induced injury recruited earlier and more extensive inflammatory cellular infiltration than did glycerol-induced injury. This study sheds light on the early events following skeletal muscle injury induced by CTX and glycerol for the first time.

INTRODUCTION

Skeletal muscle regenerates in response to various types of injury and disease (Yan *et al.*, 2003) and the healing process includes three phases: the destruction phase, in which myofibers undergo degeneration with invasion of inflammatory cells, followed by the repair phase, in which necrosed tissue is removed, myofibers start regeneration with scar formation, and finally the remodeling phase, in which the regenerated myofibers mature with reorganization of scar tissue (Jarvinen *et al.*, 2005). The efficiency of muscle repair is affected by the severity of damage and the interactions between muscle and the recruited inflammatory cells (Karalaki *et al.*, 2009).

It is necessary to develop an experimental animal model to study muscle regeneration in a controlled and reproducible manner (Horie *et al.*, 2014). Therefore, a variety of experimental injury models have been used to investigate muscle regeneration. These models are chemical models as injection of barium chloride (Hardy *et al.*, 2016), bupivacaine (Oz Gergin *et al.*, 2015), myotoxic agent as CTX (Hardy *et al.*, 2016), and glycerol (Pagano *et al.*, 2015) and mechanical models as freezing injury (Hardy *et al.*, 2016). However, the nature of the injury model influences the cellular events that occur in response to the injury (Musarò, 2014).

Intramuscular injection of CTX induces similar degenerative changes to those in muscular dystrophies and inflammatory myopathies (Ramadasan-Nair *et al.*, 2014). While injection of glycerol is a novel model to induce muscle adipogenesis (Pisani *et al.*, 2010; Uezumi *et al.*, 2010), it induces similar degenerative changes to those in patients with Duchenne muscular dystrophy (Kawai *et al.*, 1990). Therefore, CTX and glycerol injury models were chosen for this study.

Although using specific markers is a valuable method to detect different cell types, electron microscopy provides better results based on the structural characteristics of the cells. Therefore,

electron microscopy is a useful tool to study muscle pathologies as myopathies and results of electron microscopy are useful to understand the pathological mechanisms of various muscular diseases and are useful as a guide for genetics analysis (Fernandez *et al.*, 2005). We have reported that muscle regeneration is more efficient after CTX-induced injury than after glycerol-induced injury, moreover, glycerol induces adipocyte infiltration with progressive fibrosis (Mahdy *et al.*, 2015). Hardy *et al.* (2016) reported that the outcome of the regeneration process is influenced by the early stage after injury. Previous studies investigated the ultrastructural changes following glycerol-induced injury in rabbits (Kawai *et al.*, 1990) and following injury induced by injection of 3 local anesthetics, levobupivacaine, bupivacaine and ropivacaine, in rat skeletal muscles (Oz Gergin *et al.*, 2015). The present study compared the early changes in response to injury induced by injection of CTX and glycerol by light microscopy and transmission electron microscopy (TEM) to investigate the different events that take place following these injuries and also to determine the relationship between these events and the difference in regeneration between the two injury models. The present results showed that the targets of injury and the mechanisms by which muscle damage is induced are different in the two models. In addition, the time sequence and degree of immune cell infiltration were also different. To the best of my knowledge, this is the first study in which early events following skeletal muscle injury induced by CTX and glycerol were compared.

MATERIAL AND METHODS

Animals

Normal male C3H/HeN mice (CLEA Japan, Tokyo, Japan) ($n=36$) were used in the current study.

Induction of muscle injury in vivo

Muscle injury was done after intraperitoneal anaesthesia as previously described in Chapter 1. Mice were sacrificed by cervical dislocation and injured muscles were collected at different time points (1, 6, 12, 24 h and 4 days post injury). The collected samples were divided into two parts for histological analysis and transmission electron microscopy. The opposite non-injured muscles were collected as controls.

Histological assessment of muscle injury

Paraffin sections were prepared as previously described in Chapter 1 and stained with HE for histological evaluation. Representative images were photographed with a digital camera (DP71, Olympus) attached to a microscope (Olympus IX71).

Transmission electron microscopy

Muscle specimens were prepared for TEM as previously described in Chapter 1.

Morphometric analysis

For morphometric analysis, five representative blocks/animal ($n = 3$ animals/time point) were chosen for ultrathin sectioning. About 3-5 ultrathin sections/block were analyzed and

photographed. 50 images of SCs/time point were used for morphometric measurements using Image-J software (v1.46r, National Institutes of Health, Maryland, USA). To quantitatively follow SC activation, SC length was measured and the nuclear-cytoplasmic ratio was calculated (Gregory and Mars, 2004).

Immunohistochemistry

For detection of macrophages, rabbit anti-F4/80 antibody (1:500, sc-26643-R; Santa Cruz) was used as previously described in Chapter 1.

Statistical analysis

Statistical analysis was carried out as previously described in Chapter 1.

RESULTS

Time courses of muscle degeneration following CTX and glycerol injury

Light microscopy and TEM were used to evaluate the different histopathological changes in muscles injured by CTX and glycerol. Non-injured muscle exhibited closely arranged, polygonal-shaped, myofibers with peripheral nuclei. Each myofiber was surrounded by endomysium while fascicle, a group of myofibers, was surrounded by perimysium (Fig. 1A and 1B). Ultrastructurally, myofibrils were tightly arranged with normally displayed mitochondria in between. The nucleus was located under the basal lamina, while SCs were located between the basal lamina and plasma membrane (Fig. 1C and 1D). Both the outer basal lamina and the inner plasma membrane were intact (Fig. 1E). Quiescent SCs were characterized by a large nucleus with condensed heterochromatin (Fig. 1D). Moreover, Z-lines were normally arranged (Fig. 1F).

One hour after injury

Both injured muscles displayed disruption of myofiber arrangement, variation in myofiber sizes and widening of the interstitial space between myofibers (Fig. 2A and 2B). Most myofibers were swollen, while others were completely lost, leaving only an empty outer membrane, they appeared as “ghost” myofibers. Ultrastructurally, disarrangement of myofibrils was clear in both injury types. CTX-injured muscles showed an accumulation of swollen mitochondria in the subsarcolemmal region while the nuclear chromatin was clumped along the nuclear membrane (Fig. 2C). In contrast, glycerol-injured muscles showed an accumulation of small vesicles, about 40-120 nm in diameter, in the subsarcolemmal region and between myofibrils while the nuclear chromatin was condensed and fragmented. Focal disruption of the basal lamina was also

observed (Fig. 2D). On the other hand, loss of Z-lines was clear in both CTX-injured muscles and glycerol-injured muscles (Fig. 2E and 2F).

Six hours after injury

In the CTX-injured muscles, numerous mononuclear cellular infiltrations were detected in the interstitial space between myofibers with little cellular infiltration of myofibers (Fig. 3A). In contrast, individual mononuclear cellular infiltration was detected between myofibers in the glycerol-injured muscles. Hypercontracted myofibers, i.e. myofibers with partial loss of the cytoplasm leaving a gap between the cytoplasm and outer membrane, were also observed in the glycerol-injured muscles (Fig. 3B). Ultrastructurally, mononuclear cells invading the CTX-injured muscles were identified as neutrophils by their dense multi-lobed nuclei and granular cytoplasm. They were located in the interstitial space between myofibers while some myofibers were also invaded by neutrophils (Fig. 3C). In contrast, sporadic neutrophils were observed in glycerol-injured muscles. They were located in the interstitial space between myofibers only. Furthermore, myofiber hypercontraction was indicated by an undulating basal lamina which was separated from the myofiber with a gap (Fig. 3D). In addition, vesicles were still detected in the subsarcolemmal region and between myofibrils.

Twelve hours after injury

Numerous myofibers were invaded by mononuclear cellular infiltration in CTX-injured muscles (Fig. 4A) while mononuclear cellular infiltration was present in the interstitial space between myofibers in glycerol-injured muscles (Fig. 4B). Ultrastructurally,

neutrophils invaded many myofibers in CTX-injured muscles (Fig. 4C). Myofiber mitochondria were dilated and had an electron-lucent matrix with irregular and reduced number of cristae (Fig. 4E). Neutrophil infiltration in glycerol-injured muscles was only in the interstitial space between myofibers (Fig. 4D). Moreover, the plasma membrane was thickened in some areas and was discontinuous in other areas with vesicles accumulated underneath as well as between myofibrils (Fig. 4F).

Twenty four hours after injury

The number of myofibers invaded with mononuclear cellular infiltration was markedly increased in CTX-injured muscles (Fig. 5A). In contrast, only a few myofibers were invaded with mononuclear cellular infiltration in glycerol-injured muscles (Fig. 5B). Ultrastructurally, myofibers in CTX-injured muscles were invaded by numerous macrophages which identified by the prominent single euchromatic nucleus with nucleolus and cytoplasmic processes, and a few neutrophils (Fig. 5C). Eosinophils could be detected at this time point in CTX-injured muscles; they were identified by their characteristic electron-dense granules and less dense rods with peripherally located nuclear chromatin (Fig. 5E). On the other hand, myofibers in glycerol-injured muscles were invaded by neutrophils only (Fig. 5D). Furthermore, monocytes were detected at this time point in glycerol-injured muscles; they were distinguished by their characteristic kidney-shaped nucleus (Fig. 5F). Few vesicles could be detected at this time point in glycerol-injured muscles.

Four days after injury

Massive cellular infiltration, either invaded the degenerated myofibers or were located in the extracellular spaces, was detected in CTX-injured muscles. The number of cellular infiltration appeared to be larger in the CTX-injured muscles than in the glycerol-injured muscles. Ultrastructurally, the cellular infiltration in both injured muscles was mainly macrophages. The length of SCs increased markedly in both injured muscles, with appearance of some myofibrils, which suggest conversion of SCs to myoblasts (Fig. 6C and 6D). Many fibroblasts were present in the extracellular matrix in CTX-injured muscles. They were identified by their fusiform shape, elongated nucleus and well-developed rough endoplasmic reticulum (rER) in the cytoplasm which indicates active protein synthesis (Fig. 6E). On the other hand, many preadipocytes, identified by numerous rER and lipid globules, were detected in glycerol-injured muscles (Fig. 6F). Furthermore, no vesicles could be detected at this time point in glycerol-injured muscles.

Morphometric analysis of SCs

To quantitatively follow the SC activation following injury, the SC length was measured and the nuclear-cytoplasmic ratio was calculated. The quiescent SC, in non-injured muscle, was about $6.9 \pm 0.8 \mu\text{m}$ in length, while the nucleus occupied about 61.6% of the total area. At 6 h, early SCs activation was indicated by slight increase in both the length and cytoplasm-to-nucleus ratio compared to these in the quiescent condition. The increase in length and ratio continued for up to 24 h, but there was no significant difference in SC length or cytoplasm-to-nucleus ratio between CTX-injured muscles and glycerol-injured muscles at these time points. At day 4, the SCs length had increased significantly in both injured muscles compared to that in the quiescent condition. The SCs were significantly longer in the CTX-injured muscles than in the glycerol-injured

muscles while the nucleus occupied about 15.1% and 23.7% of SC total area in the CTX-injured muscles and glycerol-injured muscles, respectively ($P < 0.05$) (Fig. 7A and 7B).

Immunohistochemical detection of macrophages

Muscle sections were immunostained with anti-F4/80 antibody to detect macrophage infiltration at day 4 after injury. Massive macrophage infiltration was present in CTX-injured muscles compared to that in glycerol-injured muscles (Fig. 8A and 8B). Counting the number of F4/80-positive cells/field revealed a significantly higher content of macrophages in CTX-injured muscles, about 2.6-fold higher than that in glycerol-injured muscles ($P < 0.05$) (Fig. 8C).

DISCUSSION

Our previous study revealed significant differences in regeneration after muscle injury by CTX and glycerol. We reported an efficient regeneration with transient fibrosis and lack of adipocyte infiltration after CTX-induced injury and an impaired regeneration with progressive fibrosis and adipocyte infiltration after glycerol-induced injury (Mahdy *et al.*, 2015). Recently, a study by Hardy *et al.* (2016) reported that the outcome of regeneration is affected by the early phase after injury. Therefore, further understanding of the different cell populations during the inflammatory phase, the factors regulating their function, and the timing of their activity will help to develop therapies for acute injuries as well as myopathies associated with chronic inflammatory responses (Kharraz *et al.*, 2013). Thus, the present study was carried out to investigate the early changes following CTX- and glycerol-induced injury by using light microscopy and TEM and to determine the relationship between these changes and the difference in regeneration between the two injuries.

CTX and glycerol have different mechanisms of myofiber damage

CTX-induced injury caused mitochondrial swelling 1 h after injury as was reported after exposure to CTX *in vitro* (Wang and Wu, 2005). Moreover, lysis of the mitochondrial matrix and disruption of cristae were noted at 12 h after CTX-induced injury. It was concluded that CTX induced damage of myocytes through mitochondrial swelling and fragmentation (Wang and Wu, 2005). Moreover, mitochondrial dysfunction was reported in CTX-injured muscle as indicated by loss of enzyme histochemistry signal of mitochondrial activities and altered cristae observed by TEM (Ramadasan-Nair *et al.*, 2014). Taken together, these results suggest that myofiber mitochondria are the initial targets of CTX injury.

The results of the current study revealed that glycerol-induced injury caused myofiber hypercontraction with accumulation of small vesicles under the basal lamina and with focal disruption of the basal lamina and alteration of the plasma membrane. Similar findings were reported in rabbits following glycerol injection, and it was concluded that glycerol damages the myofiber cell membrane (Kawai *et al.*, 1990), resulting in increased permeability and subsequently cell death (Charge and Rudnicki, 2004). On the other hand, transient exposure to glycerol results in myofiber shrinkage (Demonbreun *et al.*, 2014) due to movement of water from the myofiber sarcoplasm toward the hypertonic extracellular solution (Dulhunty *et al.*, 1973). Previous studies reported disruption of plasma membrane, as shown by TEM, in calcium ionophore-treated rat muscles (Yoshimura *et al.*, 1986) and toxin-injured mice muscle (Baldo *et al.*, 2010). It is associated with vesicles accumulation under the disrupted membrane (Bansal *et al.*, 2003). Vesicle accumulation and fusion with each other or with the plasma membrane provides additional membrane for resealing the disrupted plasma membrane (Bansal and Campbell, 2004). On the other hand, exposure of myofibers to osmotic shock due to introduction and removal of glycerol resulted in vacuolation of T-tubules (Apostol *et al.*, 2009; Demonbreun *et al.*, 2014). Furthermore, plasma membrane defects and vesicles accumulation under the disrupted membrane were reported in non-necrotic myofibers from patients with dysferlinopathy (Selcen *et al.*, 2001) and dysferlin-null mice (Bansal *et al.*, 2003). Interestingly, Demonbreun *et al.* (2014) reported a similarity between damage induced by glycerol injection in young animals and dystrophic phenotype in old animals, which suggests a similar mechanism is involved in both glycerol-injury and dysferlinopathy. Taken together, the previous findings suggest that glycerol induced alteration in the myofiber osmotic property through damaging of the myofiber cell membrane.

Neutrophil infiltration following CTX and glycerol injuries

Neutrophil infiltration appeared at 6 h after both injuries. However, a larger number of neutrophils infiltration as well as earlier myofiber invasion were noticed after CTX-induced injury compared to glycerol-induced injury. These results are in harmony with results obtained by Arsic *et al.* (2004) reporting that CTX induces more severe damage and extensive inflammatory cellular infiltration than does glycerol. Neutrophils are the first cells that migrate from blood capillaries to the injury site (diapedesis), to perform phagocytosis and release pro-inflammatory cytokines (Sheshechalam *et al.*, 2014). It was reported that neutrophils were detected at 6 h after CTX injection (Kohno *et al.*, 2012) and at 12 h after glycerol injection (Suelves *et al.*, 2002). In contrast to our findings, Hardy *et al.* (2016) reported recently that neutrophil infiltration appeared at 18 h after CTX injection, moreover, Lukjanenko *et al.* (2013) reported that glycerol induces a stronger inflammatory infiltration than does CTX. The difference between these results and the results of the current study could be attributed to the difference in mouse strains used, C57BL/6 vs. C3H/HeN, and the difference in volumes of injected glycerol and CTX, 25 μ L vs. 50 μ L (Hardy *et al.*, 2016; Lukjanenko *et al.*, 2013). Strain-specific differences were reported between BALB/c and C57BL/6 mice following hind limb ischemia (McClung *et al.*, 2012) and bupivacaine injection (Lagrota-Candido *et al.*, 2010). Moreover, Ao *et al.* (2009) reported different levels of cytokines in C57BL/6 mice and C3H mice after radiation-induced pulmonary injury. Furthermore, Lukjanenko *et al.* (2013) reported that 25 μ L of 50% glycerol induced less myofiber damage than did 50 μ L of 50% glycerol.

Macrophage infiltration following CTX and glycerol injuries

Macrophages infiltration was detected at 24 h after CTX-induced injury in the present study. Similar results were reported at 24 h after CTX-induced injury (Sakaguchi *et al.*, 2014; Segawa *et al.*, 2008). In contrast, Hardy *et al.* (2016) detected macrophages for the first time at day 4 after CTX-induced injury. Although Sakaguchi *et al.* (2014) and Hardy *et al.* (2016) used the same mouse strain, C57BL/6, they injected different volumes of CTX, 50 μ L and 25 μ L, respectively, while the present study and the study by Segawa *et al.* (2008) used C3H mouse strain, but Segawa *et al.* (2008) injected 75 μ L of CTX. Despite of strain-specific differences in response to the same injury (Lagrotta-Candido *et al.*, 2010; McClung *et al.*, 2012), the difference between results of previous studies might be referred to different volumes of injected CTX rather than the mouse strain. On the other hand, macrophage infiltration was detected at 2 days after injection of glycerol (Suelves *et al.*, 2002), which could explain the inability to detect macrophages infiltration at 24 h after glycerol-induced injury in the present study.

Relationship between inflammatory cell infiltration and SC activation

Efficient tissue repair depends on inflammatory cells recruitment; the increased number of macrophages during the inflammation stage results in fast and efficient recovery of muscles (Dumont and Frenette, 2010). Delivery of proinflammatory (M1) macrophages into injured muscle 24 h after injury enhances muscle regeneration and reduces collagen accumulation (Rybalko *et al.*, 2015). The current study showed first detection of monocytes 24 h after glycerol-induced injury. At the same time, numerous macrophages invaded the CTX-injured muscle which suggests earlier recruitment of monocytes in CTX-injured muscle than in glycerol-injured muscle. This suggestion is supported by the results of Hardy *et al.* (2016) who reported a peak of monocyte chemoattractant protein-1, a chemokine that regulates monocyte infiltration, at 18 h

after CTX injection. It is worth mentioning that the recruitment time of blood monocytes to the damaged tissue and their differentiation into various macrophage phenotypes affects tissue repair and regeneration (Munoz-Canoves and Serrano, 2015). On the other hand, it was reported that co-culturing of macrophages isolated from CTX-injected muscles with primary myoblasts showed a significant increase in myotube formation (Kohno *et al.*, 2012). Infiltrating monocytes/macrophages release a high level of interleukin (IL)-6, at 24 h after CTX injury, which promotes further infiltration of macrophages and enhances myoblast proliferation (Zhang *et al.*, 2013) and Insulin-like growth factor 1 (IGF-1), at the initial stage of muscle damage after CTX injury, which enhances tissue regeneration and hastens resolution of the inflammation (Tonkin *et al.*, 2015). The present findings and those of Yan *et al.* (2003) showed early SC activation, indicated by increase in SC length and cytoplasmic content, at 6 h after CTX- and glycerol-induced injury and CTX injection, respectively. However, the morphometric analysis showed a significant increase in SC length and cytoplasmic-nuclear ratio in CTX-injured muscles compared to that in glycerol-injured muscles at day 4 after injury. This difference was associated with the significantly larger number of macrophages in CTX-injured muscles than in glycerol-injured muscles. It is notable that delayed macrophage infiltration to damaged myofibers negatively affects muscle regeneration (Scheerer *et al.*, 2013). Furthermore, early monocytes/macrophages infiltration releases signals which inhibit differentiation of fibroadipogenic progenitors (FAPs) into adipocytes (Wang *et al.*, 2014). These results could explain the results of our previous study showing more efficient regeneration after CTX-induced injury than in glycerol-induced injury (Mahdy *et al.*, 2015).

Eosinophil infiltration was observed at 24 h after CTX-induced injury. Heredia and co-workers (2013) reported that eosinophils secrete IL-4, which stimulates the proliferation of FAPs

into fibroblasts to support myogenesis and suppresses the differentiation of FAPs into adipocytes (Dong *et al.*, 2014). Intraperitoneal administration of IL-4 inhibits adipocyte accumulation in glycerol-injured muscle (Heredia *et al.*, 2013). These results support the findings of the current study showing detection of many fibroblasts in CTX-injured muscles and many preadipocytes in glycerol-injured muscle at day 4 after injury and our previous results showing increased collagen deposition after CTX-induced injury and adipocyte infiltration after glycerol-induced injury (Mahdy *et al.*, 2015). Furthermore, Murphy *et al.* (2011) reported a positive interaction between SCs and fibroblasts during muscle regeneration which supports the results of the present study showing a significant difference in myoblast length and cytoplasm content between CTX- and glycerol-induced injuries and our previous results showing efficient regeneration after CTX-induced injury compared to that after glycerol-induced injury (Mahdy *et al.*, 2015).

In conclusion, the present study investigated differences in the potential target and the mechanism of myofiber damage between injuries induced by CTX and glycerol injection. The timing and degree of inflammatory cellular infiltration were also different. CTX disrupted myofiber mitochondria, while glycerol disrupted the myofiber cell membrane and osmotic property. Moreover, CTX recruited earlier and more intense immune cell infiltration than did glycerol. The early events in response to injuries induced by CTX and glycerol might explain the differential regeneration between the two injury models. The current study showed for the first time the different events following skeletal muscle injury induced by CTX and glycerol, however, further molecular studies are also recommended.

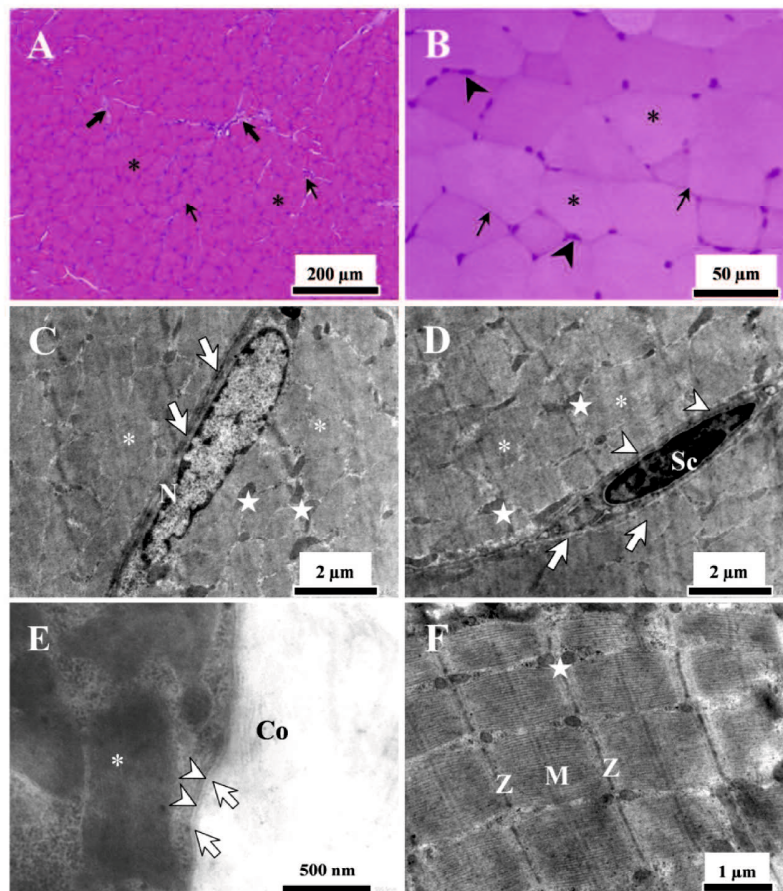


Figure 1. Morphologic structure of non-injured muscle. (A and B) Light micrograph, HE stain, showing normal muscle morphology. Myofibers (asterisk) with peripheral nuclei (arrowhead) were closely arranged. Each myofiber was surrounded by endomysium (thin arrow) while muscle fascicle was surrounded by perimysium (thick arrow). (C) TEM micrograph showing peripheral nucleus (N) lying under the basal lamina (arrows), closely arranged myofibrils (asterisk) and mitochondria (star). (D) Quiescent satellite cell (Sc) with a heterochromatic nucleus lying under the basal lamina and separated from the myofiber by the plasma membrane (arrowheads). (E) Outer basal lamina (arrows) and inner plasma membrane (arrowheads), myofibrils (asterisk) and collagen fibers (Co). (F) Longitudinal sections of normal sarcomeres showing Z-line (Z) and M-band (M)

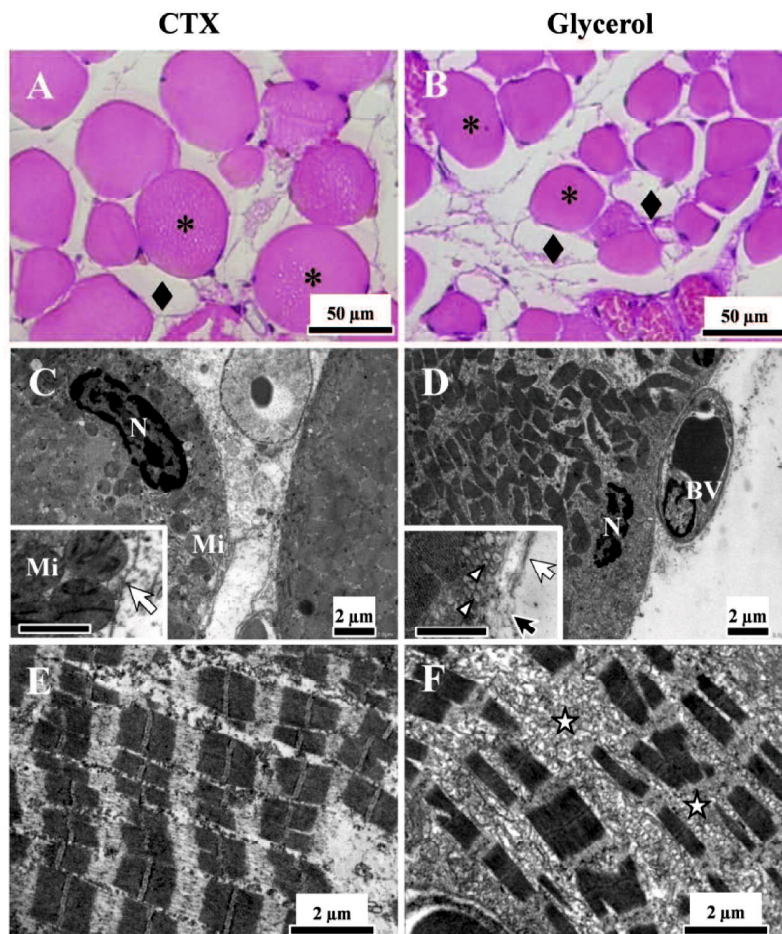


Figure 2. Changes of TA muscle at 1 h after CTX- and glycerol-induced injury. (A and B) Light micrographs, HE stain, showing CTX-injured and glycerol-injured muscles, respectively. Note myofiber swelling (asterisk) and ghost fiber (rhombus). (C and E) TEM micrographs of CTX-injured muscle and (D and F) glycerol-injured muscle. Myofiber nucleus (N), mitochondria (Mi), blood vessel (BV), basal lamina (white arrow), focal disruption of the basal lamina (black arrow) and subsarcolemmal vesicles (arrowhead). Note loss of the Z-line and accumulation of vesicles between myofibrils (star). Inset shows higher magnification, inset scale bar=1 μ m

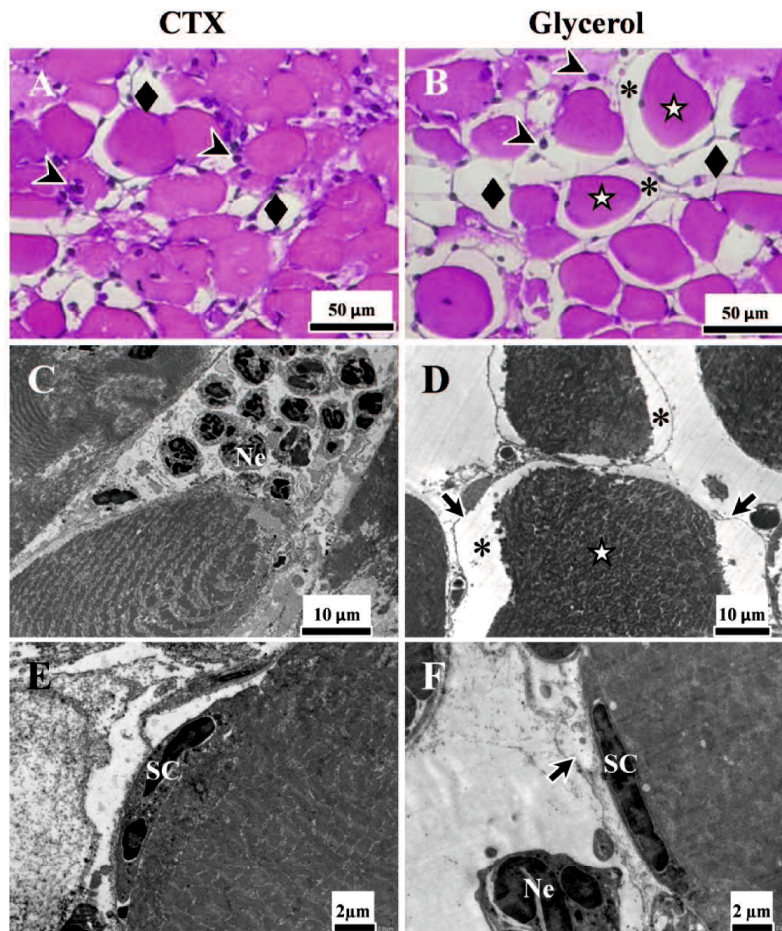


Figure 3. Changes of TA muscle at 6 h after CTX- and glycerol-induced injury. (A and B) Light micrographs, HE stain, showing mononuclear cells (arrowheads) and hypercontracted myofibers (star) with a gap (asterisk) between the myofiber and the outer membrane, and ghost fiber (rhombus). (C and E) TEM micrographs of CTX-injured muscle and (D and F) glycerol-injured muscle. Note infiltrating neutrophils (Ne), satellite cells (SC), myofiber hypercontraction (star) in glycerol-injured muscle leaving a gap (asterisk) between the cytoplasm and the outer undulating basal lamina (black arrows).

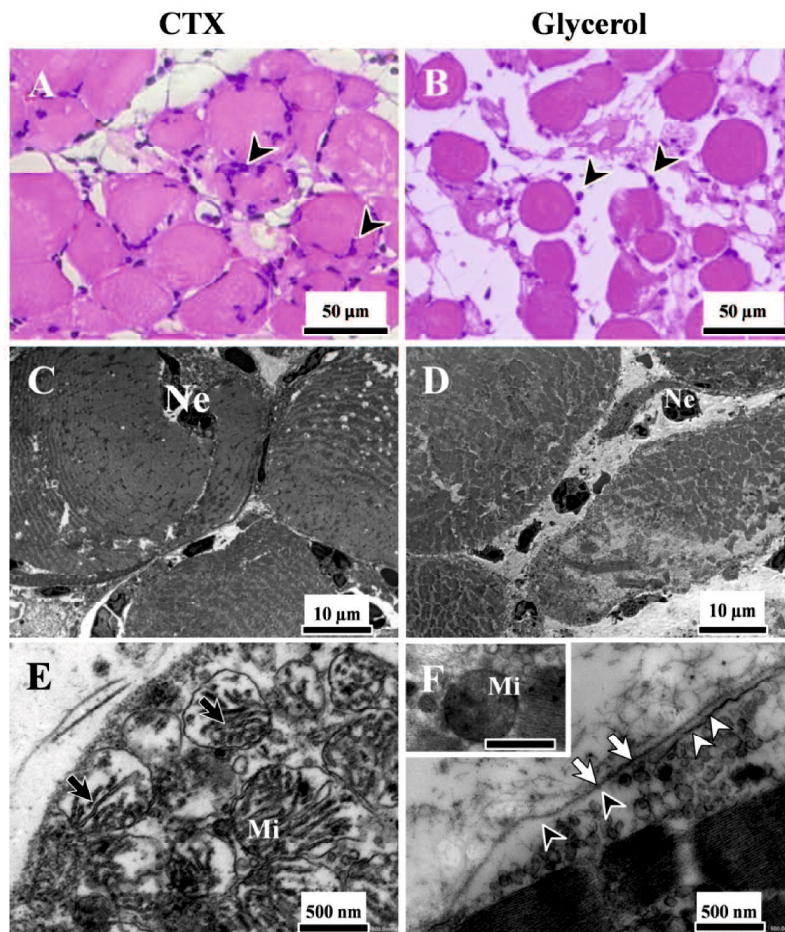


Figure 4. Changes of TA muscle at 12 h after CTX- and glycerol-induced injury. (A and B) Light micrographs, HE stain, showing some myofibers invaded with mononuclear cells (arrowheads). (C and E) TEM micrographs of CTX-injured muscle and (D and F) glycerol-injured muscle. Note necrotic myofiber invaded with neutrophils (Ne), mitochondria (Mi) with a lucent matrix, cristae (black arrows), sarcolemma (white arrow), thickened plasma membrane (white arrowheads) and loss of the plasma membrane (black arrowheads). Inset showing mitochondria (Mi) in glycerol-injured muscle, inset scale bar=500nm

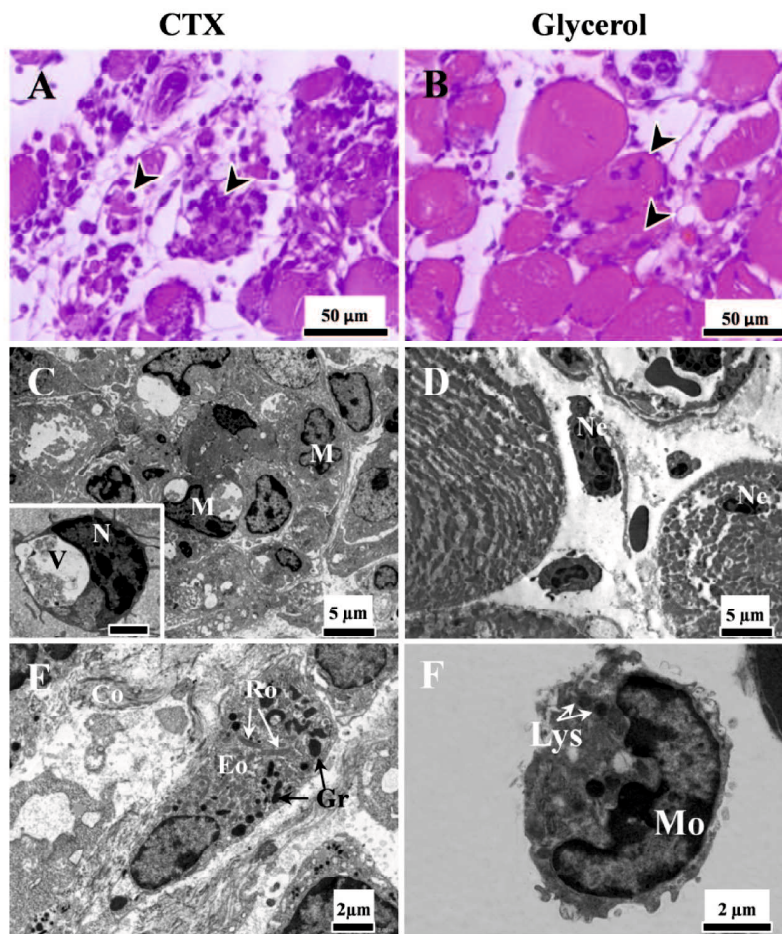


Figure 5. Changes of TA muscle at 24 h after CTX- and glycerol-induced injury. (A and B) Light micrographs, HE stain, showing myofibers invaded with mononuclear cells (arrowheads). (C and E) TEM micrographs of CTX-injured muscle and (D and F) glycerol-injured muscle. Necrotic myofibers were invaded by macrophages (M) and neutrophils (Ne). Eosinophil (EO) with dense granules (Gr) and rods (Ro) and connective tissue (Co), and monocyte (Mo) with lysosomes (Lys). Inset showing higher magnification of a macrophage with a single nucleus (N) and large phagocytic vacuole (V), inset scale bar=2 μ m

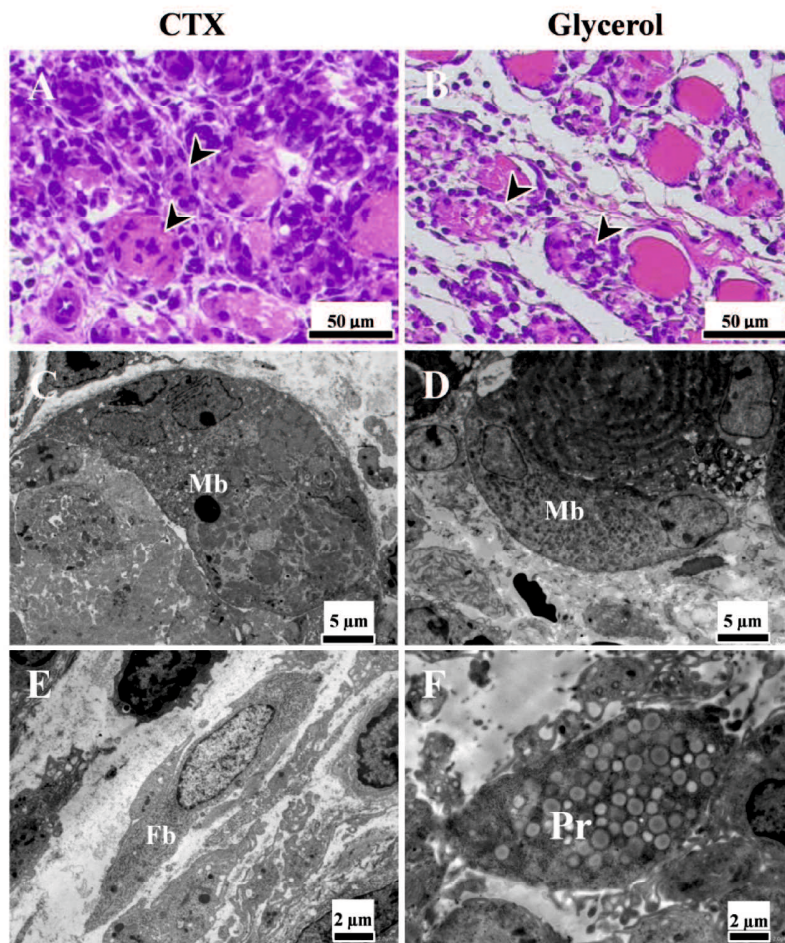


Figure 6. Changes of TA muscle at 4 days after CTX- and glycerol-induced injury. (A and B) Light micrographs, HE stain, showing myofibers extensively invaded by mononuclear cells (arrowheads). Note the larger number of macrophages (M) in CTX-injured muscle than in glycerol-injured muscle. (C and E) TEM micrographs of CTX-injured muscle and (D and F) glycerol-injured muscle. Note myoblasts (Mb), fibroblasts (Fb) and preadipocytes (Pr).

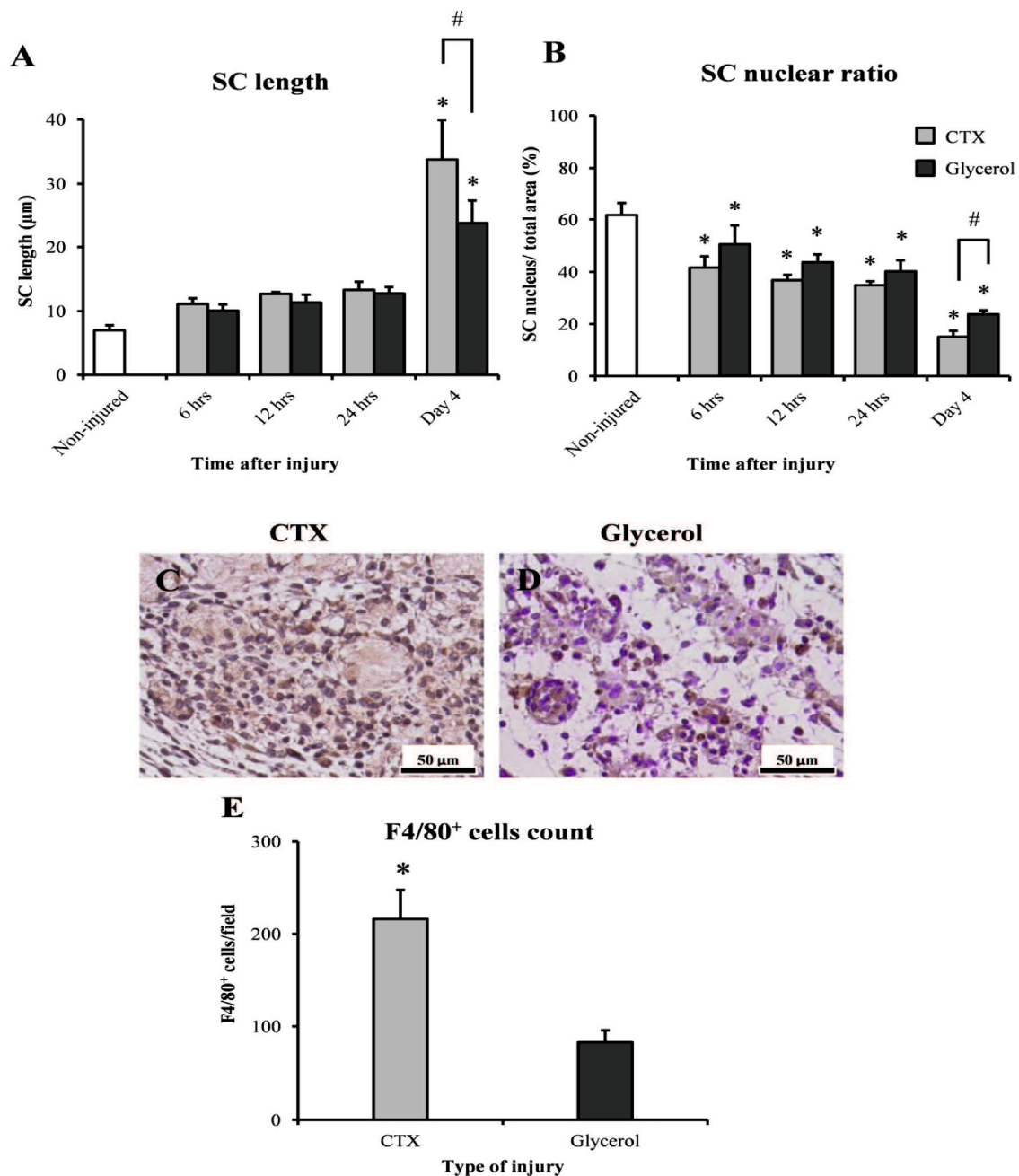


Figure 7. (A) Morphometric analysis of changes in SC length and (B) SC nuclear ratio after injuries induced by CTX and glycerol. Data are expressed as means \pm SD, * indicates significant difference from non-injured muscle, and # indicates significant difference between two injured muscles at the same time point ($P < 0.05$). (C, D) Macrophages infiltration detected by F4/80 antibody at day 4 after injury. (E) Analysis of the number of macrophages, F4/80⁺ cells, per field. * indicates significant difference ($P < 0.05$)

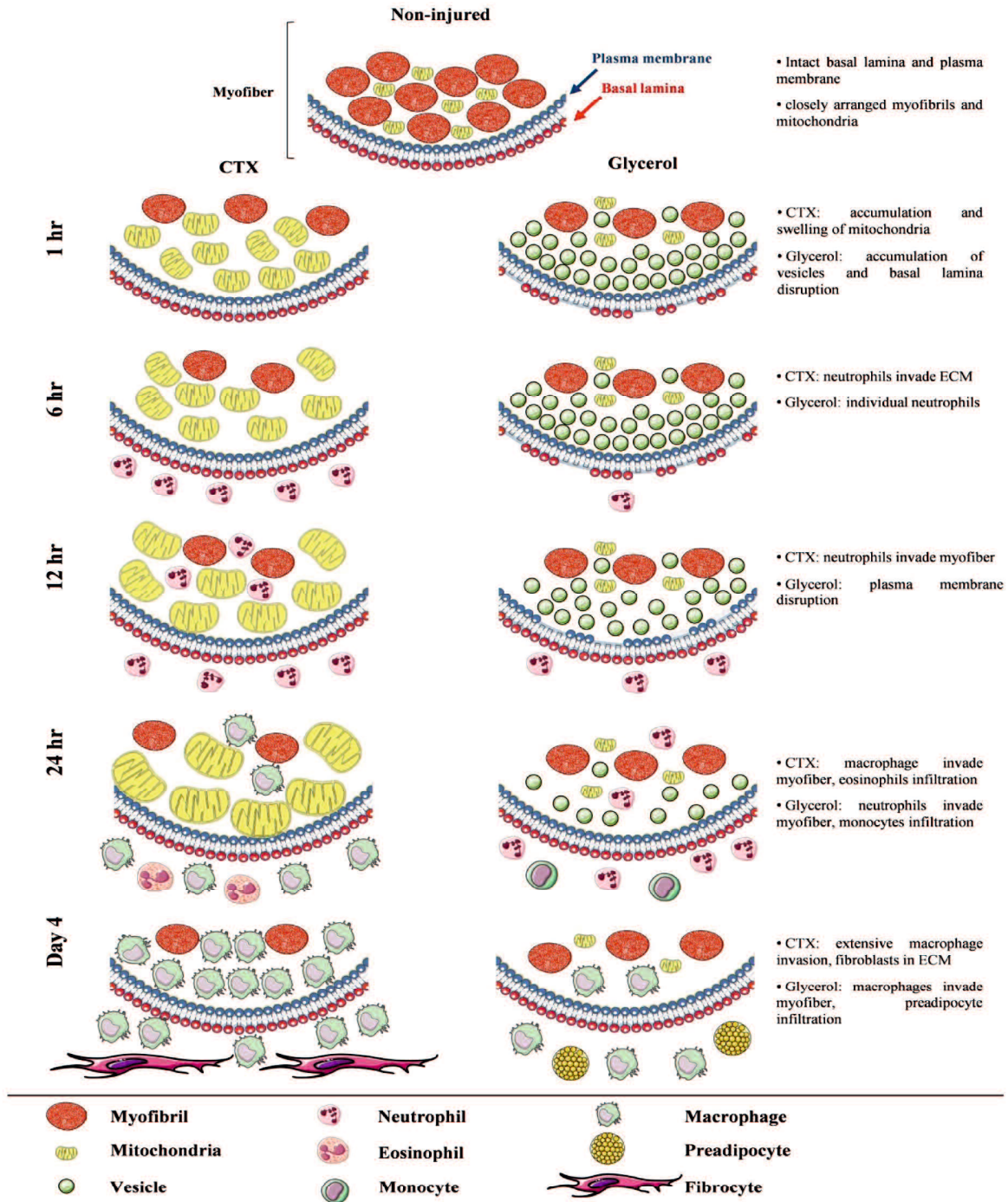


Figure 8. Schematic model showing the spatiotemporal differences of the early injury events between CTX- and glycerol-induced injury. Figures were produced using Servier Medical Art (<http://www.servier.com>).

SUMMARY

Skeletal muscle regenerates efficiently in response to injuries. However, excessive accumulations of fibrous and fat tissue are characteristic features of some pathological disorders as myopathies and advanced cases of Duchenne muscular dystrophy. For better understanding of the process of muscle regeneration in a controlled and consistent manner, various experimental animal models have been used to mimic human injuries. Although *mdx* mouse is the most accepted genetic model for studying muscle dystrophy, it shows limited fibrosis in limb muscles at about two years old. Therefore, it is important to develop either a new protocol to enhance muscle fibrosis in *mdx* mice at young age or develop new experimental models for muscle fibrosis. Hence, developing muscle fibrosis model in normal non-dystrophic muscles is easy to perform and will help evaluation of therapeutic treatment of fibrosis. The overall aim of this thesis is to investigate the detailed response of non-dystrophic muscle to injuries induced by cardiotoxin (CTX) and glycerol to determine the appropriate injury model for studying muscle fibrosis and adipogenesis.

In Chapter 1, the outcomes of regeneration following two experimental models of muscle injuries were demonstrated in non-dystrophic mice in relation to changes in intramuscular connective tissue (IMCT). Skeletal muscle responses following both injuries were different; efficient regeneration with transient endomysial fibrosis following CTX injury, while impaired regeneration with adipocyte infiltration and progressive endomysial fibrosis following glycerol injury. The association of changes in regeneration process with the variations in IMCT structure suggests that IMCT plays an important role in controlling the efficiency of muscle regeneration following injury. Next, the effects of exogenous treatment of the profibrotic cytokine, Transforming growth factor (TGF)- β 1, on muscle regeneration and adipogenesis were

investigated. TGF- β 1 treatment suppressed muscle regeneration and adipogenesis and enhanced fibrosis. The present results suggest that TGF- β 1 has a more potent effect on the early stage of muscle regeneration and adipogenesis. Moreover, combination of TGF- β 1 with glycerol-induced injury provides a simple model to enhance muscle fibrosis for future studies.

In Chapter 2, the early changes of muscle damage in response to CTX and glycerol injuries were studied in details by histological and ultrastructural analyses to further explain the difference in regeneration between the two injuries. The potential targets, the mechanisms of muscle damage and the time sequence of immune cell infiltration were different between the two injuries. Alterations of myofiber cell membrane, timing and degree of immune cells recruitment have a great impact on muscle degeneration. Moreover, these early events clarify the differential regeneration between the two injury models.

In conclusion, the data presented in this thesis provide a thorough understanding of the relationship between muscle regeneration and alteration of IMCT structure on one hand and the relationship between outcome of regeneration and early events following injury on the other hand. The glycerol-injured model provides a suitable model to study muscle fibrosis and adipogenesis for future research on defective regeneration in normal mice. In addition, combination of glycerol and TGF- β 1 treatment might be an alternative to enhance muscle fibrosis in non-dystrophic muscle which could be applied in genetically modified mice in future research.

ACKNOWLEDGEMENTS

First and foremost, all praise and thanks be to ALLAH, Lord of the worlds, who created me and provided me with all gifts during my life.

The present work was carried out at the Department of Veterinary Anatomy, Faculty of Agriculture, Tottori University, Tottori, Japan. I would like to express my sincere and deep gratitude to Prof. Dr. Yoshinao Z. Hosaka (principal supervisor), Prof. Dr. Akira Yabuki (co-supervisor, Kagoshima University), and Associate Prof. Dr. Katsuhiko Warita, for providing guidance, valuable comments, helpful advices and encouragement throughout my study. My special gratitude to the co-authors of the papers included in this study, for their cooperation and contribution, and to students of Veterinary Anatomy Department for their kind helps.

My cordial thanks are for Prof. Dr. Kamal Eldin Hashem Abdalla (Assiut University, Egypt) and Prof. Dr. Salma Ahmed Mohamed (South Valley University, Egypt), for guiding me during my first step of scientific research as well as for giving me precious advice on the personal level.

Lastly, but most importantly, the biggest acknowledgement and thanks are for my lovely family; my parents, wife and children. My parents, without your love, support, encouragement and guidance, I would not be where I am today. Thanks for continuous guidance and support from the first moment in my life. My wife, Zamzam, and my little children; Yomna, Hoor and Umar, you suffered, sacrificed and tolerated a lot of stress during these years. I love you all so much. I achieved success with your support and efforts.

Grateful acknowledgments are for the financial support from the Egyptian Government and the Ministry of Higher Education, in the form of a scholarship (No. 2/2010-2011) to obtain the PhD degree. Cordial thanks for all staff members of the Egyptian Cultural and Educational Bureau and Egyptian Embassy in Tokyo for their efforts and support during my study in Japan.

REFERENCES

- Accornero, F., Kanisicak, O., Tjondrokoesoemo, A., Attia, A.C., McNally, E.M., Molkentin, J.D., 2014. Myofiber-specific inhibition of TGF β signaling protects skeletal muscle from injury and dystrophic disease in mice. *Hum Mol Genet* 23, 6903-6915.
- Addison, O., Marcus, R.L., LaStayo, P.C., Ryan, A.S., 2014. Intermuscular fat: A review of the consequences and causes. *Int J Endocrinol* 2014, 11.
- Ao, X., Zhao, L., Davis, M.A., Lubman, D.M., Lawrence, T.S., Kong, F.M., 2009. Radiation produces differential changes in cytokine profiles in radiation lung fibrosis sensitive and resistant mice. *J Hematol Oncol* 2, 6.
- Apostol, S., Ursu, D., Lehmann-Horn, F., Melzer, W., 2009. Local calcium signals induced by hyper-osmotic stress in mammalian skeletal muscle cells. *J Muscle Res Cell Motil* 30, 97-109.
- Arsic, N., Zacchigna, S., Zentilin, L., Ramirez-Correa, G., Pattarini, L., Salvi, A., Sinagra, G., Giacca, M., 2004. Vascular endothelial growth factor stimulates skeletal muscle regeneration in vivo. *Mol Ther* 10, 844-854.
- Baldo, C., Ferreira, M., Lopes, D., Izidoro, L., Gomes, A., Ferro, E., Hamaguchi, A., Homs-Brandeburgo, M., Rodrigues, V., 2010. Action of neuwiedase, a metalloproteinase isolated from *Bothrops neuwiedi* venom, on skeletal muscle: an ultrastructural and immunocytochemistry study. *J Venom Anim Toxins incl Trop Dis* 16, 462-469.
- Bansal, D., Campbell, K.P., 2004. Dysferlin and the plasma membrane repair in muscular dystrophy. *Trends Cell Biol* 14, 206-213.
- Bansal, D., Miyake, K., Vogel, S.S., Groh, S., Chen, C.-C., Williamson, R., McNeil, P.L., Campbell, K.P., 2003. Defective membrane repair in dysferlin-deficient muscular dystrophy. *Nature* 423, 168-172.

Best, T.M., Hunter, K.D., 2000. Muscle injury and repair. *Phys Med Rehabil Clin N Am* 11, 251-266.

Brioche, T., Pagano, A.F., Py, G., Chopard, A., 2016. Muscle wasting and aging: experimental models, fatty infiltrations, and prevention. *Mol Aspects Med* 50, 56-87.

Calve, S., Odelberg, S.J., Simon, H.G., 2010. A transitional extracellular matrix instructs cell behavior during muscle regeneration. *Dev Biol* 344, 259-271.

Charge, S.B., Rudnicki, M.A., 2004. Cellular and molecular regulation of muscle regeneration. *Physiol Rev* 84, 209-238.

Cheng, M., Nguyen, M.H., Fantuzzi, G., Koh, T.J., 2008. Endogenous interferon-gamma is required for efficient skeletal muscle regeneration. *Am J Physiol Cell Physiol* 294, C1183-1191.

Choy, L., Derynck, R., 2003. Transforming growth factor-beta inhibits adipocyte differentiation by Smad3 interacting with CCAAT/enhancer-binding protein (C/EBP) and repressing C/EBP transactivation function. *J Biol Chem* 278, 9609-9619.

Cohn, R.D., van Erp, C., Habashi, J.P., Soleimani, A.A., Klein, E.C., Lisi, M.T., Gamradt, M., ap Rhys, C.M., Holm, T.M., Loeys, B.L., Ramirez, F., Judge, D.P., Ward, C.W., Dietz, H.C., 2007. Angiotensin II type 1 receptor blockade attenuates TGF- β -induced failure of muscle regeneration in multiple myopathic states. *Nat Med* 13, 204-210.

Czerwinska, A.M., Streminska, W., Ciemerych, M.A., Grabowska, I., 2012. Mouse gastrocnemius muscle regeneration after mechanical or cardiotoxin injury. *Folia Histochem Cytobiol* 50, 144-153.

Demonbreun, A.R., Rossi, A.E., Alvarez, M.G., Swanson, K.E., Deveaux, H.K., Earley, J.U., Hadhazy, M., Vohra, R., Walter, G.A., Pytel, P., McNally, E.M., 2014. Dysferlin and myoferlin regulate transverse tubule formation and glycerol sensitivity. *Am J Pathol* 184, 248-259.

Desguerre, I., Arnold, L., Vignaud, A., Cuvellier, S., Yacoub-youssef, H., Gherardi, R.K., Chelly, J., Chretien, F., Mounier, R., Ferry, A., Chazaud, B., 2012. A new model of experimental fibrosis in hindlimb skeletal muscle of adult mdx mouse mimicking muscular dystrophy. *Muscle Nerve* 45, 803-814.

Desguerre, I., Mayer, M., Leturcq, F., Barbet, J.P., Gherardi, R.K., Christov, C., 2009. Endomysial fibrosis in Duchenne muscular dystrophy: a marker of poor outcome associated with macrophage alternative activation. *J Neuropathol Exp Neurol* 68, 762-773.

Dong, Y., Silva, K.A., Dong, Y., Zhang, L., 2014. Glucocorticoids increase adipocytes in muscle by affecting IL-4 regulated FAP activity. *Faseb j* 28, 4123-4132.

Dulhunty, A.F., Gage, P.W., Barry, P.H., 1973. Differential effects of glycerol treatment on membrane capacity and excitation—contraction coupling in toad sartorius fibres. With an Appendix. *J Physiol* 234, 373-408.371.

Dumont, N., Frenette, J., 2010. Macrophages protect against muscle atrophy and promote muscle recovery in vivo and in vitro: a mechanism partly dependent on the insulin-like growth factor-1 signaling molecule. *Am J Pathol* 176, 2228-2235.

Fearing, C.M., Melton, D.W., Lei, X., Hancock, H., Wang, H., Sarwar, Z.U., Porter, L., McHale, M., McManus, L.M., Shireman, P.K., 2016. Increased adipocyte area in injured muscle with aging and impaired remodeling in female mice. *J Gerontol A Biol Sci Med Sci* 71, 992-1004.

Fernandez, C., Figarella-Branger, D., Meyronet, D., Cassote, E., Tong, S., Pellissier, J.F., 2005. Electron microscopy in neuromuscular disorders. *Ultrastruct Pathol* 29, 437-450.

Fiore, D., Judson, R.N., Low, M., Lee, S., Zhang, E., Hopkins, C., Xu, P., Lenzi, A., Rossi, F.M., Lemos, D.R., 2016. Pharmacological blockage of fibro/adipogenic progenitor expansion and suppression of regenerative fibrogenesis is associated with impaired skeletal muscle regeneration. *Stem Cell Res* 17, 161-169.

Fukada, S., Morikawa, D., Yamamoto, Y., Yoshida, T., Sumie, N., Yamaguchi, M., Ito, T., Miyagoe-Suzuki, Y., Takeda, S., Tsujikawa, K., Yamamoto, H., 2010. Genetic background affects properties of satellite cells and mdx phenotypes. *Am J Pathol* 176, 2414-2424.

Garg, K., Boppart, M.D., 2016. Influence of exercise and aging on extracellular matrix composition in the skeletal muscle stem cell niche. *J Appl Physiol* (1985) 121, 1053-1058.

Gayraud-Morel, B., Chretien, F., Tajbakhsh, S., 2009. Skeletal muscle as a paradigm for regenerative biology and medicine. *Regen Med* 4, 293-319.

Gillies, A.R., Smith, L.R., Lieber, R.L., Varghese, S., 2011. Method for decellularizing skeletal muscle without detergents or proteolytic enzymes. *Tissue Eng Part C Methods* 17, 383-389.

Gregory, M., Mars, M., 2004. Mobilisation of satellite cells following ischaemia and reperfusion in primate skeletal muscle. *S Afr J Sports Med* 16, 17-24.

Gutpell, K.M., Hrinivich, W.T., Hoffman, L.M., 2015. Skeletal muscle fibrosis in the mdx/utrn^{+/-} mouse validates its suitability as a murine model of Duchenne muscular dystrophy. *PLoS One* 10, e0117306.

Hardy, D., Besnard, A., Latil, M., Jouvion, G., Briand, D., Thepenier, C., Pascal, Q., Guguin, A., Gayraud-Morel, B., Cavaillon, J.M., Tajbakhsh, S., Rocheteau, P., Chretien, F., 2016. Comparative study of injury models for studying muscle regeneration in mice. *PLoS One* 11, e0147198.

Harris, J.B., 2003. Myotoxic phospholipases A2 and the regeneration of skeletal muscles. *Toxicon* 42, 933-945.

Heredia, J.E., Mukundan, L., Chen, F.M., Mueller, A.A., Deo, R.C., Locksley, R.M., Rando, T.A., Chawla, A., 2013. Type 2 innate signals stimulate fibro/adipogenic progenitors to facilitate muscle regeneration. *Cell* 153, 376-388.

Ho, M., Post, C.M., Donahue, L.R., Lidov, H.G., Bronson, R.T., Goolsby, H., Watkins, S.C., Cox, G.A., Brown, R.H., Jr., 2004. Disruption of muscle membrane and phenotype divergence in two novel mouse models of dysferlin deficiency. *Hum Mol Genet* 13, 1999-2010.

Horie, M., Enomoto, M., Shimoda, M., Okawa, A., Miyakawa, S., Yagishita, K., 2014. Enhancement of satellite cell differentiation and functional recovery in injured skeletal muscle by hyperbaric oxygen treatment. *J Appl Physiol* (1985) 116, 149-155.

Horsley, V., Friday, B.B., Matteson, S., Kegley, K.M., Gephart, J., Pavlath, G.K., 2001. Regulation of the growth of multinucleated muscle cells by an Nfatc2-dependent pathway. *J Cell Biol* 153, 329-338.

Inoue, T., Osatake, H., 1988. A new drying method of biological specimens for scanning electron microscopy: the t-butyl alcohol freeze-drying method. *Arch Histol Cytol* 51, 53-59.

Jarvinen, T.A., Jarvinen, T.L., Kaariainen, M., Kalimo, H., Jarvinen, M., 2005. Muscle injuries: biology and treatment. *Am J Sports Med* 33, 745-764.

Karalaki, M., Fili, S., Philippou, A., Koutsilieris, M., 2009. Muscle regeneration: cellular and molecular events. *In Vivo* 23, 779-796.

Kawai, H., Nishino, H., Kusaka, K., Naruo, T., Tamaki, Y., Iwasa, M., 1990. Experimental glycerol myopathy: a histological study. *Acta Neuropathol* 80, 192-197.

Kawanishi, N., Mizokami, T., Niihara, H., Yada, K., Suzuki, K., 2016. Macrophage depletion by clodronate liposome attenuates muscle injury and inflammation following exhaustive exercise. *Biochem Biophys Rep* 5, 146-151.

Kharraz, Y., Guerra, J., Mann, C.J., Serrano, A.L., Muñoz-Cánoves, P., 2013. Macrophage plasticity and the role of inflammation in skeletal muscle repair. *Mediators Inflamm* 2013, 9.

Kharraz, Y., Guerra, J., Pessina, P., Serrano, A.L., Munoz-Canoves, P., 2014. Understanding the process of fibrosis in Duchenne muscular dystrophy. *BioMed Res. Int.* 2014, 11.

Kohno, S., Yamashita, Y., Abe, T., Hirasaka, K., Oarada, M., Ohno, A., Teshima-Kondo, S., Higashibata, A., Choi, I., Mills, E.M., Okumura, Y., Terao, J., Nikawa, T., 2012. Unloading stress disturbs muscle regeneration through perturbed recruitment and function of macrophages. *J Appl Physiol* (1985) 112, 1773-1782.

Lagrotta-Candido, J., Canella, I., Pinheiro, D.F., Santos-Silva, L.P., Ferreira, R.S., Guimarães-Joca, F.J., Lannes-Vieira, J., Quirico-Santos, T., 2010. Characteristic pattern of skeletal muscle remodelling in different mouse strains. *Int J Experim Pathol* 91, 522-529.

Lamarche, É., Lala-Tabbert, N., Gunanayagam, A., St-Louis, C., Wiper-Bergeron, N., 2015. Retinoic acid promotes myogenesis in myoblasts by antagonizing transforming growth factor-beta signaling via C/EBP β . *Skeletal Muscle* 5, 1-14.

Li, H., Mittal, A., Makonchuk, D.Y., Bhatnagar, S., Kumar, A., 2009. Matrix metalloproteinase-9 inhibition ameliorates pathogenesis and improves skeletal muscle regeneration in muscular dystrophy. *Hum Mol Genet* 18, 2584-2598.

Li, X., McFarland, D.C., Velleman, S.G., 2008. Effect of Smad3-mediated transforming growth factor- β 1 signaling on satellite cell proliferation and differentiation in chickens. *Poult Sci* 87, 1823-1833.

Liu, W., Liu, Y., Lai, X., Kuang, S., 2012. Intramuscular adipose is derived from a non-Pax3 lineage and required for efficient regeneration of skeletal muscles. *Dev Biol* 361, 27-38.

Lu, H., Ward, M., Adeola, O., Ajuwon, K., 2013. Regulation of adipocyte differentiation and gene expression-crosstalk between TGF- β and wnt signaling pathways. *Mol Biol Rep* 40, 5237-5245.

Lukjanenko, L., Brachat, S., Pierrel, E., Lach-Trifilieff, E., Feige, J.N., 2013. Genomic profiling reveals that transient adipogenic activation is a hallmark of mouse models of skeletal muscle regeneration. *PLoS One* 8, e71084.

Mahdy, M.A.A., Lei, H.Y., Wakamatsu, J.-I., Hosaka, Y.Z., Nishimura, T., 2015. Comparative study of muscle regeneration following cardiotoxin and glycerol injury. *Ann Anat* 202, 18-27.

Malmstrom, J., Lindberg, H., Lindberg, C., Bratt, C., Wieslander, E., Delander, E., Sarnstrand, B., Burns, J., Mose-Larsen, P., Fey, S., Marko-Varga, G., 2004. Transforming growth factor-beta 1 specifically induce proteins involved in the myofibroblast contractile apparatus. *Mol Cell Proteomics* 3, 466-477.

McClung, J.M., McCord, T.J., Keum, S., Johnson, S., Annex, B.H., Marchuk, D.A., Kontos, C.D., 2012. Skeletal muscle-specific genetic determinants contribute to the differential strain-dependent effects of hindlimb ischemia in mice. *Am J Pathol* 180, 2156-2169.

McHale, M.J., Sarwar, Z.U., Cardenas, D.P., Porter, L., Salinas, A.S., Michalek, J.E., McManus, L.M., Shireman, P.K., 2012. Increased fat deposition in injured skeletal muscle is regulated by sex-specific hormones. *Am J Physiol Regul Integr Comp Physiol* 302, R331-339.

Munoz-Canoves, P., Serrano, A.L., 2015. Macrophages decide between regeneration and fibrosis in muscle. *Trends Endocrinol Metab* 26, 449-450.

Murphy, M.M., Lawson, J.A., Mathew, S.J., Hutcheson, D.A., Kardon, G., 2011. Satellite cells, connective tissue fibroblasts and their interactions are crucial for muscle regeneration. *Development* 138, 3625-3637.

Musarò, A., 2014. The basis of muscle regeneration. *Advances in Biology* 2014, 16.

Nishimura, T., Hattori, A., Takahashi, K., 1999. Structural changes in intramuscular connective tissue during the fattening of Japanese black cattle: effect of marbling on beef tenderization. *J Anim Sci* 77, 93-104.

Nishizawa, T., Tamaki, H., Kasuga, N., Takekura, H., 2003. Degeneration and regeneration of neuromuscular junction architecture in rat skeletal muscle fibers damaged by bupivacaine hydrochloride. *J Muscle Res Cell Motil* 24, 527-537.

Ohtani, O., Ushiki, T., Taguchi, T., Kikuta, A., 1988. Collagen fibrillar networks as skeletal frameworks: a demonstration by cell-maceration/scanning electron microscope method. *Arch Histol Cytol* 51, 249-261.

Osses, N., Brandan, E., 2002. ECM is required for skeletal muscle differentiation independently of muscle regulatory factor expression. *Am J Physiol Cell Physiol* 282, C383-394.

Oz Gergin, O., Yildiz, K., Bayram, A., Sencar, L., Coskun, G., Yay, A., Bicer, C., Ozdamar, S., Polat, S., 2015. Comparison of the myotoxic effects of levobupivacaine, bupivacaine, and ropivacaine: an electron microscopic study. *Ultrastruct Pathol* 39, 169-176.

Pagano, A.F., Demangel, R., Brioché, T., Jublanc, E., Bertrand-Gaday, C., Candau, R., Dechesne, C.A., Dani, C., Bonnieu, A., Py, G., Chopard, A., 2015. Muscle regeneration with intermuscular adipose tissue (IMAT) accumulation is modulated by mechanical constraints. *PLoS One* 10, e0144230.

Pessina, P., Cabrera, D., Morales, M.G., Riquelme, C.A., Gutierrez, J., Serrano, A.L., Brandan, E., Munoz-Canoves, P., 2014. Novel and optimized strategies for inducing fibrosis in vivo: focus on Duchenne muscular dystrophy. *Skelet Muscle* 4, 7.

Pessina, P., Kharraz, Y., Jardi, M., Fukada, S., Serrano, A.L., Perdiguero, E., Munoz-Canoves, P., 2015. Fibrogenic cell plasticity blunts tissue regeneration and aggravates muscular dystrophy. *Stem Cell Reports* 4, 1046-1060.

Pisani, D.F., Bottema, C.D., Butori, C., Dani, C., Dechesne, C.A., 2010. Mouse model of skeletal muscle adiposity: a glycerol treatment approach. *Biochem. Biophys. Res. Commun.* 396, 767-773.

Pohlers, D., Brenmoehl, J., Loffler, I., Muller, C.K., Leipner, C., Schultze-Mosgau, S., Stallmach, A., Kinne, R.W., Wolf, G., 2009. TGF-beta and fibrosis in different organs - molecular pathway imprints. *Biochim Biophys Acta* 1792, 746-756.

Politi, P.K., Havaki, S., Manta, P., Lyritis, G., 2006. Bupivacaine-induced regeneration of rat soleus muscle: ultrastructural and immunohistochemical aspects. *Ultrastruct Pathol* 30, 461-469.

Prisk, V., Huard, J., 2003. Muscle injuries and repair: the role of prostaglandins and inflammation. *Histol Histopathol* 18, 1243-1256.

Ramadasan-Nair, R., Gayathri, N., Mishra, S., Sunitha, B., Mythri, R.B., Nalini, A., Subbannayya, Y., Harsha, H.C., Kolthur-Seetharam, U., Srinivas Bharath, M.M., 2014. Mitochondrial alterations and oxidative stress in an acute transient mouse model of muscle degeneration: implications for muscular dystrophy and related muscle pathologies. *J Biol Chem* 289, 485-509.

Rybalko, V., Hsieh, P.L., Merscham-Banda, M., Suggs, L.J., Farrar, R.P., 2015. The development of macrophage-mediated cell therapy to improve skeletal muscle function after injury. *PLoS One* 10, e0145550.

Sakaguchi, S., Shono, J., Suzuki, T., Sawano, S., Anderson, J.E., Do, M.K., Ohtsubo, H., Mizunoya, W., Sato, Y., Nakamura, M., Furuse, M., Yamada, K., Ikeuchi, Y., Tatsumi, R., 2014. Implication of anti-inflammatory macrophages in regenerative moto-neuritogenesis: promotion of myoblast migration and neural chemorepellent semaphorin 3A expression in injured muscle. *Int J Biochem Cell Biol* 54, 272-285.

Sanes, J.R., 2003. The basement membrane/basal lamina of skeletal muscle. *J Biol Chem* 278, 12601-12604.

Schabort, E.J., van der Merwe, M., Loos, B., Moore, F.P., Niesler, C.U., 2009. TGF- β 's delay skeletal muscle progenitor cell differentiation in an isoform-independent manner. *Exp Cell Res* 315, 373-384.

Scheerer, N., Dehne, N., Stockmann, C., Swoboda, S., Baba, H.A., Neugebauer, A., Johnson, R.S., Fandrey, J., 2013. Myeloid hypoxia-inducible factor-1 α is essential for skeletal muscle regeneration in mice. *J Immunol* 191, 407-414.

Segawa, M., Fukada, S.-i., Yamamoto, Y., Yahagi, H., Kanematsu, M., Sato, M., Ito, T., Uezumi, A., Hayashi, S.i., Miyagoe-Suzuki, Y., Takeda, S.i., Tsujikawa, K., Yamamoto, H., 2008. Suppression of macrophage functions impairs skeletal muscle regeneration with severe fibrosis. *Exp Cell Res* 314, 3232-3244.

Selcen, D., Stilling, G., Engel, A.G., 2001. The earliest pathologic alterations in dysferlinopathy. *Neurology* 56, 1472-1481.

Serrano, A.L., Mann, C.J., Vidal, B., Ardite, E., Perdiguero, E., Munoz-Canoves, P., 2011. Cellular and molecular mechanisms regulating fibrosis in skeletal muscle repair and disease. *Curr Top Dev Biol* 96, 167-201.

Sheshechalam, A., Srivastava, N., Mitchell, T., Lacy, P., Eitzen, G., 2014. Granule protein processing and regulated secretion in neutrophils. *Front Immunol* 5, 1-11.

Suelves, M., Lopez-Aleman, R., Lluís, F., Anioarte, G., Serrano, E., Parra, M., Carmeliet, P., Muñoz-Canoves, P., 2002. Plasmin activity is required for myogenesis in vitro and skeletal muscle regeneration in vivo. *Blood* 99, 2835-2844.

Tidball, J.G., Vallalta, S.A., 2010. Regulatory interactions between muscle and the immune system during muscle regeneration. *Am J Physiol Regul Integr Comp Physiol* 298, R1173-1187.

Tonkin, J., Temmerman, L., Sampson, R.D., Gallego-Colon, E., Barberi, L., Bilbao, D., Schneider, M.D., Musaro, A., Rosenthal, N., 2015. Monocyte/macrophage-derived IGF-1 orchestrates murine skeletal muscle regeneration and modulates autocrine polarization. *Mol Ther* 23, 1189-1200.

Tsurutani, Y., Fujimoto, M., Takemoto, M., Irisuna, H., Koshizaka, M., Onishi, S., Ishikawa, T., Mezawa, M., He, P., Honjo, S., Maezawa, Y., Saito, Y., Yokote, K., 2011. The roles of transforming growth factor-beta and Smad3 signaling in adipocyte differentiation and obesity. *Biochem Biophys Res Commun* 407, 68-73.

Uezumi, A., Fukada, S., Yamamoto, N., Takeda, S., Tsuchida, K., 2010. Mesenchymal progenitors distinct from satellite cells contribute to ectopic fat cell formation in skeletal muscle. *Nat Cell Biol* 12, 143-152.

Uezumi, A., Ikemoto-Uezumi, M., Tsuchida, K., 2014. Roles of nonmyogenic mesenchymal progenitors in pathogenesis and regeneration of skeletal muscle. *Front Physiol* 5, 68.

Urciuolo, A., Quarta, M., Morbidoni, V., Gattazzo, F., Molon, S., Montemurro, F., Rando, T.A., Tedesco, F.S., Bonaldo, P., Blaauw, B., Cossu, G., Grumati, P., Vozzi, G., 2013. Collagen VI regulates satellite cell self-renewal and muscle regeneration. *Nat Commun* 4, 1964.

van Zoelen, E.J., Duarte, I., Hendriks, J.M., van der Woning, S.P., 2016. TGF β -induced switch from adipogenic to osteogenic differentiation of human mesenchymal stem cells: identification of drug targets for prevention of fat cell differentiation. *Stem Cell Res Ther* 7.

Waddell, J.N., Zhang, P., Wen, Y., Gupta, S.K., Yevtodiyenko, A., Schmidt, J.V., Bidwell, C.A., Kumar, A., Kuang, S., 2010. Dlk1 is necessary for proper skeletal muscle development and regeneration. *PLoS One* 5, e15055.

Wallace, G.Q., McNally, E.M., 2009. Mechanisms of muscle degeneration, regeneration, and repair in the muscular dystrophies. *Annu Rev Physiol* 71, 37-57.

Wang, C.H., Wu, W.G., 2005. Amphiphilic beta-sheet cobra cardiotoxin targets mitochondria and disrupts its network. *FEBS Lett* 579, 3169-3174.

Wang, H., Melton, D.W., Porter, L., Sarwar, Z.U., McManus, L.M., Shireman, P.K., 2014. Altered macrophage phenotype transition impairs skeletal muscle regeneration. *Am J Pathol* 184, 1167-1184.

Wang, R., Luo, D., Xiao, C., Lin, P., Liu, S., Xu, Q., Wang, Y., 2013. The time course effects of electroacupuncture on promoting skeletal muscle regeneration and inhibiting excessive fibrosis after contusion in rabbits. *Evid Based Complement Alternat Med* 2013, 16 pages.

Warren, G.L., Summan, M., Gao, X., Chapman, R., Hulderman, T., Simeonova, P.P., 2007. Mechanisms of skeletal muscle injury and repair revealed by gene expression studies in mouse models. *J Physiol* 582, 825-841.

Werner, F., Jain, M.K., Feinberg, M.W., Sibinga, N.E.S., Pellacani, A., Wiesel, P., Chin, M.T., Topper, J.N., Perrella, M.A., Lee, M.-E., 2000. Transforming growth factor- β 1 inhibition of macrophage activation is mediated via Smad3. *J Biol Chem* 275, 36653-36658.

Wicik, Z., Sadkowski, T., Jank, M., Motyl, T., 2010. Transcriptional pattern of TGF-beta1 inhibitory effect on mouse C2C12 myoblasts differentiation. *Pol J Vet Sci* 13, 629-638.

Wooddell, C.I., Radley-Crabb, H.G., Griffin, J.B., Zhang, G., 2011. Myofiber damage evaluation by evans blue dye injection. *Curr Protoc Mouse Biol* 1, 463-488.

Yan, Z., Choi, S., Liu, X., Zhang, M., Schageman, J.J., Lee, S.Y., Hart, R., Lin, L., Thurmond, F.A., Williams, R.S., 2003. Highly coordinated gene regulation in mouse skeletal muscle regeneration. *J Biol Chem* 278, 8826-8836.

Yoshimura, T., Tsujihata, M., Satoh, A., Mori, M., Hazama, R., Kinoshita, N., Takashima, H., Nagataki, S., 1986. Ultrastructural study of the effect of calcium ionophore, A23187, on rat muscle. *Acta Neuropathol* 69, 184-192.

Zhang, C., Li, Y., Wu, Y., Wang, L., Wang, X., Du, J., 2013. Interleukin-6/signal transducer and activator of transcription 3 (STAT3) pathway is essential for macrophage infiltration and myoblast proliferation during muscle regeneration. *J Biol Chem* 288, 1489-1499.

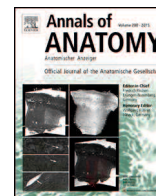
Zhang, L., Wang, X.H., Wang, H., Du, J., Mitch, W.E., 2010. Satellite cell dysfunction and impaired IGF-1 signaling cause CKD-induced muscle atrophy. *J Am Soc Nephrol* 21, 419-427.

Zhao, L., Xu, S.J., Sun, X.T., 2008. Injury and regeneration of intramuscular connective tissue subjected to various regimes of distraction. *Chin J Traumatol* 11, 67-71.

Zhao, W., Lu, H., Wang, X., Ransohoff, R.M., Zhou, L., 2016. CX3CR1 deficiency delays acute skeletal muscle injury repair by impairing macrophage functions. *FASEB J* 30.

Zimowska, M., Duchesnay, A., Dragun, P., Oberbek, A., Moraczewski, J., Martelly, I., 2009. Immunoneutralization of TGF-β1 improves skeletal muscle regeneration: effects on myoblast differentiation and glycosaminoglycan content. *Int J Cell Biol* 2009, 659372.

Živković, S.A., Clemens, P.R., 2015. Muscular dystrophy, in: Zigmond, M.J., Coyle, J.T., Rowland, L. (Eds.), *Neurobiology of brain disorders*. Academic Press, San Diego, pp. 151-166.



Research article

Comparative study of muscle regeneration following cardiotoxin and glycerol injury



Mohamed A.A. Mahdy^{a,b,c,1}, Hsiao Yin Lei^{d,1}, Jun-Ichi Wakamatsu^d,
Yoshinao Z. Hosaka^{a,b,*}, Takanori Nishimura^d

^a Laboratory of Basic Veterinary Science, United Graduate School of Veterinary Science, Yamaguchi University, Yamaguchi, Yamaguchi, Japan

^b Department of Veterinary Anatomy, Faculty of Agriculture, Tottori University, Tottori, Tottori, Japan

^c Department of Anatomy and Embryology, Faculty of Veterinary Medicine, South Valley University, Qena, Egypt

^d Laboratory of Muscle Biology and Meat Science, Research Faculty of Agriculture, Hokkaido University, Sapporo, Hokkaido, Japan

ARTICLE INFO

Article history:

Received 4 November 2014

Received in revised form 27 July 2015

Accepted 28 July 2015

Keywords:

Cardiotoxin

Cell-maceration technique

Glycerol

Intramuscular connective tissue

Muscle regeneration

ABSTRACT

In the present study, we examined muscle regeneration following two types of chemical injuries, cardiotoxin (CTX) and glycerol, in order to compare their effect on the morphological characteristics during muscle regeneration, in addition we studied the structural changes of the intramuscular connective tissue (IMCT) during the regeneration process, by scanning electron microscopy (SEM) after digestion of the cellular elements of the muscle with sodium hydroxide.

Tibialis anterior (TA) muscles of adult male mice were injected either with CTX or glycerol. Muscle degeneration was greater in the CTX-injured model than in the glycerol-injured model at day 4 post injection. Muscle regeneration started at day 7 in both the CTX and glycerol models. However, the CTX-injured model showed a higher myotube density and larger myotube diameter than the glycerol-injured model at days 10 and 14 post injection. On other hand, adipocyte infiltration was detected in the glycerol-injured model. In contrast, no adipocytes could be detected in the CTX-injured model. Furthermore, ultrastructural analysis showed a significant difference in myofiber damage and regeneration between the two models.

SEM of the IMCT showed a transient increase in endomysial collagen deposition at early stages of regeneration in the CTX-injured model. In contrast, glycerol-injured model showed slight endomysial collagen deposition. Our results suggest that changes in IMCT affect the efficiency of muscle regeneration. Studying the three dimensional structure of IMCT may help clinical therapies to reduce skeletal muscle fibrosis. To our knowledge this is the first time the changes in IMCT following CTX and glycerol injury using SEM-cell maceration technique have been compared.

© 2015 Elsevier GmbH. All rights reserved.

1. Introduction

Skeletal muscle has a remarkable capacity for regeneration in response to various types of injuries and diseases such as muscular dystrophies (Best and Hunter, 2000), the regenerated muscle in normal conditions resembles the undamaged muscle both in morphological and functional state. Several experimental models of muscle injury have been used to study the regeneration of skeletal muscles in a controlled and reproducible manner. These models either use chemical stimuli such as cardiotoxin (CTX) (Czerwinska

et al., 2012), bupivacaine (Nishizawa et al., 2003; Politi et al., 2006) and glycerol (Kawai et al., 1990; Pisani et al., 2010) injection or mechanical models such as freezing injury (Warren et al., 2007), and crush injury (Zimowska et al., 2009). However, the time course and characteristics of muscle regeneration differ according to the type of injury.

Intramuscular connective tissue (IMCT) plays an essential role during muscle growth and regeneration. It provides a skeletal muscle frame for arrangement of muscle fibers, nerves and vessels in addition to effective transmission of contractile force within the muscle. Moreover, changes in the morphology of IMCT will influence the mechanical properties of IMCT as well as the muscle function (Zhao et al., 2008).

Scanning electron microscopy (SEM)-maceration technique is a procedure in which digestion of the muscle fibers using NaOH leaving the endomysial connective tissue to visualize the

* Corresponding author at: Department of Veterinary Anatomy, Faculty of Agriculture, Tottori University, Tottori 680-8553, Tottori, Japan. Tel.: +81 857 31 5419; fax: +81 857 31 5419.

¹ These authors contributed equally to this work.

three-dimensional arrangement of the collagen fibers of IMCT. It helps to analyze the structural changes in the extracellular matrix of skeletal muscle (Gillies et al., 2011). Previous studies examined the changes in IMCT structure during muscle regeneration following strain injury (Stauber et al., 1996), tenotomy and immobilization (Jozsa et al., 1990) using SEM-maceration technique.

In the present study, we used two different types of chemically-induced muscle injury, CTX and glycerol. A recent study compared the regeneration process in glycerol and CTX-injury models by immunohistochemistry and genomic profiling (Lukjanenko et al., 2013). However, to our knowledge, no study had previously compared the changes of IMCT structure during the degeneration and regeneration process following CTX and glycerol injection. The degenerative and regenerative changes seen in chemically-injured models help to study the different events occur in muscular dystrophies. Therefore, the aim of this study was to compare the effect of a single injection of either CTX or glycerol on the process of skeletal muscle regeneration with regard to the structural changes of IMCT.

2. Materials and methods

2.1. Experimental muscle injury

Tibialis anterior (TA) muscles of 8 week old male mice (C3H/HeNjcl) were injected, at the middle part of TA muscle, either with 50 μ l of 10 μ M CTX or 50 μ l of glycerol 50% under anesthesia. The animal care and experimental plan were approved by the Laboratory Animal Care Committee, Hokkaido University and the Animal Research Committee, Tottori University, Japan. Experiments were repeated three times. Mice were sacrificed by cervical dislocation and injured TA muscles were collected at 4, 7, 10 and 14 days after injection (three mice for each time point). Non-injured TA muscles were used as controls.

2.2. Histological analysis of skeletal muscle

Muscles were fixed in 4% paraformaldehyde solution then frozen and cryosectioned. Cryosections were stained with hematoxylin and eosin (HE) for histological analysis. For evaluation of muscle regeneration, the density and the minor axis diameters (smallest diameters) of myotubes were measured using image analysis software (ImageJ; v1.46r, National Institutes of Health, USA). The minor axis diameters of myotubes were measured in three animals per time point and at least 500 myotubes per animal.

For histochemical staining of collagen fibers, muscle sections were stained with Sirius red stain. For quantification of fibrosis, four images of each muscle section, three animals per time point, at 20 \times magnification were chosen randomly and the Sirius red positive area were quantified by Image J after adjusting the threshold and expressed as percentage from the total area (Wang et al., 2013).

2.3. Scanning electron microscopy

Muscles were collected at 2, 4, 7, 10 and 14 days after injection, fixed in 2.5% glutaraldehyde, post fixed in OsO₄ (Merck, Darmstadt, Germany), critical point dried, coated with platinum and observed by SEM (S-800, Hitachi, Tokyo, Japan).

2.4. Transmission electron microscopy

Specimens were fixed in 3% glutaraldehyde overnight at 4 $^{\circ}$ C then post-fixed in 1% OsO₄, dehydrated in a graded series of ethanol, and embedded in epoxy resin (Okenshoji, Tokyo, Japan). Ultrathin sections (70 nm thickness) were cut with PT-X Power Tome ultramicrotome (RMC, Arizona, USA) and stained with uranyl acetate and lead citrate. Tissue sections were examined with JEM-1400

transmission electron microscope (JOEL, Tokyo, Japan) operated at 80 kV.

2.5. Cell maceration/scanning electron microscopy

The structure of the collagen fibers of the injured muscles was evaluated using SEM after preparation using cell maceration technique according to the previous studies (Nishimura et al., 1999; Ohtani et al., 1988), in which the cellular parts of the muscle had been removed leaving the collagen fiber network. Briefly, small pieces of TA muscles were isolated and fixed for 3 days with 2.5% glutaraldehyde in a 0.1 M phosphate buffer solution, pH 7.3, and then immersed in a 10% aqueous solution of NaOH for 4 days, and then rinsed in distilled water for 5 days (NaOH solution and distilled water were changed every 12 h). The samples were fixed in 1% tannic acid for 3 h. After rinsing in distilled water for several hours, the samples were postfixed in 1% aqueous solution of osmium tetroxide for 1 h, and then dehydrated in a series of graded concentrations of ethanol, freeze-fractured in liquid nitrogen, and freeze dried with *t*-butyl alcohol (Inoue and Osatake, 1988). The dried samples were mounted on metal stubs, coated with gold and examined using a scanning electron microscope (S-800, Hitachi) operated at 10 kV.

2.6. Statistical analysis

Data were expressed as means \pm standard deviation (SD). Statistical analysis was performed using SPSS software (IBM SPSS Statistics, version 21). Results were analyzed by one-way analysis of variance (ANOVA) followed by Bonferroni's post hoc test. Statistical significance was defined as $p < 0.05$.

3. Results

3.1. Histological analysis

The present study aims to compare the regeneration process in two different types of chemically-induced injury models; CTX and glycerol.

Myofibers in the non-injured muscles are polygonal in shape with peripheral nuclei (Fig. 1A). Both CTX and glycerol injection induced muscle degeneration with inflammatory cellular infiltration at day 4 post injection (Fig. 1B and C). However, CTX injection induced greater muscle degeneration than glycerol injection; vacuolated myofibers could be seen after CTX injection. Small regenerating myotubes with relatively large central nuclei appeared by day 7 in both models, with enlarged interstitial spaces and presence of inflammatory cellular infiltration (Fig. 1D and E). At day 10, the myotube density was higher in the CTX than the glycerol model; about 2 fold the myotube density in the glycerol model. Moreover, adipocytes infiltration was detected among the regenerated myotubes in the glycerol model only. In contrast, no adipocytes could be detected in the CTX model (Fig. 1F). At day 14, the CTX model showed a greater proportion of regenerated myotubes of varying diameters (Fig. 1H). In contrast, the glycerol model had fewer regenerated myotubes with adipocytes infiltration (Fig. 1I). The myotube density in the CTX model was about 1.1 fold that in the glycerol model. The average diameter was significantly increased at day 14 compared with that at day 7 in both models ($p < 0.05$). The average myotube diameter was significantly larger in the CTX model than in the glycerol model ($p < 0.05$) (Fig. 3A). Moreover, the regenerating myotubes in the CTX model showed better organization compared to those in the glycerol model.

Muscle sections were stained with Sirius red stain to visualize collagen fibers deposition after injury. Collagen fibers deposition increased in response to CTX and glycerol injection (Fig. 2). Although collagen deposition was significantly higher in the CTX

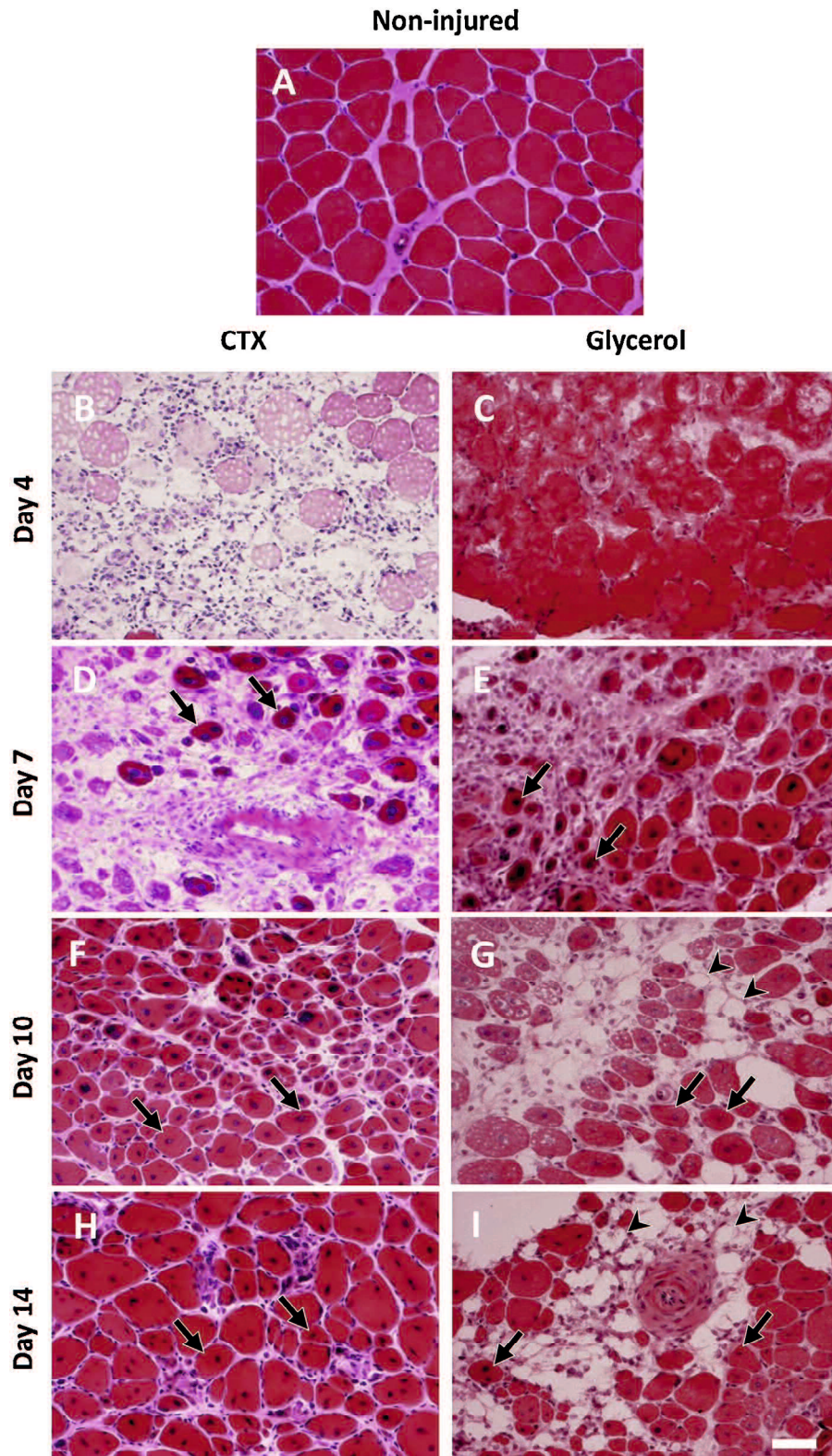


Fig. 1. Morphological changes of TA muscle following either CTX or glycerol injection. (A) Non-injured muscles, (B, D, F and H) CTX-injured muscles and (C, E, G and I) glycerol-injured muscles at 4, 7, 10 and 14 days after injection were stained with HE stain. Regenerating myotubes with central nuclei (arrows) appeared in both models at day 7, while adipocytes (arrowheads) could be detected only in glycerol model, scale bar: 50 μ m.

model than that in the glycerol model at both day 4 and day 7 ($p < 0.05$) (Fig. 3B), it decreased significantly in the CTX model compared to the glycerol model at day 14. On other hand, collagen deposition increased with regeneration in the glycerol model.

3.2. Scanning electron microscopy

To confirm the effect of glycerol on muscle regeneration, glycerol-injured TA muscles were examined with SEM. The

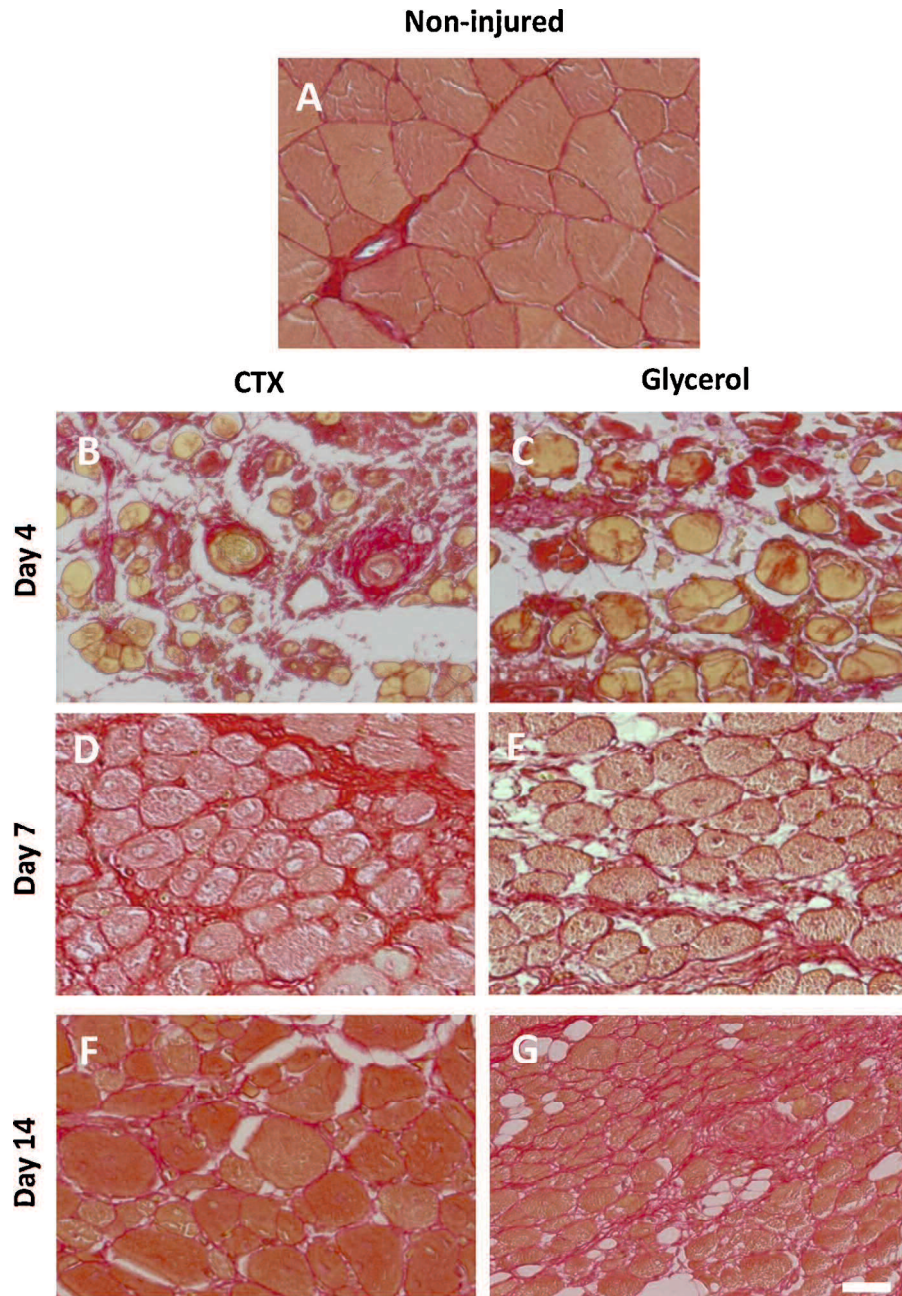


Fig. 2. Histochemical analysis of collagen fiber in TA muscle following either CTX or glycerol injection. (A) Non-injured muscles, (B, D and F) CTX-injured muscles and (C, E and G) glycerol-injured muscles at 4, 7 and 14 days after injection were stained with Sirius red stain, scale bar: 50 μ m.

non-injured muscle showed polygonal shaped myofibers, they were closely arranged to each other. Glycerol-injured muscle showed loss and degradation of myofibers at day 2 and day 4 post injection, the surviving myofibers were disorganized, rounded in shape and have smaller diameters than that in non-injured muscle, in addition to increased extracellular spaces. The myofibers were separated from the endomysial tubes by gaps indicating contraction of the myofibers (data not shown). At day 7, few numbers of small rounded myotubes with small spherical-shaped lipid droplets could be seen between them (Fig. 4B). At day 14, the spaces between the myofibers decreased and being infiltrated with lipid droplets which were surrounded by a membrane and contain fat in amorphous state. Thin delicate reticular fibers were connecting the lipid droplets (Fig. 4C).

3.3. Transmission electron microscopy (TEM)

The non-injured muscle showed myofibers with peripherally located myonuclei under the basal lamina, while the quiescent satellite cell was located between the myofiber and the basal lamina. It had a large nucleus with condensed heterochromatin and little cytoplasm (Fig. 5A). The degenerated myofibers in the CTX-injured muscle showed disintegrated cytoplasm and pyknotic nuclei while the basal lamina was intact (Fig. 5B). Vacuoles of different shapes and sizes lined by single membranes were present in the cytoplasm (Fig. 5C). Inflammatory cells invasion into the myofibers could not be detected. At day 7, myoblasts become close together. Some of the adjacent myoblasts appeared as apparently fused (Fig. 5D). At day 14, some myotubes were in the process of maturation, having both central and peripheral nuclei, while

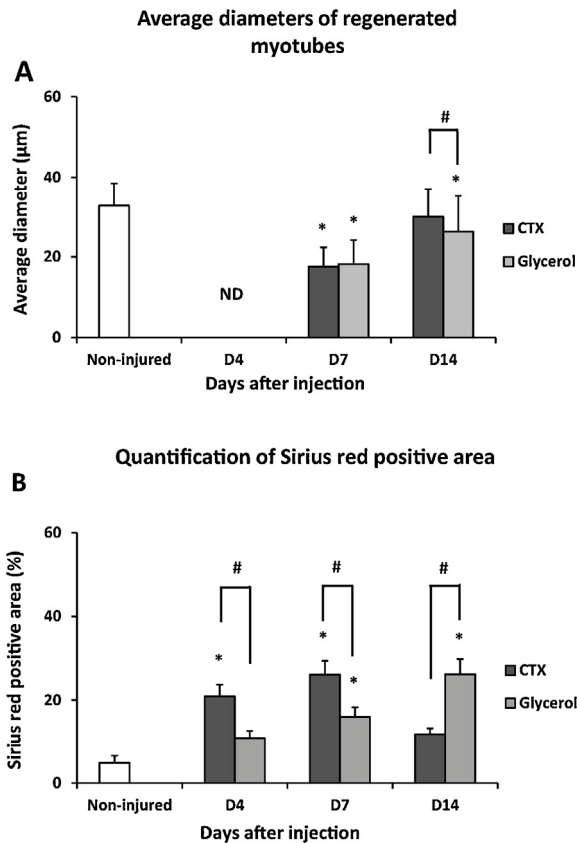


Fig. 3. Morphometric analysis of regenerated muscle following either CTX or glycerol injection. (A) Changes in the diameters of regenerated myotubes at different time points after CTX or glycerol injection. (B) Quantification of Sirius red positive area. Data are expressed as means \pm SD. (ND, not detected, * indicates significant difference from non-injured muscle, # indicates significant difference between two models, $p < 0.05$).

others became matured, having peripheral elongated nuclei. Satellite cells were detected in their original position (Fig. 5E and F).

On other hand, the glycerol-injured muscle showed degenerated myofibers at day 4 post injection. The degenerated myofibers showed amorphous cytoplasm with loss of myofibrils and disruption of the basal lamina. Many mononuclear cells either invade the degenerated myofibers. Most of these cells were macrophages; having ovoid nucleus and cell projections (Fig. 6A and B). At day 7, large number of oval, spindle-shaped and elongated myoblasts could be observed. Each myoblast had a large nucleus with distinct nucleolus but lack myofibrils (Fig. 6C). Few myotubes containing one or more central nuclei and few myofibrils were detected. Adipocytes could be detected between myoblasts and myotubes (Fig. 6D). At day 14, all myotubes had central nuclei and the satellite cells were separated from the myotube by the plasma membrane (Fig. 6E). Fibroblasts were detected between the myotubes (Fig. 6F).

3.4. Three dimensional structure of IMCT

We examined the alteration of the IMCT structure as a response to either CTX or glycerol injection. The TA muscles were prepared by cell-maceration technique to remove all cellular structures leaving the collagen fibers network. SEM micrographs of the non-injured muscle showed endomysial connective tissue surrounding empty tubular structures that were occupied by myofibers before maceration, they have polygonal shapes and arranged in a honeycomb structure (Fig. 7A). At day 4, the CTX-injured muscle showed alteration of the honeycomb structure, the endomysial tubes have

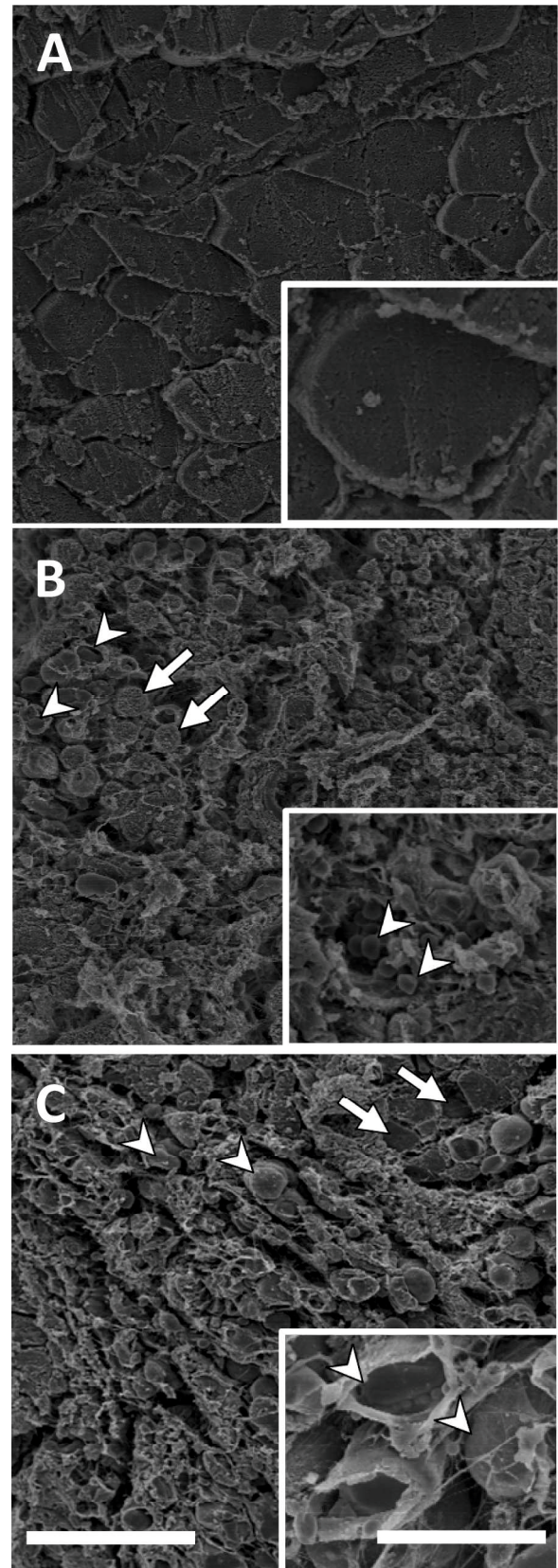


Fig. 4. SEM micrograph of glycerol-injured muscle. (A) Non-injured and (B and C) glycerol-injured TA muscle at 7 and 14 days post injection. Inset showing higher magnification. Regenerating myotubes (arrows) were infiltrated with adipocytes (arrowheads), scale bar: 100 μ m, inset scale bar: 30 μ m.

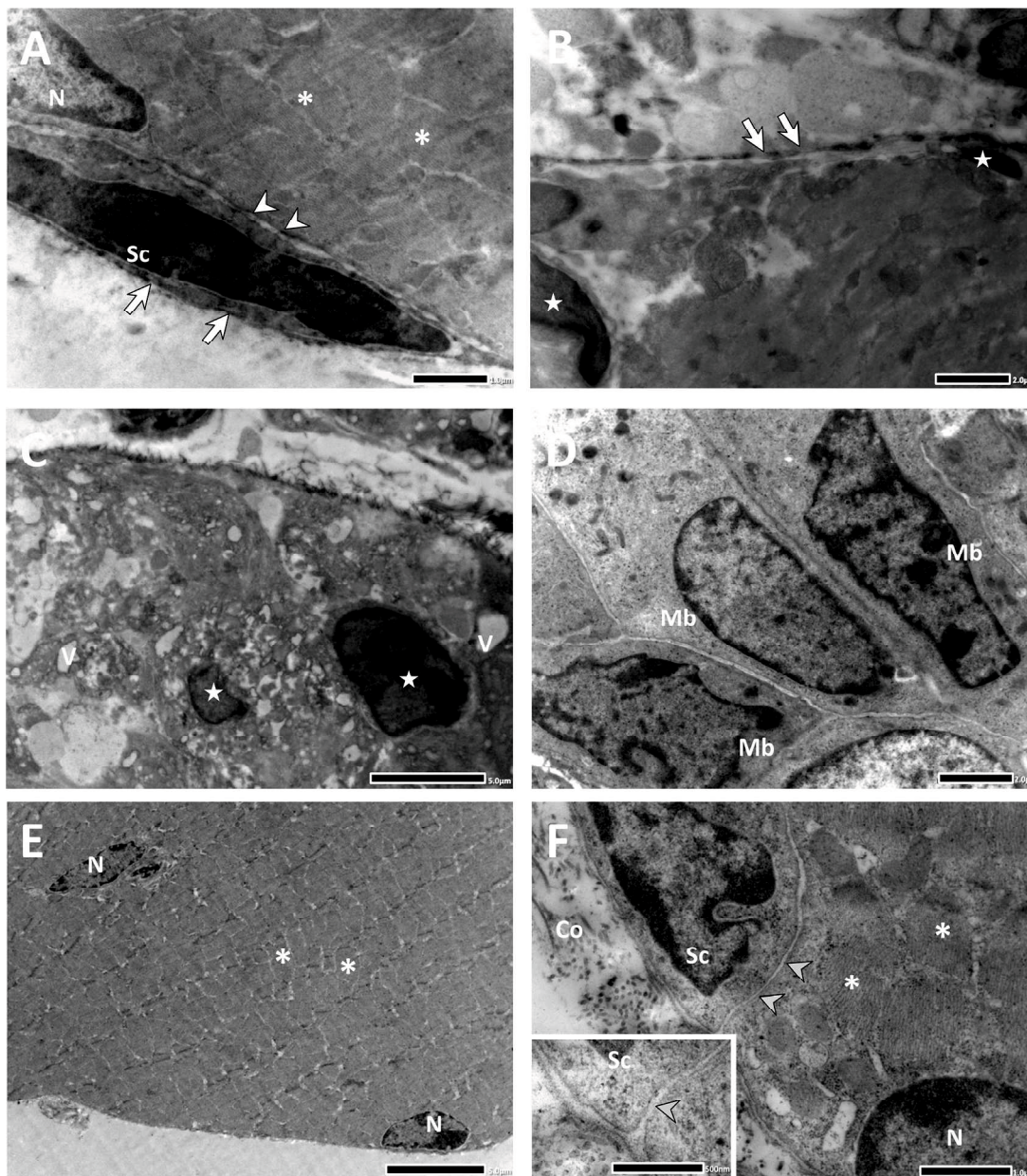


Fig. 5. TEM analysis of muscle regeneration following CTX injury. (A) Non-injured muscle with peripheral nucleus (N), normal myofibrils (asterisks) and satellite cell (Sc) was located under basal lamina (arrows) and separated from myofiber by plasma membrane (arrowheads), (B and C) degenerated myofiber at day 4 showed disintegrated cytoplasm and pyknotic nucleus (star), intact basal lamina (arrows), cytoplasmic vacuoles (V), (D) regenerative changes at day 7 showed myoblasts (Mb) appear as apparently fused, (E and F) regenerated muscle at day 14 showed myotube in the process of maturation with central and peripheral nuclei (N), and mature myofiber with peripheral nucleus (N), normal myofibrils (asterisk), connective tissue (Co), and satellite cell (Sc) in normal position separated from myotube by plasma membrane (arrowhead), inset showing higher magnification.

varying sizes and shapes with an increase in the endomysial connective tissue, it appear as wavy sheets (Fig. 7B) while the glycerol-injured muscle showed loss of the honey comb structure with disruption of the endomysial connective tissue, the collagen fibers were irregular and had mushy-shape with few number of endomysial tubes (Fig. 7C). At day 7, the CTX-injured muscle restored the honey comb appearance but with an increase in perimysial and endomysial connective tissue with marked fibrosis around blood vessels (Fig. 7D), while the glycerol-injured muscle showed appearance of small number of endomysial tubes indicating muscle regeneration (Fig. 7E). The thickness of the endomysial sheath was decreased in CTX-injured muscle up to day 14 (Fig. 7F and H), but the endomysium still thicker at day 14 than the normal level. On the other hand, the glycerol-injured muscle showed

large number of endomysial tubes of varying diameters with spaces between them, these spaces comprise the collagen fibril baskets remained after dissolving of adipocytes during sample preparation. The endomysial connective tissue was thinner than that of CTX-injured muscle at day 10 and 14 but was slightly thicker than the control level (Fig. 7G and I).

4. Discussion

The present study aims to compare the regeneration process of mice TA muscle after two different types of chemically-induced injuries; CTX and glycerol, with regard to the structural changes of IMCT and its effect on the process of muscle regeneration in these injury models.

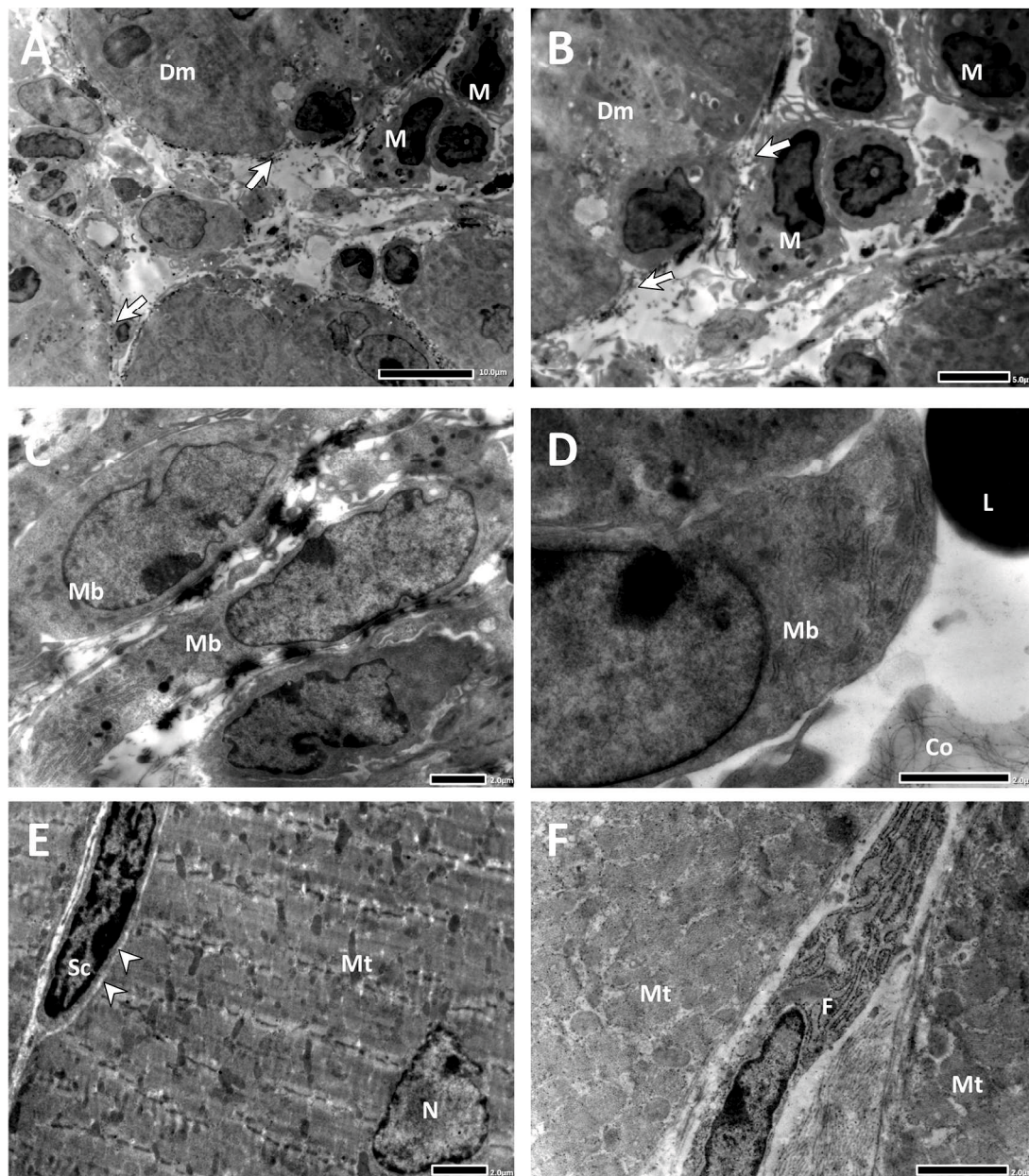


Fig. 6. TEM analysis of muscle regeneration following glycerol injury. (A and B) Degenerated myofiber (Dm) at day 4 was invaded by macrophages (M) through the disrupted basal lamina, (C and D) regenerative changes at day 7 showed elongated myoblasts (Mb) in close contact with connective tissue (Co), and lipid droplet (L), (E and F) immature myotubes at day 14 showing myotube (Mt) with central nucleus (N) and satellite cell (Sc) in normal position separated from myotube by plasma membrane (arrowhead), fibroblast (F) and connective tissue (Co).

The pathological events seen in CTX-injured model resemble those seen in muscular dystrophies and inflammatory myopathies (Ramadasan-Nair et al., 2014). Moreover, the glycerol-injured model showed similar degenerative changes to those seen in Duchenne Muscular Dystrophy (DMD) (Kawai et al., 1990). Therefore, studying muscle fibrosis in normal, non-dystrophic, mice will help understanding the mechanism, cells and factors that play role in fibrosis development (Pessina et al., 2014), and consequently help in development of new therapies to compete skeletal muscle fibrosis.

Our results showed that both CTX and glycerol injection induced muscle degeneration followed by regeneration. Although muscle regeneration started at day 7 post injection in both models, our morphometrical analysis showed better regeneration in the CTX-injured model than the glycerol-injured one which was indicated

by a greater number of regenerated myotubes, larger diameters and better organization than in the glycerol-injured model at day 14 post injection. This result is in agreement with the result of the previous study (Lukjanenko et al., 2013). The difference in regeneration between the two injury models may be due to their different effects on muscle, it was reported that injury models with minimum disruption to the basal lamina show better regeneration than injury models that destroy the basal lamina (Sanes, 2003). Ultrastructural analysis of injured muscles showed a significant difference between damaged myofibers in the two models; the glycerol-injured muscle showed amorphous cytoplasm and disruption of the basal lamina with invasion of macrophages into degenerated myofiber while the CTX-injured muscle showed disintegrated cytoplasm, pyknotic nuclei and intact basal lamina with no invasion of macrophages into the myofibers. Our results are in agreement of those of

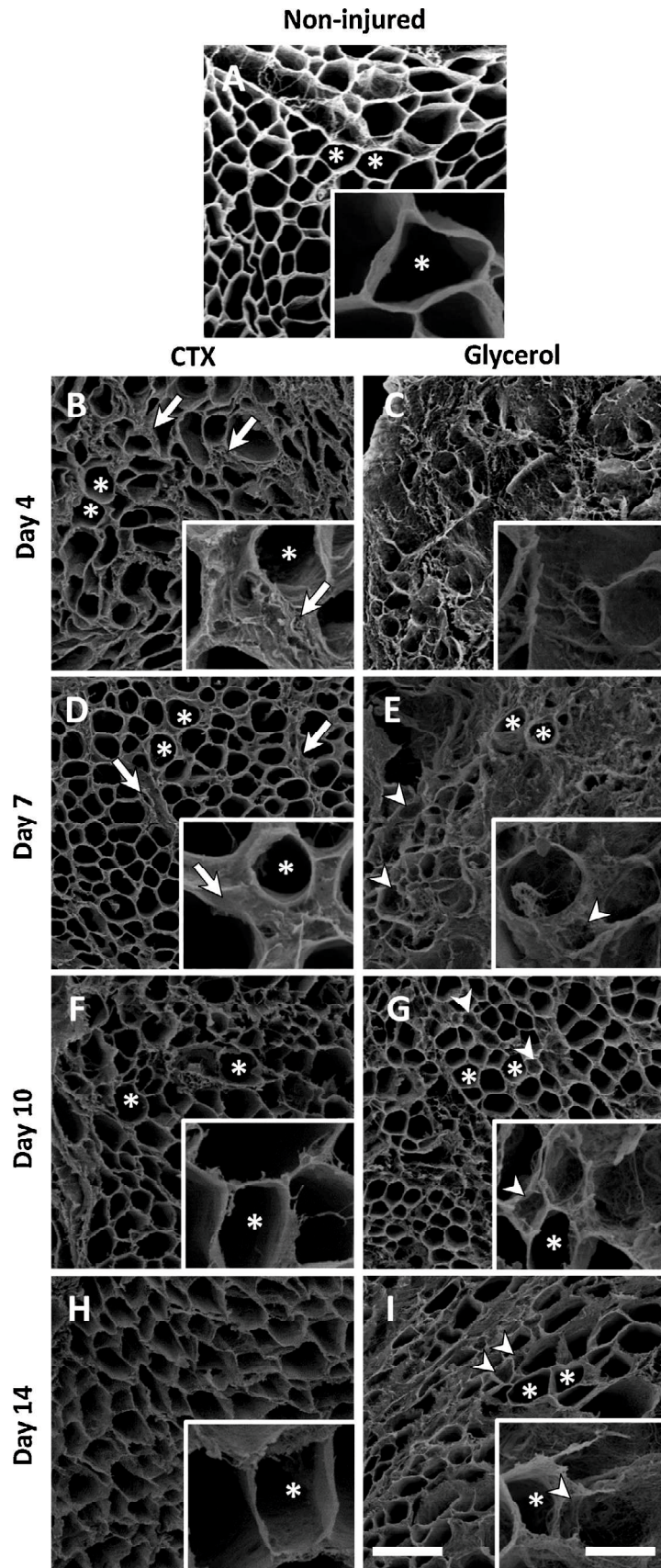


Fig. 7. Structural changes of the IMCT of macerated TA muscle following either CTX or glycerol injection. (A) Non-injured, (B, D, F and H) CTX-injured muscles and (C, E, G and I) glycerol-injured muscles at 4, 7, 10 and 14 days post injection. Endomysial collagen (arrows) surrounding endomysial tubes (asterisks). Collagen baskets of adipocytes (arrow heads) could be observed in glycerol model but not in CTX model. Inset showing higher magnification. Scale bar: 100 μm , inset scale bar: 30 μm .

previous studies which reported that CTX induces muscle fiber necrosis and degeneration leaving the basal lamina intact (Harris, 2003), while glycerol disrupts the basal lamina (Kawai et al., 1990). Our SEM findings confirm the before mentioned results, the endomysial tubes were preserved after CTX injection while they were destroyed after glycerol injection. Moreover, CTX injection stimulates neovascularization of the injected muscle (Vignaud et al., 2007), as a proper blood supply improve myofiber regeneration (Wang et al., 2013).

The present study revealed an impaired regeneration following glycerol injury, which was indicated by greater adipocyte infiltration compared with that following CTX injury, while no adipocytes infiltration could be detected in CTX model. Ectopic adipocytes were detected in skeletal muscle following glycerol injection (Kawai et al., 1990; Lukjanenko et al., 2013; Pisani et al., 2010), glycerol affects the macrophages function negatively resulting in both fat deposition and delayed regeneration (Pisani et al., 2010). Injured muscle with CTX (Liu et al., 2012) and Notexin (Lee et al., 2013) showed good regeneration with the absence of adipocytes in young mice, in contrast, poor regeneration with adipocyte infiltration was detected in old mice. Moreover, the mouse strain plays a role in fat deposition following CTX injection; no adipocyte was detected in C57BL/6 mice either after single or repeated injections, while fat accumulation was detected after repeated CTX injections (in BALB/c, C3H/HeN and DBA/2 mice strains) but could not be detected in any examined mice strain following single injections (Fukada et al., 2010), this result supports the results of the present study.

Our results showed an increased endomysial connective tissue in CTX-injured muscle in the early stages of regeneration that decreased at later stages, but did not return to the control level. Our results are in agreement with those of Pessina and colleagues who reported mild and transient fibrosis following CTX injury (Pessina et al., 2014), and the results of Murphy and colleagues who reported that interactions between fibroblasts and satellite cells are essential for muscle regeneration; positive fibroblast–satellite interactions in early stages stimulate regeneration followed by suppression of fibroblasts activity at later stages to decrease fibrosis (Murphy et al., 2011). Moreover, the regenerating myofibers produce transforming growth factor- β 1 (TGF- β 1) at early time points after CTX injury, TGF- β 1 stimulate the differentiation of myoblasts into myofibroblasts (Li et al., 2004), a marked expression of alpha-smooth actin, a marker of activated myofibroblasts, was detected 10 days post CTX-injury (Pelosi et al., 2007).

In conclusion, our study showed a significant difference during the process of degeneration and regeneration between CTX-injured muscle and the glycerol-injured one. Moreover, adipocyte infiltration in glycerol-injured muscle persists up to 14 days post injection, on the contrary, no adipocytes were detected in CTX-injured muscle. It seems that a transient increase in IMCT at the early stages stimulate muscle regeneration in the CTX-injured model, on the contrary, adipocyte infiltration impaired muscle regeneration in the glycerol-injured model. Future studies are required to clarify the factors correlated with changes in the connective tissue structure during muscle regeneration. To our knowledge, this is the first study to compare the regeneration process following CTX and glycerol injury using cell-maceration technique.

Acknowledgements

This study was supported by JSPS/MEXT KAKENHI Grant numbers 24658222 and 24248045. M. A. A. Mahdy was supported by a scholarship (no. 2–2010/2011) from the Egyptian Government to obtain PhD degree.

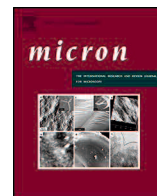
Appendix A. Supplementary data

Supplementary material related to this article can be found, in the online version, at <http://dx.doi.org/10.1016/j.aanat.2015.07.002>.

References

- Best, T.M., Hunter, K.D., 2000. Muscle injury and repair. *Phys. Med. Rehabil. Clin. N. Am.* 11, 251–266.
- Czerwinska, A.M., Stremimska, W., Ciemerych, M.A., Grabowska, I., 2012. Mouse gastrocnemius muscle regeneration after mechanical or cardiotoxin injury. *Folia Histochem. Cytobiol.* 50, 144–153.
- Fukada, S., Morikawa, D., Yamamoto, Y., Yoshida, T., Sumie, N., Yamaguchi, M., et al., 2010. Genetic background affects properties of satellite cells and mdx phenotypes. *Am. J. Pathol.* 176, 2414–2424.
- Gillies, A.R., Smith, L.R., Lieber, R.L., Varghese, S., 2011. Method for decellularizing skeletal muscle without detergents or proteolytic enzymes. *Tissue Eng. C: Methods* 17, 383–389.
- Harris, J.B., 2003. Myotoxic phospholipases A2 and the regeneration of skeletal muscles. *Toxicol.* 42, 933–945.
- Inoue, T., Osatake, H., 1988. A new drying method of biological specimens for scanning electron microscopy: the *t*-butyl alcohol freeze-drying method. *Arch. Histol. Cytol.* 51, 53–59.
- Jozsa, L., Kannus, P., Thoring, J., Refly, A., Jarvinen, M., Kvist, M., 1990. The effect of tenotomy and immobilisation on intramuscular connective tissue. A morphometric and microscopic study in rat calf muscles. *J. Bone Joint Surg. Br.* 72, 293–297.
- Kawai, H., Nishino, H., Kusaka, K., Naruo, T., Tamaki, Y., Iwasa, M., 1990. Experimental glycerol myopathy: a histological study. *Acta Neuropathol.* 80, 192–197.
- Lee, A.S., Anderson, J.E., Joya, J.E., Head, S.I., Pather, N., Kee, A.J., et al., 2013. Aged skeletal muscle retains the ability to fully regenerate functional architecture. *Bioarchitecture* 3, 25–37.
- Li, Y., Foster, W., Deasy, B.M., Chan, Y., Prisk, V., Tang, Y., et al., 2004. Transforming growth factor- β 1 induces the differentiation of myogenic cells into fibrotic cells in injured skeletal muscle: a key event in muscle fibrogenesis. *Am. J. Pathol.* 164, 1007–1019.
- Liu, W., Liu, Y., Lai, X., Kuang, S., 2012. Intramuscular adipose is derived from a non-Pax3 lineage and required for efficient regeneration of skeletal muscles. *Dev. Biol.* 361, 27–38.
- Lukjanenko, L., Brachet, S., Pierrel, E., Lach-Trifileff, E., Feige, J.N., 2013. Genomic profiling reveals that transient adipogenic activation is a hallmark of mouse models of skeletal muscle regeneration. *PLoS ONE* 8, e71084.
- Murphy, M.M., Lawson, J.A., Mathew, S.J., Hutcheson, D.A., Kardon, G., 2011. Satellite cells, connective tissue fibroblasts and their interactions are crucial for muscle regeneration. *Development* 138, 3625–3637.
- Nishimura, T., Hattori, A., Takahashi, K., 1999. Structural changes in intramuscular connective tissue during the fattening of Japanese black cattle: effect of marbling on beef tenderization. *J. Anim. Sci.* 77, 93–104.
- Nishizawa, T., Tamaki, H., Kasuga, N., Takekura, H., 2003. Degeneration and regeneration of neuromuscular junction architecture in rat skeletal muscle fibers damaged by bupivacaine hydrochloride. *J. Muscle Res. Cell Motil.* 24, 527–537.
- Ohtani, O., Ushiki, T., Taguchi, T., Kikuta, A., 1988. Collagen fibrillar networks as skeletal frameworks: a demonstration by cell-maceration/scanning electron microscope method. *Arch. Histol. Cytol.* 51, 249–261.
- Pelosi, L., Giacinti, C., Nardis, C., Borsellino, G., Rizzuto, E., Nicoletti, C., et al., 2007. Local expression of IGF-1 accelerates muscle regeneration by rapidly modulating inflammatory cytokines and chemokines. *FASEB J.* 21, 1393–1402.
- Pessina, P., Cabrera, D., Morales, M.G., Riquelme, C.A., Gutierrez, J., Serrano, A.L., et al., 2014. Novel and optimized strategies for inducing fibrosis in vivo: focus on Duchenne Muscular Dystrophy. *Skelet. Muscle* 4, 7.
- Pisani, D.F., Bottema, C.D., Butori, C., Dani, C., Dechesne, C.A., 2010. Mouse model of skeletal muscle adiposity: a glycerol treatment approach. *Biochem. Biophys. Res. Commun.* 396, 767–773.
- Politi, P.K., Havaki, S., Manta, P., Lyritis, G., 2006. Bupivacaine-induced regeneration of rat soleus muscle: ultrastructural and immunohistochemical aspects. *Ultrastruct. Pathol.* 30, 461–469.
- Ramadasan-Nair, R., Gayathri, N., Mishra, S., Sunitha, B., Mythri, R.B., Nalini, A., et al., 2014. Mitochondrial alterations and oxidative stress in an acute transient mouse model of muscle degeneration: implications for muscular dystrophy and related muscle pathologies. *J. Biol. Chem.* 289, 485–509.
- Sanes, J.R., 2003. The basement membrane/basal lamina of skeletal muscle. *J. Biol. Chem.* 278, 12601–12604.
- Stauber, W.T., Knack, K.K., Miller, G.R., Grimmett, J.C., 1996. Fibrosis and intercellular collagen connections from four weeks of muscle strains. *Muscle Nerve* 19, 423–430.
- Vignaud, A., Hourde, C., Butler-Browne, G., Ferry, A., 2007. Differential recovery of neuromuscular function after nerve/muscle injury induced by crude venom from *Notechis scutatus*, cardiotoxin from *Naja atra* and bupivacaine treatments in mice. *Neurosci. Res.* 58, 317–323.

- Wang, R., Luo, D., Xiao, C., Lin, P., Liu, S., Xu, Q., et al., 2013. The time course effects of electroacupuncture on promoting skeletal muscle regeneration and inhibiting excessive fibrosis after contusion in rabbits. *Evid. Based Complement. Alternat. Med.* 2013, 16.
- Warren, G.L., Summan, M., Gao, X., Chapman, R., Hulderman, T., Simeonova, P.P., 2007. Mechanisms of skeletal muscle injury and repair revealed by gene expression studies in mouse models. *J. Physiol.* 582, 825–841.
- Zhao, L., Xu, S.J., Sun, X.T., 2008. Injury and regeneration of intramuscular connective tissue subjected to various regimes of distraction. *Chin. J. Traumatol.* 11, 67–71.
- Zimowska, M., Duchesnay, A., Dragun, P., Oberbek, A., Moraczewski, J., Martelly, I., 2009. Immunoneutralization of TGF- β 1 improves skeletal muscle regeneration: effects on myoblast differentiation and glycosaminoglycan content. *Int. J. Cell Biol.* 2009 (659372).



Early ultrastructural events of skeletal muscle damage following cardiotoxin-induced injury and glycerol-induced injury



Mohamed A.A. Mahdy^{a,b,1}, Katsuhiko Warita^{a,b}, Yoshinao Z. Hosaka^{a,b,*}

^a Laboratory of Basic Veterinary Science, United Graduate School of Veterinary Science, Yamaguchi University, Yamaguchi, Japan

^b Department of Veterinary Anatomy, Faculty of Agriculture, Tottori University, Tottori, Japan

ARTICLE INFO

Article history:

Received 2 August 2016

Received in revised form

27 September 2016

Accepted 27 September 2016

Available online 28 September 2016

Keywords:

Basal lamina

Cardiotoxin (CTX)

Glycerol injury

Satellite cells

Ultrastructure

ABSTRACT

In this study, we investigated the early changes of skeletal muscle damage in response to injuries induced by cardiotoxin (CTX) and glycerol by using both light microscopy and transmission electron microscopy. Normal, non-dystrophic, adult male mice were used in this study. Tibialis anterior (TA) muscles were injected either with CTX or glycerol. Samples were collected at intervals starting from 1 h up to 4 days after injury. Injured muscles were subjected to both histological and ultrastructural analyses. CTX-induced injury caused mitochondrial accumulation and swelling followed by lysis, while glycerol-induced injury caused accumulation of vesicles with focal disruption of the basal lamina, indicating that the injuries have different mechanisms of damage to myofibers. Moreover, inflammatory cells, including neutrophils and macrophages, were recruited earlier and in larger numbers after CTX-induced injury than after glycerol-induced injury. On the other hand, satellite cells (SCs) activation started at 6 h after both injuries, as indicated by an increase in both the length and cytoplasmic-to-nuclear ratio. However, there were significantly longer SCs with a higher cytoplasmic-to-nuclear ratio in the CTX-injured muscles than in the glycerol-injured muscles at day 4. In conclusion, our results demonstrated a difference between CTX and glycerol in their damage to myofibers; CTX damages myofiber mitochondria, while glycerol damages the myofiber cell membrane and alters osmosis. In addition, CTX-induced injury caused earlier and more extensive inflammatory infiltration than did glycerol-induced injury. This study is the first study to shed light on the early events following skeletal muscle injury induced by CTX and glycerol.

© 2016 Elsevier Ltd. All rights reserved.

1. Introduction

Skeletal muscle has a notable capacity for regeneration in response to various types of injury and disease (Yan et al., 2003). The healing process of an injured muscle consists mainly of three phases: the destruction phase, characterized by degeneration of myofibers and inflammatory reaction, followed by the repair phase, characterized by removal of necrosed tissue, regeneration of myofibers and scar formation, and finally the remodeling phase, characterized by maturation of regenerated myofibers and reorganization of scar tissue (Jarvinen et al., 2005). The efficiency of

muscle repair is affected by the extent of muscle damage and the interactions between muscle and the recruited inflammatory cells (Karakaki et al., 2009).

The development of an experimental animal model is necessary to study muscle regeneration in a controlled and reproducible manner (Horie et al., 2014). Different experimental models of muscle injury have been used to investigate skeletal muscle regeneration. These models include chemical models such as barium chloride injection (Hardy et al., 2016) and bupivacaine injection (Oz Gergin et al., 2015), injection of a myotoxic agent such as cardiotoxin (CTX) (Hardy et al., 2016), and glycerol injection (Kawai et al., 1990) and mechanical models such as freezing injury (Hardy et al., 2016). However, the nature of the injury model affects the cellular events that occur in response to the injury (Musarò, 2014).

Glycerol-induced injury is a novel model to induce muscle adipogenesis (Pisani et al., 2010; Uezumi et al., 2010). Injection of glycerol induces similar degenerative changes to those in patients with Duchenne Muscular Dystrophy (Kawai et al., 1990). On the other hand, CTX-induced injury produces similar degener-

* Corresponding author at: Department of Veterinary Anatomy, Faculty of Agriculture, Tottori University, Tottori 680-8553, Japan.

E-mail addresses: drmohamedhady@yahoo.com (M.A.A. Mahdy), waritak@muses.tottori-u.ac.jp (K. Warita), y-hosa@muses.tottori-u.ac.jp (Y.Z. Hosaka).

¹ Permanent address: Department of Anatomy and Embryology, Faculty of Veterinary Medicine, South Valley University, Qena, Egypt.

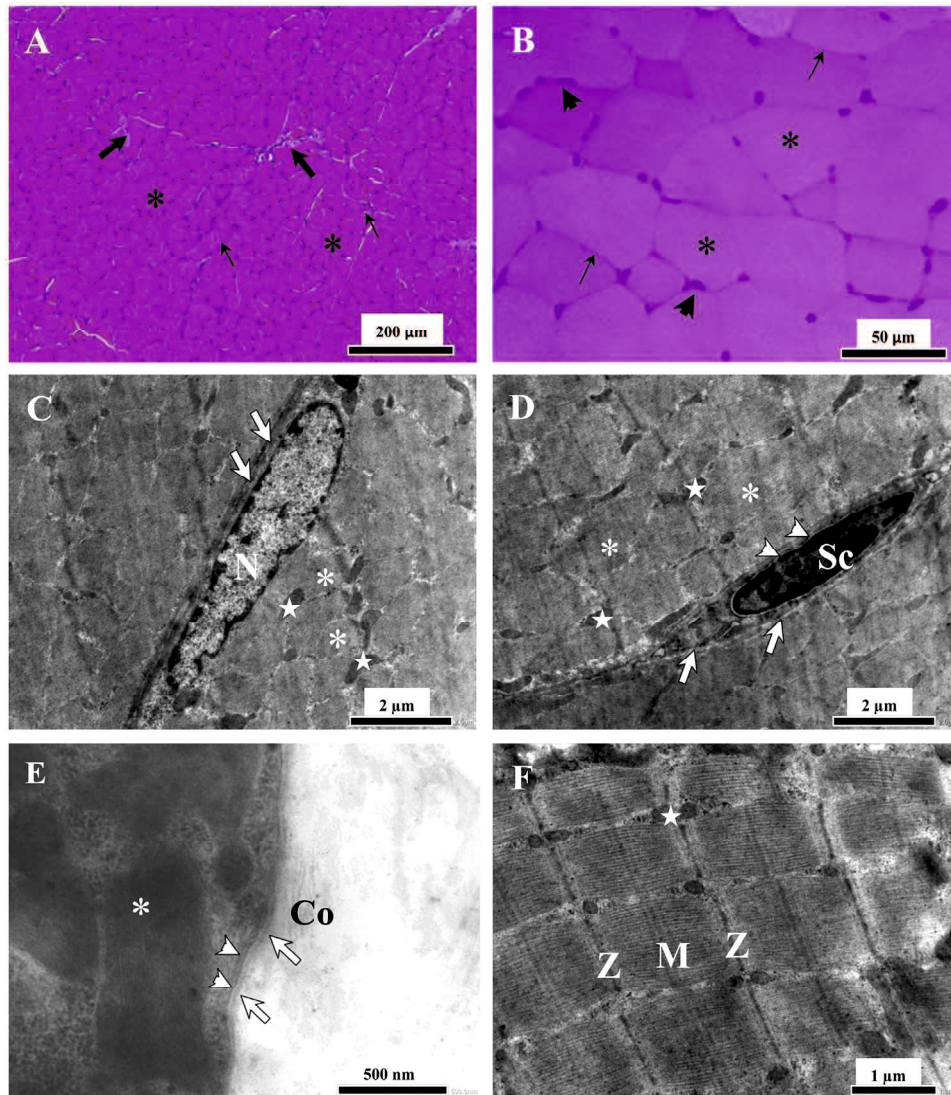


Fig. 1. Morphologic structure of non-injured muscle. (A and B) Light micrograph, HE stain, showing normal morphology of muscle. Myofibers (asterisk) with peripheral nuclei (arrowhead) were closely arranged. Each myofiber was surrounded by endomysium (thin arrow) while muscle fascicle was surrounded by perimysium (thick arrow). (B) TEM micrograph showing peripheral nucleus (N) lying under the basal lamina (arrows), closely arranged myofibrils (asterisk) and mitochondria (star). (C) Quiescent satellite cell (Sc) with a heterochromatic nucleus lying under the basal lamina and separated from the myofiber by the plasma membrane (arrowheads). (D) Outer basal lamina (arrows) and inner plasma membrane (arrowheads), myofibrils (asterisk) and collagen fibers (Co). (E) Longitudinal sections of normal sarcomeres showing Z-line (Z) and M-band (M).

ative changes to those in muscular dystrophies and inflammatory myopathies (Ramadasan-Nair et al., 2014). Therefore, CTX-induced injury and glycerol-induced injury were chosen for this study.

Although the use of markers for different cell types provides valuable information, ultrastructural analysis provides better results according to the structural characteristics of the cells. Therefore, electron microscopy is used as a tool to study muscle pathologies as myopathies and results of electron microscopy are useful for understanding the pathological mechanisms of numerous muscular diseases and are useful as a guide for genetics analysis (Fernandez et al., 2005). In our previous study, we compared muscle regeneration following CTX-induced injury and that following glycerol-induced injury, and we found that muscle regeneration is more efficient after CTX-induced injury. It has also been reported that glycerol induced progressive fibrosis with adipocyte infiltration (Mahdy et al., 2015). Recently, it was reported that the outcome of the regeneration process is influenced by the early phase after

injury (Hardy et al., 2016). Ultrastructural changes were studied after glycerol-induced injury in rabbits (Kawai et al., 1990) and after injury induced by injection of 3 local anesthetics, levobupivacaine, bupivacaine and ropivacaine, in rat skeletal muscles previously (Oz Gergin et al., 2015). In the present study, we compared the early changes following CTX-induced injury and glycerol-induced injury by light and transmission electron microscopy (TEM) in order to clarify the different events that take place in response to these injuries and also to determine the relationship between these events and the difference in regeneration between the two models. We found that the targets of injury and the mechanisms by which muscle injury is induced are different in the two models. The time sequence and degree of immune cell infiltration were also different. To our knowledge, this is the first study in which early events following skeletal muscle injury induced by CTX and glycerol were compared.

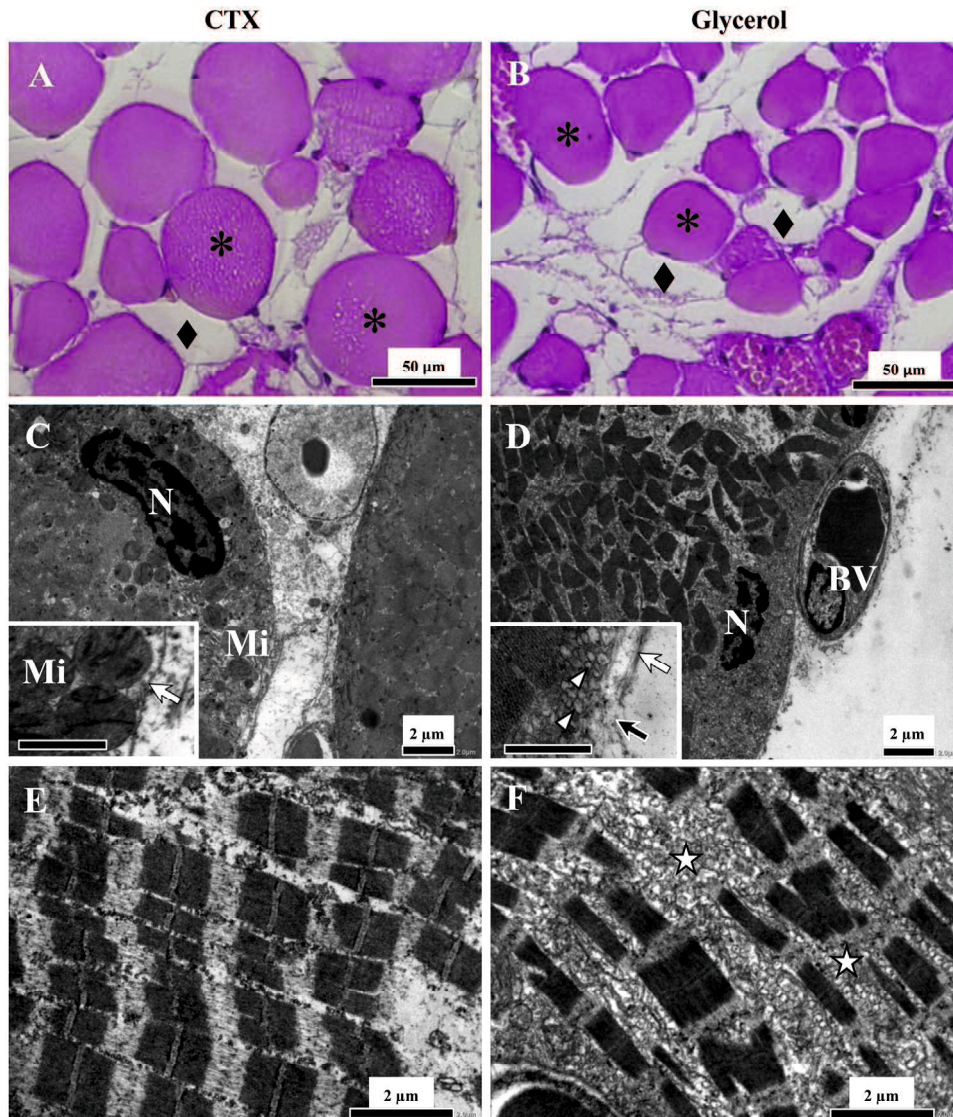


Fig. 2. Changes of TA muscle at 1 h after CTX-induced injury and glycerol-induced injury. (A and B) Light micrographs, HE stain, showing CTX-injured and glycerol-injured muscles, respectively. Note myofiber swelling (asterisk) and ghost fiber (rhombus). (C and E) TEM micrographs of CTX-injured muscle and (D and F) glycerol-injured muscle showing the nucleus (N), mitochondria (Mi), blood vessel (BV), basal lamina (white arrow), focal disruption of the basal lamina (black arrow) and subsarcolemmal vesicles (arrowhead). Note loss of the Z-line and accumulation of vesicles between myofibrils (star). Inset shows higher magnification, inset scale bar = 1 μm .

2. Material and methods

2.1. Animals and ethics approval

Animal experiments were performed using normal male C3H/HeN mice at 8 weeks of age with body weights of about 20–24 g (CLEA Japan, Tokyo, Japan). The animals were kept in the Experimental Animal Facility of Tottori University, Japan under controlled temperature, light and humidity. Animal care and experimental protocols were approved by the Animal Research Committee, Tottori University, Japan (Approval number: 15-T-24).

2.2. Induction of muscle injury in vivo

Mice were anesthetized with an intraperitoneal injection of pentobarbital sodium [0.02 mg/body weight (g)]. The anterolateral aspect of the left hind limb was shaved and the skin was disinfected.

Then 50 μl of either 10 μM CTX² (Sigma-Aldrich, St. Louis, MO, USA) or 50% glycerol (v/v) (Wako, Osaka, Japan) in sterile phosphate-buffered saline (PBS; pH 7.4) was injected along the length of the left tibialis anterior (TA) muscle as previously described (Mahdy et al., 2015). Each animal was kept on a heating pad at approximately 38 °C to maintain body temperature until full recovery.

Mice were sacrificed by cervical dislocation after inhalation anesthesia with isoflurane (Intervet, Tokyo, Japan). Injured TA muscles were collected at different time points (1, 6, 12, 24 h and 4 days post injury), and samples were taken from three animals at each time point. The collected samples were divided into two halves for histological assessment and transmission electron microscopy. Non-injured muscles in the right legs were collected as controls.

² CTX used in this study was from *Naja mossabica*, product number (C9759). According to Sigma website, it is a discontinued product. An alternative is CTX from *Naja pallida* (Latoxan, France) product number (L8102).

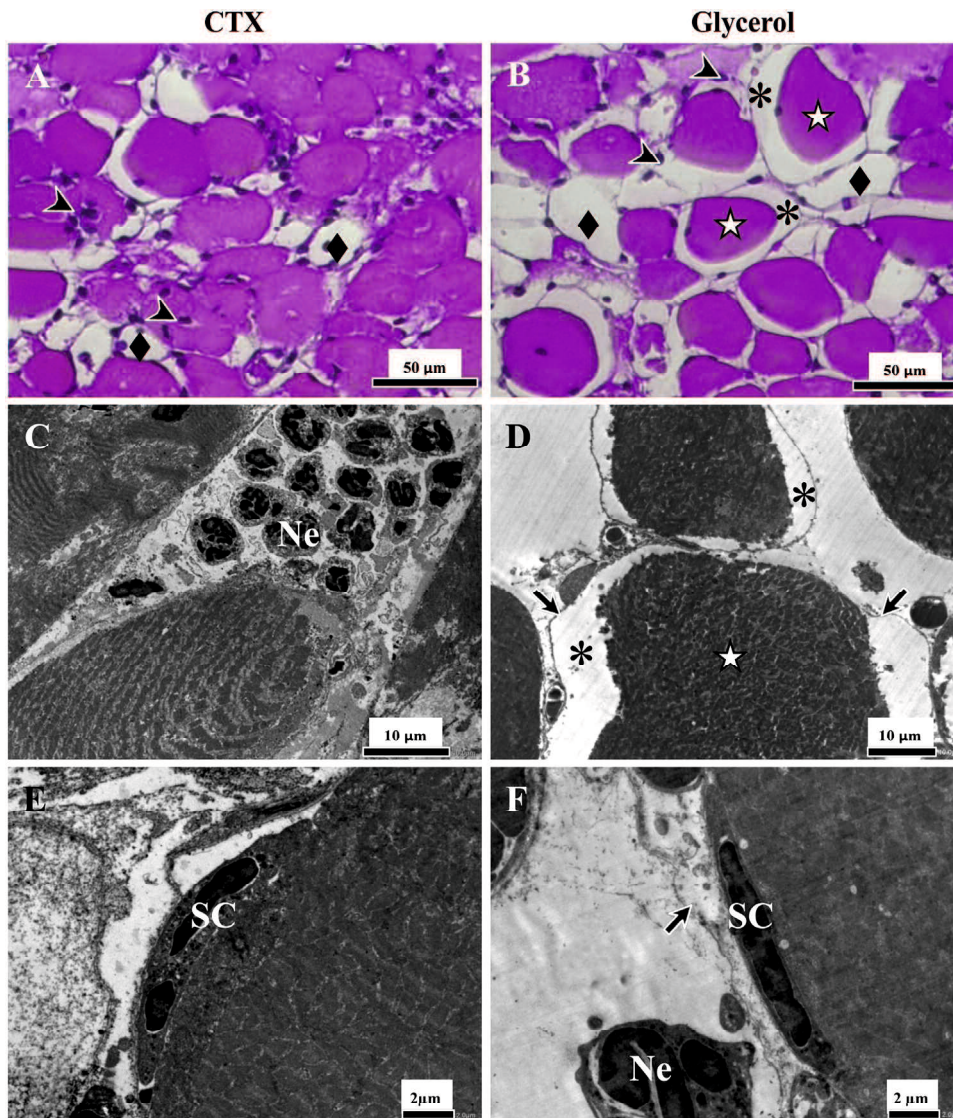


Fig. 3. Changes of TA muscle at 6 h after CTX-induced injury and glycerol-induced injury. (A and B) Light micrographs, HE stain, showing mononuclear cells (arrowheads) and hypercontracted myofibers (star) with a gap (asterisk) between the myofiber and the outer membrane, and ghost fiber (rhombus). (C and E) TEM micrographs of CTX-injured muscle and (D and F) glycerol-injured muscle showing neutrophils (Ne) and satellite cells (SC). Note myofiber hypercontraction (star) in glycerol-injured muscle leaving a gap (asterisk) between the cytoplasm and the outer undulating basal lamina (black arrows).

2.3. Histological assessment of muscle injury

Paraffin sections (5 μm in thickness) were obtained and stained with hematoxylin and eosin (HE) for histological evaluation. Representative images were taken with a digital camera (DP71, Olympus, Tokyo, Japan) attached to a microscope (Olympus IX71).

2.4. Transmission electron microscopy

Muscle specimens were fixed in 3% glutaraldehyde (Wako) overnight at 4 $^{\circ}\text{C}$ (Li et al., 2009) and post-fixed for one hour in 1% OsO₄ (Merck, Darmstadt, Germany), dehydrated in ethanol (Wako), and embedded in rubber molds with epoxy resin (Okenshoji, Tokyo, Japan) and then polymerized in an oven at 60 $^{\circ}\text{C}$. Semithin sections (1 μm in thickness) were cut using a PT-X Power Tome Ultramicrotome (RMC, Arizona, USA) and stained with toluidine blue (Merck), and then ultrathin sections (70 nm in thickness) were cut and mounted on coated copper grids (Nisshin EM, Tokyo, Japan) and double-stained with 2% uranyl acetate (Merck) and lead cit-

rate (Wako). Tissue sections were examined with a JEM-1400 TEM (JOEL, Tokyo, Japan) with an accelerating voltage of 80 Kv.

2.5. Morphometric analysis

For morphometric analysis, three animals/time point were used and five representative blocks/animal were chosen for ultrathin sectioning. About 3–5 ultrathin sections/block were examined and photographed. 50 images of satellite cells (SCs)/time point were used for morphometric measurements using Image-J software, v1.46r (National Institutes of Health, Maryland, USA). To quantitatively follow SC activation, SC length was measured and the nuclear-cytoplasmic ratio was calculated (Gregory and Mars, 2004).

2.6. Immunohistochemistry (IHC)

Paraffin sections were permeabilized with 0.5% Triton X-100 (Nacalai, Kyoto, Japan). Endogenous peroxidase activity was eliminated with 3% hydrogen peroxide (Wako) in distilled water for

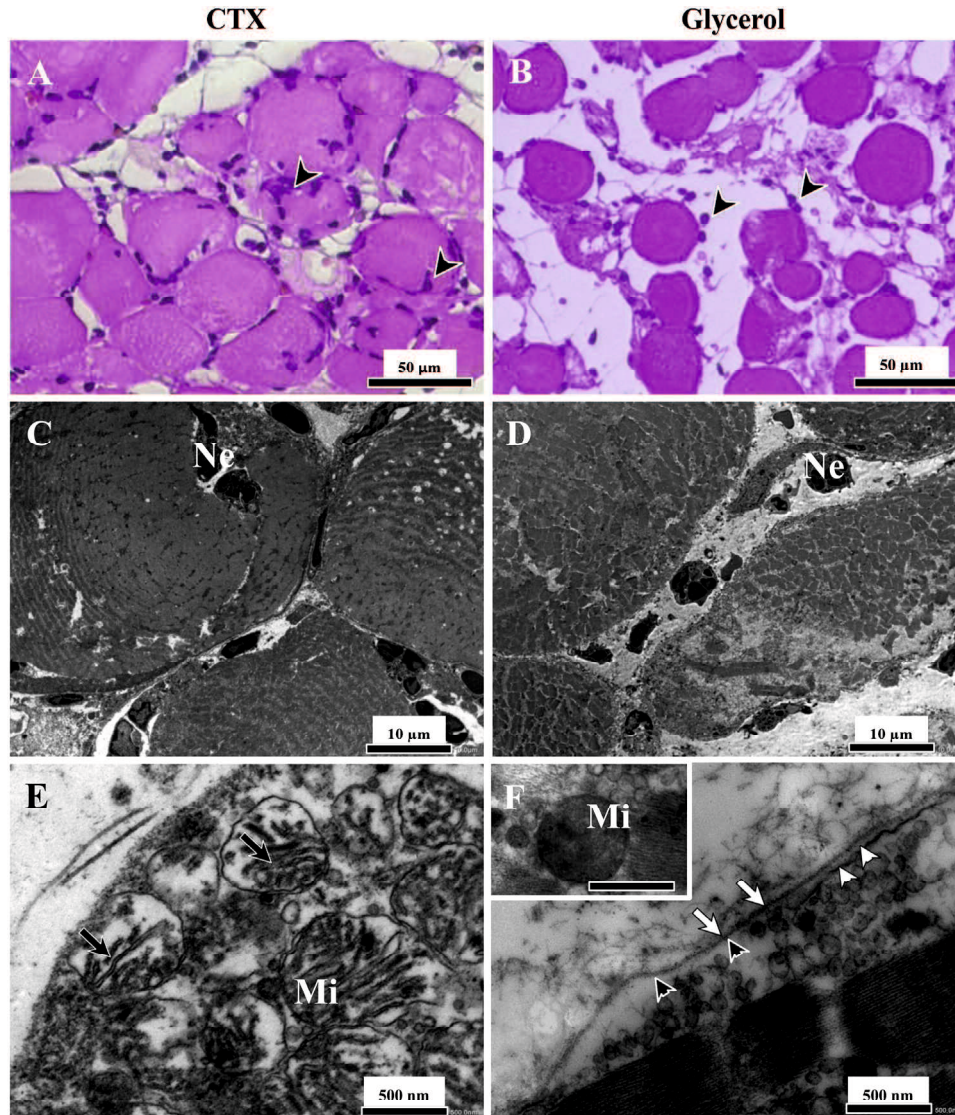


Fig. 4. Changes of TA muscle at 12 h after CTX-induced injury and glycerol-induced injury. (A and B) Light micrographs, HE stain, showing some myofibers invaded with mononuclear cells (arrowheads). (C and E) TEM micrographs of CTX-injured muscle and (D and F) glycerol-injured muscle showing necrotic myofiber invaded with neutrophils (Ne), mitochondria (Mi) with a lucent matrix, cristae (black arrows), sarcolemma (white arrow), thickened plasma membrane (white arrowheads) and loss of the plasma membrane (black arrowheads). Inset showing mitochondria (Mi) in glycerol-injured muscle, inset scale bar = 500 nm.

10 min at room temperature. Antigen retrieval was done with proteinase K (Abcam, Cambridge, UK) at 37 °C for 5 min. Non-specific binding was blocked with 5% BSA (Sigma-Aldrich) for 2 h. Sections were incubated with rabbit anti-F4/80 antibody (1:500, Santa Cruz Biotechnology, Santa Cruz, USA), a marker for macrophages (Kawanishi et al., 2016), in 0.05% Tween-PBS overnight at 4 °C. Immunoreactivity was detected with 0.05% 3, 3'-diaminobenzidine (DAB) (Wako), and slides were counterstained with hematoxylin. Negative control sections without a primary antibody were included in every staining.

2.7. Statistical analysis

Data were expressed as means \pm standard deviation (SD). Statistical analysis was carried out using SPSS software (IBM SPSS Statistics, Chicago, Illinois, version 21). Data were analyzed by one-way analysis of variance (ANOVA) followed by Dunnett's post-hoc test to compare groups with the control. The *t*-test followed by

Bonferroni's post-hoc test was used for comparison between treatments. Statistical significance was defined as $p < 0.05$.

3. Results

3.1. Time courses of muscle degeneration after cardiotoxin-induced injury and glycerol-induced injury

Sections from muscles injured by CTX and glycerol were examined by light microscopy and TEM to assess the different histopathological changes.

Non-injured muscle exhibited closely arranged myofibers that were polygonal in shape with peripherally located nuclei. Endomysium surrounded myofiber while perimysium surrounded a group of myofibers called fascicle (Fig. 1A and B). Ultrastructurally, both the basal lamina and plasma membrane were intact with closely arranged myofibrils. The nucleus was located peripherally under the basal lamina, while SCs were located between the basal lamina and plasma membrane (Fig. 1C and D). Both the outer basal lamina

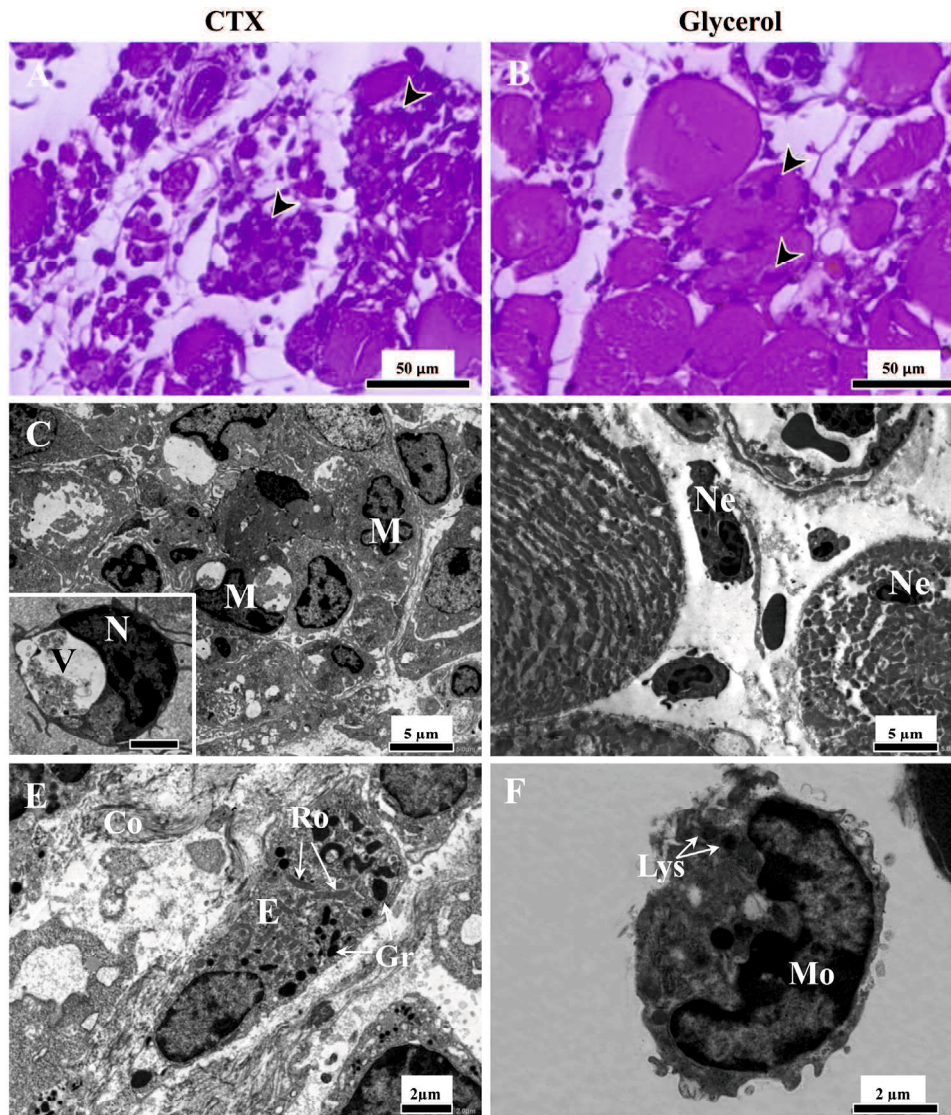


Fig. 5. Changes of TA muscle at 24 h after CTX-induced injury and glycerol-induced injury. (A and B) Light micrographs, HE stain, showing myofibers invaded with mononuclear cells (arrowheads). (C and E) TEM micrographs of CTX-injured muscle and (D and F) glycerol-injured muscle showing necrotic myofibers invaded by macrophages (M) and neutrophils (Ne). Eosinophil (Eo) with dense granules (Gr) and rods (Ro) and connective tissue (Co), and monocyte (Mo) with lysosomes (Lys). Inset showing higher magnification of a macrophage with a single nucleus (N) and large phagocytic vacuole (V), inset scale bar = 2 μ m.

and the inner plasma membrane were intact (Fig. 1E). Quiescent SCs were characterized by a large nucleus with condensed heterochromatin (Fig. 1D). In addition, Z-lines were normally arranged (Fig. 1F).

At 1 h after injury, both CTX-injured muscles and glycerol-injured muscles displayed disruption of myofiber arrangement, variation in myofiber sizes and widening of the interstitial space between myofibers (Fig. 2A and 2B). Most myofibers were swollen, while others were completely lost, leaving an empty outer membrane with the appearance of “ghost” myofibers. Ultrastructurally, disarrangement of myofibrils was clear in both CTX-injured muscles and glycerol-injured muscles. CTX-injured muscles showed a subsarcolemmal accumulation of swollen mitochondria. The nuclear chromatin was clumped along the nuclear membrane (Fig. 2C). In contrast, the swollen myofibers in glycerol-injured muscles showed an accumulation of small vesicles, about 40–120 nm in diameter, in the subsarcolemmal region and between myofibrils. The nuclear chromatin was condensed and fragmented. Focal disruption of the basal lamina was also observed (Fig. 2D).

On the other hand, loss of Z-lines was detected in both CTX-injured muscles and glycerol-injured muscles (Fig. 2E and 2F).

At 6 h after injury, multiple mononuclear cellular infiltrations were detected in the interstitial space between myofibers in the CTX-injured muscles. There was little cellular infiltration of myofibers (Fig. 3A). In the glycerol-injured muscles, individual mononuclear cellular infiltration was detected between myofibers. Hypercontracted myofibers, i.e. myofibers with partial loss of the cytoplasm resulting in a gap between the cytoplasm and outer membrane, were also observed in the glycerol-injured muscle (Fig. 3B). Ultrastructurally, mononuclear cells infiltrating the CTX-injured muscles were identified as neutrophils by their dense multi-lobed nuclei and granular cytoplasm and they were located in the interstitial space between myofibers. Some myofibers were also invaded by neutrophils (Fig. 3C). In contrast, sporadic neutrophils were observed in glycerol-injured muscles. They were located in the interstitial space between myofibers. Furthermore, myofiber hypercontraction was indicated by an undulating basal lamina separated from the myofiber with a gap (Fig. 3D). Vesicles were still detected in the subsarcolemmal region and between myofibrils.

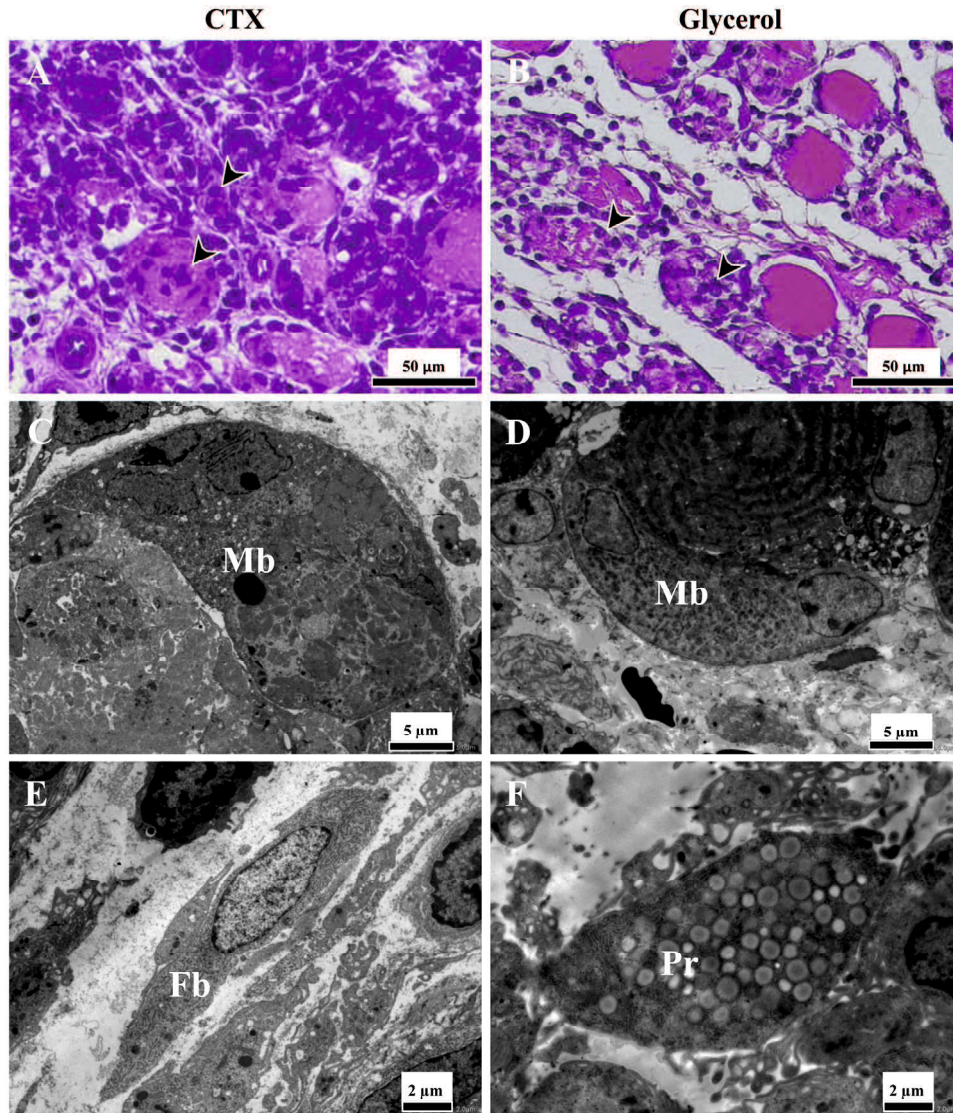


Fig. 6. Changes of TA muscle at 4 days after CTX-induced injury and glycerol-induced injury. (A and B) Light micrographs, HE stain, showing myofibers extensively invaded by mononuclear cells (arrowheads). Note the larger number of macrophages (M) in CTX-injured muscle than in glycerol-injured muscle. (C and E) TEM micrographs of CTX-injured muscle and (D and F) glycerol-injured muscle showing myoblasts (Mb), fibroblasts (Fb) and preadipocytes (Pr).

At 12 h after injury, many myofibers were infiltrated by mononuclear cells in CTX-injured muscles (Fig. 4A) while mononuclear cells were distributed in the interstitial space between myofibers in glycerol-injured muscles (Fig. 4B). Ultrastructurally, many myofibers were invaded by neutrophils in CTX-injured muscles (Fig. 4C). The mitochondria were dilated and had an electron-lucent matrix with irregular and reduced number of cristae (Fig. 4E). Neutrophil infiltration in glycerol-injured muscles was only in the interstitial space between myofibers (Fig. 4D). Moreover, the plasma membrane was thickened in some parts and was discontinuous in other parts with vesicles accumulated underneath as well as between myofibrils (Fig. 4F).

At 24 h after injury, the number of myofibers infiltrated with mononuclear cells was markedly increased in CTX-injured muscles (Fig. 5A). In contrast, only a few myofibers were infiltrated with mononuclear cells in glycerol-injured muscles (Fig. 5B). Ultrastructurally, myofibers in CTX-injured muscles were invaded by numerous macrophages, identified by the prominent single euchromatic nucleus with nucleolus and cytoplasmic processes, and a few neutrophils (Fig. 5C). Eosinophils could be detected at this time point in CTX-injured muscles; they were distinguished

by their characteristic electron-dense granules and less dense rods, while nuclear chromatin was located at the periphery of the nucleus (Fig. 5E). On the other hand, myofibers in glycerol-injured muscles were invaded only by neutrophils only (Fig. 5D). Monocytes were detected at this time point in glycerol-injured muscles; they were characterized by their characteristic kidney-shaped nucleus (Fig. 5F). Few vesicles could be detected at this time point in glycerol-injured muscles.

At 4 days after injury, massive cellular infiltration was detected in CTX-injured muscles. The cells had either invaded the degenerated myofibers or were located in the extracellular spaces. Although glycerol-injured muscles were infiltrated with a large number of mononuclear cells, the number of mononuclear cells appeared to be larger in the CTX-injured muscles than in the glycerol-injured muscles. Ultrastructurally, the infiltrating cells were mainly macrophages in both muscles. The length of SCs increased markedly both in the CTX-injured muscles and glycerol-injured muscles, the SCs contained some myofibrils, suggesting their conversion to myoblasts (Fig. 6C and D). Many fibroblasts were detected in the extracellular matrix in CTX-injured muscles. They were characterized by their fusiform shape, elongated

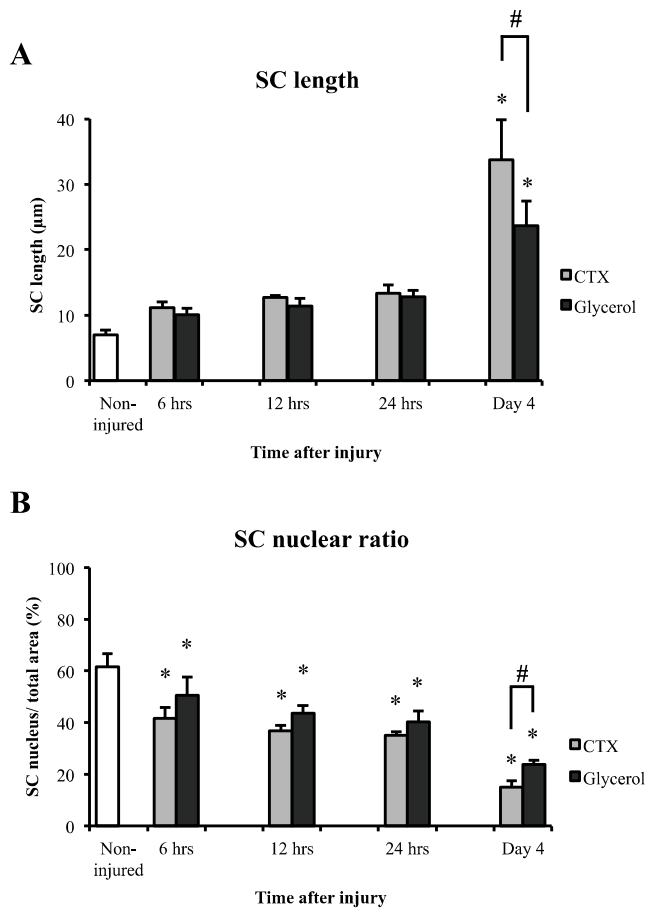


Fig. 7. Morphometric analysis of changes in SC length (A) and SC nuclear ratio (B) following CTX-induced injury and glycerol-induced injury. Data are expressed as means \pm SD, * indicates significant difference from non-injured muscle, and # indicates significant difference between CTX-injured and glycerol-injured muscles at the same time point ($P < 0.05$, $n = 50$ SCs).

nucleus and well-developed rough endoplasmic reticulum in the cytoplasm, indicating active protein synthesis (Fig. 6E). On the other hand, numerous preadipocytes, characterized by numerous RER and lipid globules, were detected in glycerol-injured muscles (Fig. 6F). Furthermore, vesicles could not be detected at this time point in glycerol-injured muscles.

3.2. Morphometric analysis of SCs

To quantitatively follow the SC activation state in response to injury, the length of SCs was measured and the nuclear-cytoplasmic ratio was calculated. The average length of quiescent SCs, in non-injured muscle was about $6.9 \pm 0.8 \mu\text{m}$, and the nucleus occupied about 61.6% of the total area. At 6 h, early activation of SCs was indicated by slight increase in both the length and cytoplasm-to-nucleus ratio compared to these in the quiescence state. The increase in length and ratio continued for up to 24 h, but there was no significant difference in SC length or cytoplasm-to-nucleus ratio between CTX-injured muscles and glycerol-injured muscles at these time points. At day 4, the length of SCs had increased significantly both in the CTX-injured muscles and glycerol-injured muscles compared to that in the quiescent state. The SCs were significantly longer in the CTX-injured muscles than in the glycerol-injured muscles. The nucleus occupied about 15.1% and 23.7% of SC total area in the CTX-injured muscles and glycerol-injured muscles, respectively ($P < 0.05$) (Fig. 7A and B).

3.3. Immunohistochemical detection of macrophages

Immunostaining of F4/80 was performed to detect macrophage infiltration at day 4 after injury. Extensive macrophage infiltration was detected in CTX-injured muscles compared to that in glycerol-injured muscles (Fig. 8A and B). Quantification of the number of macrophages revealed a significantly higher content of macrophages in CTX-injured muscles, about 2.6-fold higher than that in glycerol-injured muscles ($P < 0.05$) (Fig. 8C).

4. Discussion

Our previous study revealed efficient regeneration with transient fibrosis and absence of adipocyte infiltration following CTX-induced injury and impaired regeneration with progressive fibrosis and adipocyte infiltration following glycerol-induced injury (Mahdy et al., 2015). Recently, it was reported that the early phase after injury affects the outcome of regeneration (Hardy et al., 2016). A further understanding of the different cell subtypes during the inflammatory phase, the factors that regulate their function, and the timing of their activity will help to develop therapies for acute injuries as well as myopathies associated with chronic inflammatory responses (Kharraz et al., 2013). Therefore, the present study was carried out to compare the early changes following CTX-induced injury and glycerol-induced injury by light microscopy and TEM and to determine the relationship between these changes and the difference in regeneration between the two injuries (Fig. 9).

CTX-induced injury caused mitochondrial swelling as was reported after exposure to CTX in vitro (Wang and Wu, 2005). Moreover, mitochondrial matrix lysis and disrupted cristae were noted at 12 h after CTX-induced injury. It was concluded that the CTX-induced necrosis of myocytes is mediated through mitochondrial swelling and fragmentation (Wang and Wu, 2005). Moreover, mitochondrial dysfunction was reported in CTX-injected muscle as indicated by loss of enzyme histochemistry signal of mitochondrial activities and altered cristae observed by TEM (Ramadasan-Nair et al., 2014). Taken together, the results suggest that myofiber mitochondria are the initial targets of CTX injury.

The results of the present study revealed that glycerol-induced injury caused myofiber hypercontraction with formation of small vesicles under the basal lamina and with focal disruption of the basal lamina. Similar findings were reported in rabbits after glycerol injection, and it was concluded that glycerol damages the myofiber cell membrane (Kawai et al., 1990), resulting in increased permeability and finally cell death (Charge and Rudnicki, 2004). It was also reported that transient exposure to glycerol results in myofiber shrinkage (Démonbreun et al., 2014) due to movement of water from the myofiber sarcoplasm to the hypertonic extracellular solution (Dulhunty et al., 1973). Disruption of plasma membrane was detected by TEM in calcium ionophore-treated rat muscles (Yoshimura et al., 1986) and toxin-injured mice muscle (Baldo et al., 2010). It is associated with accumulations of vesicles under the disrupted membrane (Bansal et al., 2003). Vesicle accumulation and fusion with each other or with the plasma membrane provides additional membrane to reseal the disrupted plasma membrane (Bansal and Campbell, 2004). On the other hand, exposure of myofibers to osmotic shock through glycerol introduction and removal resulted in vacuolation of T-tubules (Apostol et al., 2009; Démonbreun et al., 2014). The previous findings suggest that glycerol damaged the myofiber cell membrane and induced alteration in the myofiber osmotic property.

Our results showed the appearance of neutrophil infiltration at 6 h after both injuries. However, CTX induced infiltration of a larger number of neutrophils and earlier myofiber invasion than did glycerol. These results are consistent with results obtained by

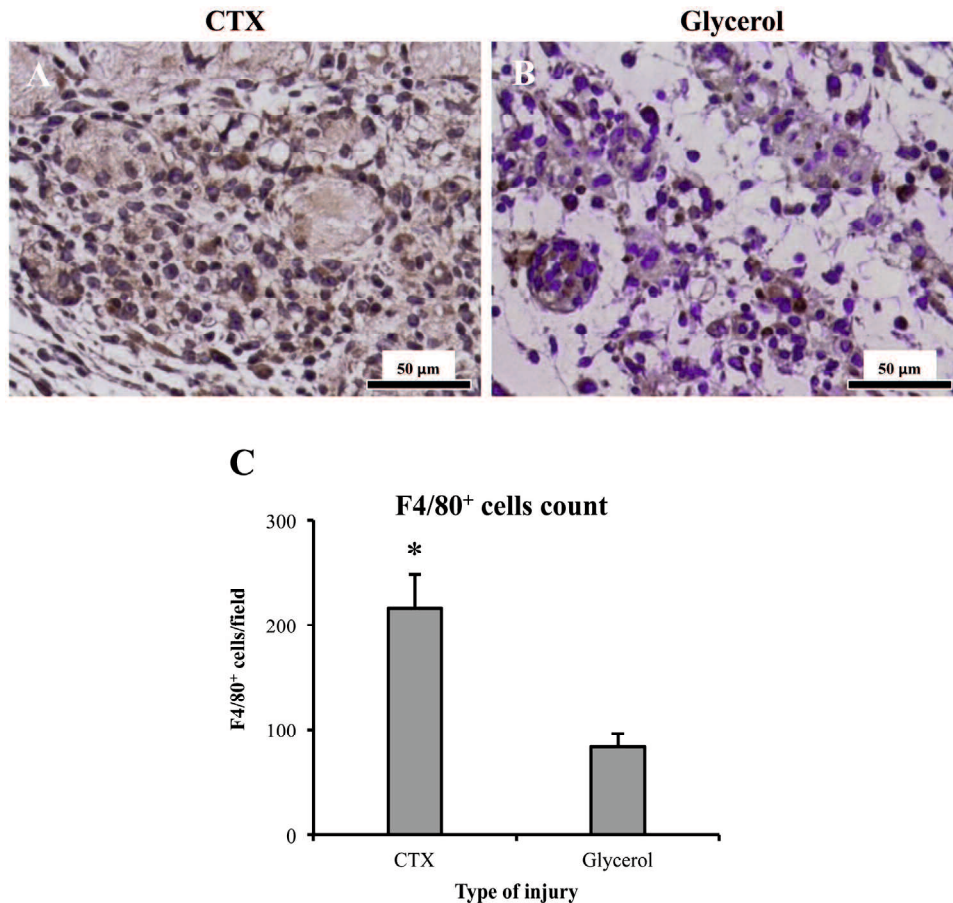


Fig. 8. Macrophage infiltration at day 4 after CTX-induced injury and glycerol-induced injury. (A, B) Representative images showing macrophages (arrowhead) detected by IHC staining with F4/80 antibody. (C) Analysis of the number of macrophages, F4/80⁺ cells, per field. Data are expressed as means ± SD, * indicates significant difference ($P < 0.05$, $n = 12$ field).

Arsic et al. (2004) showing that CTX induces more severe damage and extensive infiltration of inflammatory cells than does glycerol. Neutrophils are the first cells to migrate from blood capillaries to the injury site (diapedesis), and they have a phagocytic function and release pro-inflammatory cytokines (Sheshchalam et al., 2014). It was reported that neutrophils appeared at 6 h after CTX injection (Kohno et al., 2012) and at 12 h after glycerol injection (Suelves et al., 2002). In contrast to our findings, a recent study showed neutrophil infiltration at 18 h after CTX injection (Hardy et al., 2016), and Lukjanenko et al. (2013) reported that glycerol induces a stronger inflammatory response than does CTX. The difference between these results and our results might be due to the difference in mouse strains used, C57BL/6 vs. CH3/HeN, and the difference in volumes of injected glycerol and CTX, 25 μl vs. 50 μl (Hardy et al., 2016; Lukjanenko et al., 2013). Strain-specific differences were reported between BALB/c and C57BL/6 mice following ischemia (McClung et al., 2012) and bupivacaine injection (Lagrotta-Candido et al., 2010). Moreover, different levels of cytokines in C57BL/6 mice and C3H mice following radiation-induced pulmonary injury were reported (Ao et al., 2009). It was also reported that 25 μl of 50% glycerol induced less myofiber damage than did 50 μl of 50% glycerol (Lukjanenko et al., 2013).

Infiltration of macrophages was detected at 24 h after CTX-induced injury in the present study. Similar findings were reported at 24 h after CTX injury (Sakaguchi et al., 2014; Segawa et al., 2008). On the other hand, Hardy et al. (2016) detected macrophages for the first time at day 4 after CTX-induced injury. Although Sakaguchi et al. (2014) and Hardy et al. (2016) used the same mouse strain,

C57BL/6, they injected different volumes, 50 μl and 25 μl, respectively, while the CH3 mouse strain was used in the present study and in the study by Segawa et al. (2008), but Segawa et al. (2008) injected 75 μl of CTX. Although there are strain-specific differences in response to the same injury (Lagrotta-Candido et al., 2010; McClung et al., 2012), the difference between results of previous studies might be due to different volumes of injected CTX rather than the mouse strain. In addition, macrophage infiltration was detected 2 days after glycerol-induced injury (Suelves et al., 2002), which might explain the inability to detect macrophages at 24 h after glycerol-induced injury in the current study.

Efficient tissue repair depends on the recruitment of inflammatory cells; the increased number of macrophages during the inflammation phase results in fast and complete recovery of muscles (Dumont and Frenette, 2010). Delivery of proinflammatory (M1) macrophages into injured muscle 24 h after injury improves muscle regeneration and decreases collagen accumulation (Rybalko et al., 2015). Monocytes were first detected at 24 h after glycerol-induced injury in the present study. At the same time, the CTX-injured muscles were invaded by numerous macrophages, suggesting earlier recruitment of monocytes in CTX-induced injury than in glycerol-induced injury. This suggestion is supported by the results of a recent study showing a peak of monocyte chemoattractant protein 1, a chemokine that regulates monocyte migration and infiltration, at 18 h after CTX-induced injury (Hardy et al., 2016). The timing of recruitment of blood monocytes to the damaged tissue and the differentiation of the monocytes into different macrophage subtypes influence tissue repair and regeneration (Munoz-Canoves

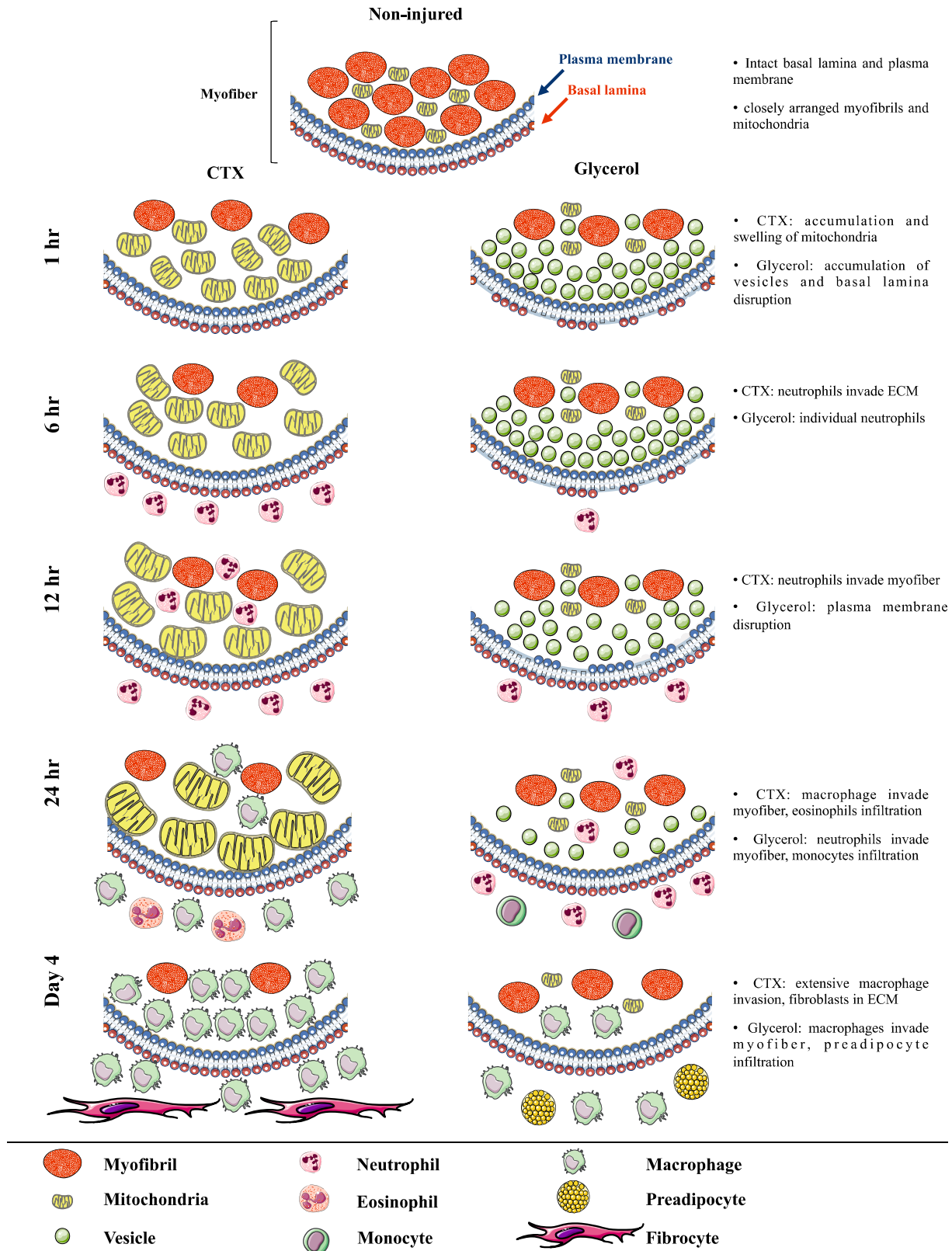


Fig. 9. Schematic model showing the spatiotemporal differences of the early injury events between CTX-induced injury and glycerol-induced injury. Figures were produced using Servier Medical Art (<http://www.servier.com>).

and Serrano, 2015). On the other hand, it was reported that macrophages isolated from CTX-injected muscles co-cultured with primary myoblasts showed a significant increase in myotube formation (Kohno et al., 2012). Infiltrating monocytes/macrophages

produce a high level of interleukin (IL)-6 at 24 h after CTX-induced injury. IL-6 stimulates further infiltration of macrophages and promotes myoblast proliferation (Zhang et al., 2013). Our findings and those of Yan et al. (2003) showed early SC activation, indicated by

increase in the length and cytoplasmic content, at 6 h after CTX and glycerol-induced injury and CTX injury, respectively. However, a significant increase in the length and cytoplasmic/nuclear content in CTX-injured muscles compared to that in glycerol-injured muscles was recorded at day 4 after injury. This difference was associated with the significantly larger number of macrophages in CTX-injured muscles than in glycerol-injured muscles. It was reported that delayed macrophage invasion to damaged myofibers negatively affects muscle regeneration (Scheerer et al., 2013). These results might explain the results of our previous study showing more efficient regeneration after CTX-induced injury than in glycerol-induced injury (Mahdy et al., 2015).

Eosinophil infiltration was detected at 24 h after CTX-induced injury, being in agreement with the results of Heredia et al. (2013). They reported that eosinophils secrete IL-4, which induces the proliferation of fibroadipogenic progenitors (FAPs) into fibroblasts to support myogenesis and inhibits the differentiation of FAPs into adipocytes (Dong et al., 2014). Intraperitoneal administration of IL-4 inhibits adipocyte infiltration in glycerol-injured muscle (Heredia et al., 2013). These results support our observations of many fibroblasts in CTX-injured muscles and many preadipocytes in glycerol-injured muscle at day 4 after injury. These results are consistent with our recent results showing increased collagen deposition after CTX-induced injury and adipocyte infiltration after glycerol-induced injury (Mahdy et al., 2015). Furthermore, the results of the previous study showed a positive interaction between SCs and fibroblasts during muscle regeneration (Murphy et al., 2011). These results supports our results showing a significant difference in myoblast length and cytoplasm ratio between CTX-induced and glycerol-induced injuries and our previous results showing efficient regeneration following CTX-induced injury compared to that following glycerol-induced injury (Mahdy et al., 2015).

5. Conclusions

The present study demonstrated differences in the possible target and the mechanism of muscle damage between CTX-induced and glycerol-induced injuries. The timing and degree of immune cell infiltration were also different. CTX targeted myofiber mitochondria, while glycerol targeted the myofiber cell membrane and osmotic property. Moreover, CTX triggered earlier and more intense immune cell infiltration than did glycerol. The early events following injuries induced by CTX and glycerol might explain the difference in regeneration between the two models. Although the current study showed for the first time the chronology of events following skeletal muscle injury induced by CTX and glycerol, further molecular studies are also recommended.

Funding

This work was supported by Japan Society for the Promotion of Science/Ministry of Education, Culture, Sports, Science and Technology (JSPS/MEXT) KAKENHI Grant Numbers 26450444 and 16H0258 (to Y. Z. H.).

Declaration of interest

The authors have no conflicts of interest.

Acknowledgments

The first author was supported financially by a scholarship from the Egyptian Government (no. 2-2010/2011) to obtain a PhD degree (to M.M.).

References

- Ao, X., Zhao, L., Davis, M.A., Lubman, D.M., Lawrence, T.S., Kong, F.M., 2009. Radiation produces differential changes in cytokine profiles in radiation lung fibrosis sensitive and resistant mice. *J. Hematol. Oncol.* 2, 6, <http://dx.doi.org/10.1186/1756-8722-2-6>.
- Apostol, S., Ursu, D., Lehmann-Horn, F., Melzer, W., 2009. Local calcium signals induced by hyper-osmotic stress in mammalian skeletal muscle cells. *J. Muscle Res. Cell Motil.* 30, 97–109, <http://dx.doi.org/10.1007/s10974-009-9179-8>.
- Arsic, N., Zacchigna, S., Zentilin, L., Ramirez-Correa, G., Pattarini, L., Salvi, A., Sinagra, G., Giacca, M., 2004. Vascular endothelial growth factor stimulates skeletal muscle regeneration in vivo. *Mol. Ther.* 10, 844–854, <http://dx.doi.org/10.1016/j.ythm.2004.08.007>.
- Baldo, C., Ferreira, M., Lopes, D., Izidorio, L., Gomes, A., Ferro, E., Hamaguchi, A., Homs-Brandeburgo, M., Rodrigues, V., 2010. Action of neuwiedase, a metalloproteinase isolated from Bothrops neuwiedi venom, on skeletal muscle: an ultrastructural and immunocytochemistry study. *J. Venomous Anim. Toxins Incl. Trop. Dis.* 16, 462–469.
- Bansal, D., Campbell, K.P., 2004. Dysferlin and the plasma membrane repair in muscular dystrophy. *Trends Cell Biol.* 14, 206–213, <http://dx.doi.org/10.1016/j.tcb.2004.03.001>.
- Bansal, D., Miyake, K., Vogel, S.S., Groh, S., Chen, C.-C., Williamson, R., McNeil, P.L., Campbell, K.P., 2003. Defective membrane repair in dysferlin-deficient muscular dystrophy. *Nature* 423, 168–172.
- Charge, S.B., Rudnicki, M.A., 2004. Cellular and molecular regulation of muscle regeneration. *Physiol. Rev.* 84, 209–238, <http://dx.doi.org/10.1152/physrev.00019.2003>.
- Demonbreun, A.R., Rossi, A.E., Alvarez, M.G., Swanson, K.E., Deveaux, H.K., Earley, J.U., Hadhazy, M., Vohra, R., Walter, G.A., Pytel, P., McNally, E.M., 2014. Dysferlin and myoferlin regulate transverse tubule formation and glycerol sensitivity. *Am. J. Pathol.* 184, 248–259, <http://dx.doi.org/10.1016/j.ajpath.2013.09.009>.
- Dong, Y., Silva, K.A.S., Dong, Y., Zhang, L., 2014. Glucocorticoids increase adipocytes in muscle by affecting IL-4 regulated FAP activity. *FASEB J.* 28, 4123–4132, <http://dx.doi.org/10.1096/fj.14-254011>.
- Dulhunty, A.F., Gage, P.W., Barry, P.H., 1973. Differential effects of glycerol treatment on membrane capacity and excitation–contraction coupling in toad sartorius fibres. With an Appendix. *J. Physiol.* 234 (234–408), 371.
- Dumont, N., Frenette, J., 2010. Macrophages protect against muscle atrophy and promote muscle recovery in vivo and in vitro: a mechanism partly dependent on the insulin-like growth factor-1 signaling molecule. *Am. J. Pathol.* 176, 2228–2235, <http://dx.doi.org/10.2353/ajpath.2010.090884>.
- Fernandez, C., Figarella-Branger, D., Meyronet, D., Cassote, E., Tong, S., Pellissier, J.F., 2005. Electron microscopy in neuromuscular disorders. *Ultrastruct. Pathol.* 29, 437–450, <http://dx.doi.org/10.1080/01913120500323175>.
- Gregory, M.A., Mars, M., 2004. Mobilisation of satellite cells following ischaemia and reperfusion in primate skeletal muscle. *S. Afr. J. Sports Med.* 16, 17–24.
- Hardy, D., Besnard, A., Latil, M., Jouvion, G., Briand, D., Thépenier, C., Pascal, Q., Guguin, A., Gayraud-Morel, B., Cavailion, J.-M., Tajbaksh, S., Rocheteau, P., Chrétien, F., 2016. Comparative study of injury models for studying muscle regeneration in mice. *PLoS One* 11, e0147198, <http://dx.doi.org/10.1371/journal.pone.0147198>.
- Heredia, J.E., Mukundan, L., Chen, F.M., Mueller, A.A., Deo, R.C., Locksley, R.M., Rando, T.A., Chawla, A., 2013. Type 2 innate signals stimulate fibro/adipogenic progenitors to facilitate muscle regeneration. *Cell* 153, 376–388, <http://dx.doi.org/10.1016/j.cell.2013.02.053>.
- Horie, M., Enomoto, M., Shimoda, M., Okawa, A., Miyakawa, S., Yagishita, K., 2014. Enhancement of satellite cell differentiation and functional recovery in injured skeletal muscle by hyperbaric oxygen treatment. *J. Appl. Physiol.* 116, 149–155, <http://dx.doi.org/10.1152/jappphysiol.00235.2013>.
- Jarvinen, T.A., Jarvinen, T.L., Kaariainen, M., Kalimo, H., Jarvinen, M., 2005. Muscle injuries: biology and treatment. *Am. J. Sports Med.* 33, 745–764, <http://dx.doi.org/10.1177/0363546505274714>.
- Karalaki, M., Fili, S., Philippou, A., Koutsilieris, M., 2009. Muscle regeneration: cellular and molecular events. *In Vivo* 23, 779–796.
- Kawai, H., Nishino, H., Kusaka, K., Naruo, T., Tamaki, Y., Iwasa, M., 1990. Experimental glycerol myopathy: a histological study. *Acta Neuropathol.* 80, 192–197.
- Kawanishi, N., Mizokami, T., Niihara, H., Yada, K., Suzuki, K., 2016. Macrophage depletion by clodronate liposome attenuates muscle injury and inflammation following exhaustive exercise. *Biochem. Biophys. Rep.* 5, 146–151, <http://dx.doi.org/10.1016/j.bbrep.2015.11.022>.
- Kharraz, Y., Guerra, J., Mann, C.J., Serrano, A.L., Pura, M.-C., 2013. Macrophage plasticity and the role of inflammation in skeletal muscle repair. *Mediators Inflamm.* 2013, 9, <http://dx.doi.org/10.1155/2013/491497>.
- Kohno, S., Yamashita, Y., Abe, T., Hirasaka, K., Oarada, M., Ohno, A., Teshima-Kondo, S., Higashibata, A., Choi, I., Mills, E.M., Okumura, Y., Terao, J., Nikawa, T., 2012. Unloading stress disturbs muscle regeneration through perturbed recruitment and function of macrophages. *J. Appl. Physiol.* 112, 1773–1782, <http://dx.doi.org/10.1152/jappphysiol.00103.2012>.
- Lagrotta-Candido, J., Canella, I., Pinheiro, D.F., Santos-Silva, L.P., Ferreira, R.S., Guimarães-Joca, F.J., Lannes-Vieira, J., Quirico-Santos, T., 2010. Characteristic pattern of skeletal muscle remodelling in different mouse strains. *Int. J. Exp. Pathol.* 91, 522–529, <http://dx.doi.org/10.1111/j.1365-2613.2010.00737.x>.
- Li, H., Mittal, A., Makonchuk, D.Y., Bhatnagar, S., Kumar, A., 2009. Matrix metalloproteinase-9 inhibition ameliorates pathogenesis and improves

- skeletal muscle regeneration in muscular dystrophy. *Hum. Mol. Genet.* 18, 2584–2598, <http://dx.doi.org/10.1093/hmg/ddp191>.
- Lukjanenko, L., Brachat, S., Pierre, E., Lach-Trifilieff, E., Feige, J.N., 2013. Genomic profiling reveals that transient adipogenic activation is a hallmark of mouse models of skeletal muscle regeneration. *PLoS One* 8, e71084, <http://dx.doi.org/10.1371/journal.pone.0071084>.
- Mahdy, M.A.A., Lei, H.Y., Wakamatsu, J.-I., Hosaka, Y.Z., Nishimura, T., 2015. Comparative study of muscle regeneration following cardiotoxin and glycerol injury. *Ann. Anat.* 202, 18–27, <http://dx.doi.org/10.1016/j.aanat.2015.07.002>.
- McClung, J.M., McCord, T.J., Keum, S., Johnson, S., Annex, B.H., Marchuk, D.A., Kontos, C.D., 2012. Skeletal muscle-specific genetic determinants contribute to the differential strain-dependent effects of hindlimb ischemia in mice. *Am. J. Pathol.* 180, 2156–2169, <http://dx.doi.org/10.1016/j.ajpath.2012.01.032>.
- Munoz-Canoves, P., Serrano, A.L., 2015. Macrophages decide between regeneration and fibrosis in muscle. *Trends Endocrinol. Metab.* 26, 449–450, <http://dx.doi.org/10.1016/j.tem.2015.07.005>.
- Murphy, M.M., Lawson, J.A., Mathew, S.J., Hutcheson, D.A., Kardon, G., 2011. Satellite cells, connective tissue fibroblasts and their interactions are crucial for muscle regeneration. *Development* 138, 3625–3637, <http://dx.doi.org/10.1242/dev.064162>.
- Musarò, A., 2014. The basis of muscle regeneration. *Adv. Biol.* 2014, 16, <http://dx.doi.org/10.1155/2014/612471>.
- Oz Gergin, O., Yildiz, K., Bayram, A., Sencar, L., Coskun, G., Yay, A., Bicer, C., Ozdamar, S., Polat, S., 2015. Comparison of the myotoxic effects of levobupivacaine, bupivacaine, and ropivacaine: an electron microscopic study. *Ultrastruct. Pathol.* 39, 169–176, <http://dx.doi.org/10.3109/01913123.2015.1014610>.
- Pisani, D.F., Bottema, C.D., Butori, C., Dani, C., Dechesne, C.A., 2010. Mouse model of skeletal muscle adiposity: a glycerol treatment approach. *Biochem. Biophys. Res. Commun.* 396, 767–773, <http://dx.doi.org/10.1016/j.bbrc.2010.05.021>.
- Ramadasan-Nair, R., Gayathri, N., Mishra, S., Sunitha, B., Mythri, R.B., Nalini, A., Subbannayya, Y., Harsha, H.C., Kolthur-Seetharam, U., Srinivas Bharath, M.M., 2014. Mitochondrial alterations and oxidative stress in an acute transient mouse model of muscle degeneration: implications for muscular dystrophy and related muscle pathologies. *J. Biol. Chem.* 289, 485–509, <http://dx.doi.org/10.1074/jbc.M113.493270>.
- Rybalko, V., Hsieh, P.L., Merscham-Banda, M., Suggs, L.J., Farrar, R.P., 2015. The development of macrophage-mediated cell therapy to improve skeletal muscle function after injury. *PLoS One* 10, e0145550, <http://dx.doi.org/10.1371/journal.pone.0145550>.
- Sakaguchi, S., Shono, J., Suzuki, T., Sawano, S., Anderson, J.E., Do, M.K., Ohtsubo, H., Mizunoya, W., Sato, Y., Nakamura, M., Furuse, M., Yamada, K., Ikeuchi, Y., Tatsumi, R., 2014. Implication of anti-inflammatory macrophages in regenerative moto-neuritogenesis: promotion of myoblast migration and neural chemorepellent semaphorin 3A expression in injured muscle. *Int. J. Biochem. Cell Biol.* 54, 272–285, <http://dx.doi.org/10.1016/j.biocel.2014.05.032>.
- Scheerer, N., Dehne, N., Stockmann, C., Swoboda, S., Baba, H.A., Neugebauer, A., Johnson, R.S., Fandrey, J., 2013. Myeloid hypoxia-inducible factor-1 α is essential for skeletal muscle regeneration in mice. *J. Immunol.* 191, 407–414, <http://dx.doi.org/10.4049/jimmunol.1103779>.
- Segawa, M., Fukada, S.-i., Yamamoto, Y., Yahagi, H., Kanematsu, M., Sato, M., Ito, T., Uezumi, A., Hayashi, S.i., Miyagoe-Suzuki, Y., Takeda, S.i., Tsujikawa, K., Yamamoto, H., 2008. Suppression of macrophage functions impairs skeletal muscle regeneration with severe fibrosis. *Exp. Cell Res.* 314, 3232–3244, <http://dx.doi.org/10.1016/j.yexcr.2008.08.008>.
- Sheshechalam, A., Srivastava, N., Mitchell, T., Lacy, P., Eitzen, G., 2014. Granule protein processing and regulated secretion in neutrophils. *Front. Immunol.* 5, <http://dx.doi.org/10.3389/fimmu.2014.00448>.
- Suelves, M., Lopez-Alemany, R., Lluís, F., Aniorte, G., Serrano, E., Parra, M., Carmeliet, P., Munoz-Canoves, P., 2002. Plasmin activity is required for myogenesis in vitro and skeletal muscle regeneration in vivo. *Blood* 99, 2835–2844.
- Uezumi, A., Fukada, S., Yamamoto, N., Takeda, S., Tsuchida, K., 2010. Mesenchymal progenitors distinct from satellite cells contribute to ectopic fat cell formation in skeletal muscle. *Nat. Cell Biol.* 12, 143–152, <http://dx.doi.org/10.1038/ncb2014>.
- Wang, C.H., Wu, W.G., 2005. Amphiphilic beta-sheet cobra cardiotoxin targets mitochondria and disrupts its network. *FEBS Lett.* 579, 3169–3174, <http://dx.doi.org/10.1016/j.febslet.2005.05.006>.
- Yan, Z., Choi, S., Liu, X., Zhang, M., Schageman, J.J., Lee, S.Y., Hart, R., Lin, L., Thurmond, F.A., Williams, R.S., 2003. Highly coordinated gene regulation in mouse skeletal muscle regeneration. *J. Biol. Chem.* 278, 8826–8836, <http://dx.doi.org/10.1074/jbc.M209879200>.
- Yoshimura, T., Tsujihata, M., Satoh, A., Mori, M., Hazama, R., Kinoshita, N., Takashima, H., Nagataki, S., 1986. Ultrastructural study of the effect of calcium ionophore A23187, on rat muscle. *Acta Neuropathol.* 69, 184–192, <http://dx.doi.org/10.1007/bf00688293>.
- Zhang, C., Li, Y., Wu, Y., Wang, L., Wang, X., Du, J., 2013. Interleukin-6/signal transducer and activator of transcription 3 (STAT3) pathway is essential for macrophage infiltration and myoblast proliferation during muscle regeneration. *J. Biol. Chem.* 288, 1489–1499, <http://dx.doi.org/10.1074/jbc.M112.419788>.